Dynamic Modeling and Optimal Operation of District Heating Systems

LianZhong, Li

A thesis in
Department of Building, Civil and Environmental Engineering

Presented in Partial Fulfillment of the Requirements
For the Degree of Master of Applied Science at
Concordia University
Montreal, Quebec, Canada

August 2003

Your file Votre référence
ISBN: 0-612-83859-5
Our file Notre référence
ISBN: 0-612-83859-5

ABSTRACT

Dynamic Modeling and Optimal Operation of District Heating Systems

Lianzhong Li

District Heating Systems (DHS) are widely utilized for space heating in residential and commercial buildings. They offer economic benefits to consumers in terms of lower heating costs. The energy efficiency of DHS can be further improved by optimally controlling the operating parameters of the system. With this as a motivation, dynamic modeling and optimal operation strategies of DHS are explored in this thesis.

Two typical District Heating Systems namely Direct District Heating System (DDHS) and Indirect District Heating System (IDHS) are considered. Using typical system configurations the components of the DHS were sized. Dynamic models of the designed DHSs useful for control analysis were developed. Open loop tests subject to constant inputs and loads were conducted to evaluate the time response characteristics of DHS.

A methodology for computing optimal operating parameters of DHS is presented. These optimal parameters so computed are used as set points for PID controllers. The

DHS by virtue of its long distribution network is subject to large transportation time delays. To compensate such time delays, a PID controller augmented with a Smith Predictor is developed. The designed controller is used to simulate closed loop operation of DHS under variable load conditions. Results show that the optimal set point strategy can save 10%~15% energy compared to conventional control strategies.

ACKNOWLEDGEMENTS

I would like to express my sincere gratitude to Dr. M. Zaheer-Uddin for his constant guidance, help, sustained interest, and financial support throughout the whole span of this thesis.

My thanks are also to the staff in BCEE Department, as well as my colleagues, especially to Wenzhen Huang.

I would like to dedicate this thesis to my wife, Tong Zhang, and my lovely daughter, Jiameng Li for their patience, understanding and support during my whole studies.

TABLE OF CONTENTS

List of Figures

List of Tables

Nomenclature

af_i	value related to heat transfer area and conductance of terminal heaters of zone i (w/℃)
A_1	heated floor area for point 1 (m^2)
A_2	heated floor area for point 2 (m^2)
A_{eq}	matrix or array of linear equality constraints
A_{floori}	floor area of zone i (m^2)
A_{ij}	area of each part of enclosure in each building (m^2)
A_j	transfer area of each heat exchanger (m^2)
A_{roofi}	roof area of zone i (m^2)
A_{wall_si}	south-facing wall area of zone i (m^2)
A_{wothi}	non-south-facing wall area of zone i (m^2)
A_{win_si}	south-facing window area of zone i (m^2)
$A_{othwini}$	non-south-facing window area of zone i (m^2)
A_{zi}	heated floor area of zone i (m^2)
b_{eq}	linear equality constraints
bh	factor in terminal heater conductance equation, $k=f(T_{hav}-T_z)^{bh}$
c_w	specific heat of water (J/kg℃)
c_z	specific heat of air (J/kg℃)
C_b	thermal capacity of boiler (J/℃)
C_{bi}	thermal capacity of internal pipe segment i in boiler (J/℃)
C_{2j}	thermal capacity of j^{th} secondary system (J/℃)
C_{fi}	thermal capacity of floor of zone i (J/℃)
C_{h1j}	thermal capacity of heat exchanger j in primary side (J/℃)
C_{h2j}	thermal capacity of heat exchanger j in secondary side (J/℃)
C_{opb11}	thermal capacity of outside piping network of zone 1 (J/℃)
C_{opc3}	thermal capacity of outside piping network of zone 3 (J/℃)
C_{opd2}	thermal capacity of outside piping network of zone 2 (J/℃)
C_{rfi}	thermal capacity of roof of zone i (J/℃)
C_{wsi}	thermal capacity of south-facing wall of zone i (J/℃)
C_{wothi}	thermal capacity of non-south-facing wall of zone i (J/℃)
C_{u1}	thermal capacity of users of zone 1 (J/℃)
C_{u2}	thermal capacity of users of zone 2 (J/℃)
C_{u3}	thermal capacity of users of zone 3 (J/℃)
C_{zi}	thermal capacity of zone i (J/℃)
C_{zj}	thermal capacity of zone j (J/℃)
d_e	insulation thickness of pipe (m)
d_{intk}	inter diameter of k^{th} pipe segment (m)
d_z	density of air (kg/m^3)

d_w	density of water (kg/m^3)
e_1	efficiency of primary system (%)
e_2	efficiency of secondary system (%)
e_b	boiler efficiency (%)
e_{bmax}	maximum boiler efficiency (%)
E_p	price of electricity (CND/kwh)
f	factor in conductance equation of terminal heaters
f_d	factor
f_{foul}	fouling factor of heat exchangers
f_{ea}	excess heat transfer area factor of heat exchangers
f_f	safety factor of water flow rate
f_g	safety factor related to heat losses
f_r	safety factor of water friction resistance
f_{ha}	excess heat transfer area factor of terminal heaters
f_m	factor in boiler efficiency calculation
f_n	factor in boiler efficiency calculation
f_{se}	ratio of exhaust fan power to supply fan power
f_{sp}	safety factor of makeup water pressure set point
f_{sw}	ratio of makeup water (%)
F_{boiler}	factor in calculating boiler efficiency
g	gravity acceleration (m/s^2)
G	water flow rate (kg/s)
G_{1d}	design water flow rate in primary system (kg/s)
G_{1dj}	design water flow rate of heat exchanger j in primary side (kg/s)
G_{2d}	design water flow rate in secondary system (kg/s)
G_{2dj}	design water flow rate of heat exchanger j in secondary side (kg/s)
G_{2dzi}	design water flow rate of zone i (kg/s)
G_c	transfer function of nominal controller
G_{cp}	circulating water flow rate of pump (kg/s)
G_{cpd}	design water flow rate of pump (kg/s)
G_{csp}	transfer function of controller with Smith Predictor
G_{ef}	airflow rate of exhaust fan (m^3/s)
G_f	flow rate of fuel (kg/s)
G_{fmax}	maximum flow rate of fuel (kg/s)
G_{mp}	makeup water flow rate (kg/s)
G_o	overall transfer function
G_p	transfer function of nominal plant
G_r	transfer function of real plant
G_{re}	return water flow rate (kg/s)
G_{rls}	transfer function of root locus
G_s	supply water flow rate (kg/s)

G_{sf}	airflow rate of supply fan (m^3/s)
G_{sw}	make up water flow rate (kg/s)
G_{szi}	circulating water flow rate of zone i (kg/s)
G_t	circulating water flow rate of pump (kg/s)
h_i	convection heat transfer coefficient inside room or inside surface of pipe ($w/m^2℃$)
hv	heating value of fuel (J/kg)
h_w	convection heat transfer coefficient of water inside pipe ($w/m^2℃$)
J	operating cost (CND)
J_e	electricity cost (CND/s)
J_f	fuel cost (CND/s)
J_w	water cost (CND/s)
k	pipe segment
k_i	integral gain
k_{ins}	thermal conductivity of outside pipe insulation ($w/m℃$)
k_p	proportional gain
K	conductance of heat exchanger ($w/m^2℃$)
K_a	absolute roughness (m)
KF_j	heat transfer rate of heat exchanger j ($w/℃$)
l	time delay of pipe segment (s)
L	length or thickness (m)
L_k	length of pipe segment (m)
LMTD	logarithmic mean temperature difference (℃)
$LMTD_{ex}$	logarithmic mean temperature difference of heat exchanger (℃)
n	number of heat exchanger selected in the j^{th} heat exchange station or number of story
N_{cp}	operating power of circulating water pump (kw)
N_{ef}	operating power of exhaust fan (kw)
N_l	total amount of water loop
N_{mp}	operating power of makeup water pump (kw)
N_{pk}	number of pipe segment according to the water flow direction
N_{sf}	operating power of supply fan (kw)
O_p	price of heavy oil (CND/kg)
P_m	makeup water pressure (Pa)
P_{min}	minimum makeup water pressure (Pa)
P_{max}	maximum makeup water pressure (Pa)
P_{sp}	makeup water pressure set point (Pa)
q_2	heat loss owing to stack gas (%)
q_3	heat loss owing to chemical incomplete combustion (%)
q_4	heat loss owing to physical incomplete combustion (%)
q_5	heat loss owing to radiation and natural convection of combustion (%)

q_6	heat loss owing to slag removed from the surface (%)
$\bar{q}_{d1}$	heating load per m^2 for point 1 (w/m^2)
$\bar{q}_{d2}$	heating load per m^2 for point 2 (w/m^2)
q_{ex}	total heating load of heat exchangers (w)
q_{exj}	heating load of heat exchanger j (w)
$q_{heateri}$	heating load of terminal heaters of zone i (w)
q_{ins}	piping network insulation (w)
q_{int}	internal loads (w)
q_{inthig}	internal loads of high energy users (w)
q_{intlow}	internal loads of low energy users (w)
q_{intpub}	internal loads of public buildings (w)
q_{inttot}	total internal loads (w)
q_t	total heating load in IDHS (w)
q_{zi}	heating load of zone i in DDHS(w)
q_z	total heating load in DDHS (w)
q_{zdi}	design heating load of zone i in DDHS (w)
Q	design heating load (w)
Q_{boiler}	nominal heating load of boiler (w)
Q_f	radiation heat flux (w)
Q_{fi}	radiation heat flux of internal pipe segment i in boiler (w)
r_e	outer radius of pipe (m)
r_i	inter radius of pipe (m)
r_Q	heating load ratio of boiler
R_k	friction resistance of pipe (Pa)
R_m	friction resistance of m^{th} loop (Pa)
R_{rk}	friction rate of k^{th} pipe segment (Pa/m)
R_{win}	thermal resistance of window ($m^2℃/w$)
S_{rfi}	solar radiation of roof of zone i (w)
S_{wall_si}	solar radiation of south-facing wall of zone i (w)
S_{win_si}	solar radiation of south-facing window of zone i (w)
T	time delay (s)
T_b	supply water temperature of boiler (℃)
T_{bi}	water temperature of boiler in segment i (℃)
T_{bd}	design supply water temperature of boiler (℃)
T_{b_d}	supply water temperature in design operating condition (℃)
T_{bmax}	maximum supply temperature of boiler (℃)
T_{bsp}	optimal set point of supply water temperature (℃)
T_{bspzi}	supply water set point of zone i (℃)
T_{bspavg}	average value of supply water temperature set point in zone 1, 2, and 3 (℃)

T_e	environment temperature (℃)
T_{fi}	floor temperature of zone i (℃)
T_h	supply water temperature of heat exchanger (℃)
T_{hj}	supply water temperature of heat exchanger j in secondary side (℃)
T_{hd}	design supply water temperature in secondary side (℃)
T_{h_d}	supply water temperature of heat exchanger in design operating condition (℃)
T_{hav}	average water temperature of terminal heater (℃)
T_{ij}	temperature of node i in zone j (℃)
T_{in}	air temperature of entering boiler (℃)
T_o	outdoor air temperature (℃)
T_o'	equivalent outdoor air temperature (℃)
T_{oact}	actual outdoor air temperature (℃)
T_{od}	design outdoor temperature (℃)
T_{oequ}	equivalent outdoor air temperature considered by internal loads (℃)
T_{oint}	equivalent temperature affected by internal loads (℃)
T_{ou}	gas temperature at boiler exit (℃)
T_{re}	return water temperature (℃)
T_{red}	design return water temperature (℃)
T_{re_d}	return water temperature in design operating condition (℃)
T_{re1}	return water temperature in primary system (℃)
T_{re1j}	return water temperature of heat exchanger j in primary side (℃)
T_{re1d}	design return water temperature in primary system (℃)
T_{re1_d}	return water temperature of primary side in design operating condition (℃)
T_{re2}	return water temperature in secondary system (℃)
T_{re2j}	return water temperature of heat exchanger j in secondary side (℃)
T_{re2d}	design return water temperature in secondary system (℃)
T_{re2_d}	return water temperature of secondary side in design operating condition (℃)
T_{rfi}	roof temperature of zone i (℃)
T_s	supply water temperature (℃)
T_{sd}	design supply water temperature (℃)
T_{s_d}	supply water temperature in design operating condition (℃)
T_{sw}	makeup water temperature (℃)
T_{soil}	soil temperature (℃)
T_{wsii}	inside temperature of south-facing wall of zone i (℃)
T_{wothii}	inside temperature of non-south-facing wall of zone i (℃)
T_{zdij}	design indoor air temperature in each room in winter (°C)
T_{zi}	indoor air temperature of zone i (℃)
T_{zj}	indoor air temperature of room j (℃)
T_{zd}	design indoor air temperature (℃)
T_{zlow}	zone temperature on lowest floor of building (℃)

T_{zup}	zone temperature on highest floor of building (℃)
U_b	normalized energy input of boiler
U_{f1}	conductance of pipe network in primary side (w/℃)
U_{f2}	conductance of pipe network in secondary side (w/℃)
U_{f1i}	combined conductance of floor surface in zone i (w/℃)
U_{fi}	conductance of floor surface in zone i (w/℃)
U_{fii}	conductance of inside floor surface in zone i (w/℃)
U_{ij}	conductance of each part of enclosure in each building ($W/m^2{}^\circ C$)
U_{ins}	conductance of pipe insulation (w/℃)
U_{rfi}	conductance of roof in zone i (w/℃)
U_{rf1i}	combined conductance of roof surface in zone i (w/℃)
U_{rfii}	conductance of inside roof surface in zone i (w/℃)
U_t	conductance of building enclosure (w/℃)
U_{wsi}	conductance of south-facing wall in zone i (w/℃)
U_{wsii}	conductance of inside south-facing wall surface in zone i (w/℃)
U_{wsoi}	conductance of outside south-facing wall surface in zone i (w/℃)
U_{wothi}	conductance of non-south-facing wall in zone i (w/℃)
U_{wotho}	conductance of outside non-south-facing wall surface in zone i (w/℃)
V_{air}	theoretical combustion airflow rate per kg fuel (Nm^3/kg)
V_b	water content of boiler (m^3)
V_e	water velocity in pipe system (m/s)
V_{ex1}	water content of heat exchanger in primary side (m^3)
V_{ex2}	water content of heat exchanger in secondary side (m^3)
V_{ij}	volume of each room in each building (m^3)
V_{op}	water content of outdoor piping network (m^3)
V_p	water content of piping network (m^3)
V_u	water content of users (m^3)
V_z	volume of zone air (m^3)
W_p	price of water (CND/t)
X	optimal variables
α	excess air coefficient
β_k	equivalent length factor of local friction resistance
λ_k	friction factor of pipe segment

Subscripts

1	referring to parameter of IDHS
2	referring to parameter of DDHS
ab, bc, cd, bb1, de, ef, fg, bh, hi	referring to pipe segment
act	referring to actual

air	referring to air
av	referring to average
b	referring to boiler or building
b11, d2, c3	referring to pipe segment
cp	referring to circulating water pump
d	referring to design condition
eq, equ	referring to equality constraint
ex	referring to heat exchanger
f	referring to fuel
f, fl, floor	referring to floor
h	referring to output of heat exchanger
hig	referring to high-energy users
heater	referring to terminal heater
i	referring to sequent number, internal surface, or number of heated buildings
ins	referring to insulation
int	referring to internal load
j	referring to sequent number, part of enclosure in buildings, room, or heat exchange station
low	referring to the lowest-floor of building or low-energy users
m	referring to number of loop
max	referring to maximum valve
min	referring to minimum valve
mp	referring to makeup water pump
o	referring to external surface
op	referring to outdoor piping network
oth	referring to non-south-facing enclosure
p	referring to piping network
pub	referring to public building
re	referring to return water
rf, roof	referring to roof
s	referring to supply water or south-facing enclosure
soil	referring to soil
sp	referring to set point or Smith Predictor
sw	referring to makeup water
t, tot	referring to total
u	referring to user side
up	referring to the highest-floor of building
w	referring to water
win	referring to window
win_oth, othwin	referring to non- south-facing window

win_s	referring to south-facing window
woth	referring to non-south-facing wall
ws, wall_s	referring to south-facing wall
z	referring to zone
z1, z2, z3	referring to pipe segment in zone 1, 2, and 3

Abbreviations

ACH	air change per hour
ASHRAE	American society of heating, refrigerating and air-conditioning engineers
DDHS	direct district heating system
DHS	district heating system
HES	heat exchange station
HVAC	heating, ventilating, and air conditioning
OLT	open loop test
PI	proportional plus integral controller
PID	proportional plus integral and derivative controller
IDHS	indirect district heating system
SP	Smith Predictor
VSD	variable speed device

Chapter 1 Introduction and Literature Review

1.1 Introduction

District heating systems are widely utilized for space heating in residential, commercial, and industrial buildings. Since heating technology and equipment have greatly developed in recent decades, the trend is to build larger district heating systems. The larger the district heating systems are, larger is the energy consumption. Therefore, it is of interest to consider energy conservation, through improved operating control strategies. Generally, district heating systems can be divided into three types according to the kind of heat source: heating from power plants, district boiler houses and others. In this thesis, a district heating system with a district boiler house will be studied because it is the one with higher potential for energy savings of all types of district heating systems.

1.1.1 Definition of a district heating system

A district heating system transmits and distributes heat from one or more energy sources to residential, commercial, and industrial consumers for space conditioning, hot water heating, and industrial processes. The definition includes, therefore, very small schemes sometimes referred to group heating schemes or block centrals, and very large schemes encompassing an entire city as well. District heating systems are extensively used for space heating, especially where the thermal load density is high or the annual load factor is high.

Based on economical and technical analysis, a district heating system can be

grouped into two types based on their structure. One is called a direct district heating system (DDHS), which usually has heated floor area ranging between 50000m^2 to 250000m^2. In this range they are the most cost-effective. If the heating area is larger than this range, an alternate heating system, which is called an indirect district heating system (IDHS), is recommended. Recently, several indirect district heating systems have already been built with 10Mm^2 heated floor area. Both types of district heating systems consist of production plant, transmission and distribution systems, and in-building equipment. However, the main structural distribution between the two types of systems is that indirect district heating systems consist of several heat exchange stations.

District heating systems are developing rapidly because of their advantages. District heating systems offer several benefits not only environmental benefits but also consumer economic benefits. For example, consumers can reduce energy consumption according to their needs, they do not require additional space for housing the heating equipment, and also they have less equipment maintenance.

A district heating system (DHS) is referred to as a direct district heating system (DDHS) in which hot water from a boiler passes through piping network to each terminal device directly and returns back to the heat source. On the other hand, in an indirect district heating system (IDHS) hot water passes through primary piping network to each heat exchange station and returns back to heat source directly. The secondary loop system in each heat exchange station obtains heat from the primary system. The secondary system works similarly to a direct district heating system. Some larger district heating

systems have several heat sources, hundreds of heat exchange stations, and more complex configuration.

1.1.2 Importance of this research

The use of DHS in cold climates especially in China has increased at a rapid rate and continues to grow at significant rates. For example as shown in Table 1.1 and 1.2 over a period of 8 years, the heated floor area in China has increased by 340%. Given such growth potential, it is obvious that energy conservation in DHS plays a significant economic role. If reasonable technologies are utilized in order to improve operating efficiency, for example 1%, the energy saving obtained will be about 8.35 MGJ in the year 2000. In addition, other advantages of improving operating efficiency are reducing air pollution and reduction in CO_2 levels exhausted in environment.

Table 1.1 Statistical data of DHSs

Year		1992	1998	1999	2000
Number of metropolis		517	668	668	668
Number of DHSs in metropolis		158	286	286	286
Heated floor area	10^8m^2	3.28	8.70	9.68	11.08
The amount of vapor supplied	10^8t	-	1.70	2.20	2.40
The amount of heat supplied	$10^{17}J$	-	6.50	6.98	8.35
Length of steam piping network	km	-	6933	7733	7963
Length of water piping network	km	-	27000	30506	35785

Table 1.2 Percentage of the types of heat source and heated floor area in 1998

Heated floor area for different heat sources		
Heat power plant	%	62.90
District boiler house	%	35.75
Others	%	1.35
Total	%	100
Heated floor area for different users		
Commercial building	%	33.12
Residential building	%	59.77
Others	%	7.11
Total	%	100

Improved operating strategies can save significant energy in DHS. For instance, the use of variable speed pumps and optimal control of boiler in response to changing loads on the system should be explored in order to improve overall energy efficiency of DHS.

It should be noted that, control strategies for large heating systems are quite different compared with nominal control design method because of the transport time delays that are usually large. Therefore, special control strategies have to be considered.

The motivation for this study is based on the following observations.

(1) A district heating system has a large heated floor area; therefore, it consumes large amount of energy during heating season.

(2) Many heating systems currently do not operate based on automization; thus, the potential of energy saving can be fulfilled by utilizing optimal operating set points and appropriate control strategies.

(3) Because the transport time delay and disturbances cannot be neglected, there is a need to develop an effective control strategy to handle the large time delay and disturbances as well.

(4) Internal loads should be utilized in order to achieve more energy savings.

1.1.3 The scope and objectives

The focus of the thesis is to develop dynamic models, find optimal set points, develop a control strategy, and simulate energy performance of DHS under realistic operating conditions.

The main objectives of this study are as follows:

(1) To design two typical district heating systems using practical guidelines and steady state methods and examine the influence of design parameters on system operation.

(2) To develop dynamic models of DDHS and IDHS suitable for control analysis and design. The models can be used to study the effects of building load, indoor air temperature, outdoor air temperature, solar radiation, circulating water flow rate, heat exchanger area, and supply and return water temperatures. The dynamic models can be used to analyze and simulate the responses of the DHS.

(3) To obtain optimal set of operating parameters by using multi-variable constraint objective function optimization technique for energy efficient operation.

(4) To design a control strategy embedded with a Smith Predictor for compensating the effect of large transport time delays that exist in piping networks and improve the system performance.

(5) To carry out simulation runs to study the operating performance of DHS, evaluate energy saving potential under different operating conditions.

1.2 Literature review

A literature review related to design, operation, optimization, dynamic models, and control strategies of district heating systems is presented. Also, papers dealing with large transportation delay have been reviewed. Since hot water space heating systems have similar characteristics, some guidelines employed in space heating system design are also

reviewed.

1.2.1 Design and operation of district heating systems

District heating system design plays an important role not only in its first cost but also in its operating cost. Normally, design of DHSs includes several subsystems such as heat source, distribution system, terminal heaters, and heat exchangers. These components should be selected properly; otherwise, the first cost and the operating cost increase significantly. For example, if variable speed water circulating pump and variable speed supply air fan are designed for a heating system, pumping cost to the order of 15%~60% can be saved.

ASHRAE Handbook (2000) [1] stated several guidelines for hot water heating system design. Appropriate pipe sizing was determined from an economic study of the life-cycle cost based on construction and operation of heating systems. According to the economic study, the design method based on maximum flow velocity is optimal. Also, ASHRAE Handbook describes methods for the calculation of heat losses from insulated, underground-buried pipes, which are extensively used in DHS. Moreover, the advantages and the use of plate heat exchangers were addressed. These include high heat transfer efficiency, smaller size, low maintenance, and one-third to one-half the surface area required by shell-and-tube units for the same operating conditions.

The use of plate heat exchangers to enhance heat transfer rate between water-to-water in DHS is studied by Liu (1997) [14]. The paper gives an approach for designing and calculating high efficiency plate heat exchangers using steady state design theory.

However, the design method is not validated. The calculation method and a computer program for design and selection of plate water-to-water heat exchanger, plate condenser, and plate evaporate were reported. The theoretical analysis makes several simplifying assumptions as such the accuracy of the model needs verification.

Li (1982) [16] formulated the principles and design methods of district heating systems. Steady state design including heating load and circulating water flow rate calculation, distribution system, equipment selection, make-up water, and operating curves were focused on different types of heating systems such as direct district heating systems and indirect district heating systems. Optimal operating parameters for direct district heating systems depending on adjusting simultaneously supply water temperature and circulating water flow rate were developed. In addition, a method of calculating pressure drop in piping network and devices in heating systems is developed. However, few factors such as excess area factor of terminal heaters and heat exchangers were not considered.

Many researchers have studied pipe sizing of hot water heating systems. Besides ASHRAE Handbook (2000) [1], Europeans researchers have used the criterion that pressure losses of pipe should be limited to 100Pa/m as stated by BΦhm (1988) [4]. Studies indicated that higher levels of pressure losses could be acceptable as shown by Stewart and Dona (1987) [28] and warranted from an economical standpoint according to BΦhm (1986) [3] and Phetteolace (1989) [7]. Also, Siegenthaler (1995) [19] pointed out that several factors such as flow velocity, erosion corrosion, and operating cost enter into

the selection of a pipe sizes for a given application. Flow velocities in piping network of less than 1.2m/s were recommended. When the flow through a pipe increased, the heat loss associated with the flow increased rapidly. The greater the heat loss was, the more pumping power was needed to offset the heat losses. The determination of an optimal pipe size based on minimizing total owning and operating cost could be a complex process. To mitigate this difficulty, some equations and figures were presented to estimate the theoretical annual operating cost of a piping system.

Hansen (1985) [6] formulated a steady state design method related to pressurization of closed hot water systems in primary and secondary loops. Pressurizing at pump suction, pump discharge, remote pressurization from return profiles were presented. Pressures in user systems were governed by a number of variables, for instance, pipe resistance and elevation. To keep the fluids separated, a primary-secondary system separation was employed. The method was shown to be appropriate with both constant and variable volume flow systems.

Bobenhausen (1994) [29] addressed how to design hot water heating systems using steady state methodologies, such as calculation of hot water flow rate, selection of piping system, boiler, and terminal devices. Also, for a closed heating system, the weight of the column of water going up in the supply pipes was balanced by the weight of the water coming down the return pipes. Therefore, the circulating water pump only overcame the friction caused by flow through the pipes and fittings rather than the height of the water column. The pressure drop of a distribution system was computed for several different

field operating conditions.

Basu, Kefa, and Jestin (2000) [21] described fuel and combustion calculation, burners design, corrosion and erosion prevention, and gas and air duct system design for a boiler used in a DHS. Steady state method was used in the calculations. Based on heat balance principle, the heat released by fuel combustion should be absorbed by circulating water flow. However, for a variety of reasons, the released heat would not be utilized completely because several heat losses occur in the heat transfer processes. A heat balance between the thermal efficiency and heat losses was shown. The heat losses included: heat loss though stack gas, incomplete combustion, owing to unburned carbon, owing to convection, and radiation from the furnace exterior, through the sensible heat of ash and slag. Some measured data was used in order to improve the accuracy of the model.

It is noted from the above studies that most of the published research work are related to the design aspects of DHS. The methodology used is based on steady state analysis and design technologies. This points to the lack of suitable methods for dynamic analysis and control design of DHS. To this end, in the next set of papers reviewed the attention is focused on dynamic analysis and control methods used in hot water heating systems, which are the closest to DHS in terms of operating characteristics.

1.2.2 Dynamic models for simulation and control design

Dynamic models of district heating systems are essential for simulation and control design. A district heating system consists of several subsystems. Therefore, subsystem

models have to be developed for the boiler, pipe network, heat exchangers, terminal heaters, and building enclosure. Solar radiation and internal loads in buildings should be considered because they are important factors for dynamic responses and energy savings. Much of the work is done in developing dynamic models of single zone or multi-zone buildings. However, there are no comprehensive dynamic models for the whole district heating system.

Zhang (2001) [31] developed a simple and relatively accurate dynamic model of a radiant floor heating system, which included a boiler, distribution system, floor slab, and building enclosure. The model was utilized to determine effective and simple strategies for operating the radiant floor heating system. By using the logarithmic-mean-temperature-difference approach, significant reduction of the dynamic equations was achieved. Validation between experimental results and predictions from the model represented that the predictions were in agreement with the experimental data. Three control strategies such as a multistage control, an augmented constant gain control, and a variable gain control for improving the temperature regulation of the heating systems were proposed. The limitations of the dynamic model were that the heat transfer process of the floor slab was assumed as one-dimensional problem.

Saboksayr (1995) [24] developed a control strategy for a multi-zone space heating system including a boiler and associated distribution network. The control system was a multi-input multi-output system, which was consisted of five input signals and three output signals. An analytical method was presented, and robust controller and

decentralized control concept were addressed. Furthermore, three design methods, which were linear robust servomechanism design, decentralized controller design, and nonlinear decentralized servomechanism design, were provided. All of the three designed controllers yielded similar performance. The decentralized neural network controller was a nonlinear time varying and designed on minimizing decentralized cost function. The controller had good performance over a wide range of operation and gave better disturbance rejection compared to the existing controllers published before.

Zaheer-Uddin et al. (1993) [17] described a single zone space heating system by a seventh-order linear model. The heat generated in a hot water boiler was transferred to the zone air. The zone temperature was controlled by burner modulation and the hot water valve associated with the heating coil. Optimal P and PI controller were designed by using the reduced-order model of the heating system. The PI controller was used for simulation with the full-order model. The simulation results show good regulation of room temperature. In addition, a multi-input controller was designed by using a linear model of the heating system.

Chen (1997) [5] developed a complex building transfer process model for a floor heating system with a thermal network. The established thermal network was based on not only the physical similarity but also the principle of equivalence. Thermal mass was utilized in order to lower both peak loads and operating cost as well as to reduce room temperature swings by predictive control while utilizing solar gains to reduce energy consumption. A method was presented for the semi-symbolic network analysis of

buildings. The algorithm based on Cayley's expansion was then described to generate a symbolic transfer function. Application of the techniques to the floor heating system shows that significant operating cost savings might be achieved by predictive control when the heating system was properly designed and operated. The limitation of the model was that the internal loads were ignored.

Practical modeling and control design methods have been explored by Letherman (1981) [11]. The examples presented illustrated application to heating and cooling systems.

1.2.3 Optimization of hot water heating systems

The focus in this review is to examine the optimization techniques used in hot water heating systems. Most studies have used optimization method to determine optimal operating parameters by minimizing an objective function. Also, some studies have shown how to develop cost functions in different systems in order to attain optimal parameters.

Zheng (1997) [30] developed dynamic models and optimal control for a multi-zone HVAC system. The nonlinear dynamic models integrated the building loads and all the components of the multi-zone HVAC system. A methodology was developed for multiple stage dynamic optimal operation problems in order to determine the optimal set point profiles. The potential for energy savings was estimated by analyzing several simulations. A global optimal control methodology to handle multiple stage operation and multiple time scale processes was presented. The best solution that achieves an optimal balance

among zone load, operating schedules, energy storage, energy price, and the comfort requirement was determined.

Larsson and Mahgary (1977) [10] developed a general optimization model for a district heating system by minimizing a cost function. The model consisted of numerous sub-models so that the modular optimization was also possible. These sub-models were the electrical system optimization model, the turbine model, the heat transport system model, and the distribution and utilization model. Some preliminary results of the first runs were presented with the general optimization model, showing the influence of different parameters on the cost of heat delivery. One-way heat transport systems in connection with low-temperatures were also evaluated and compared to conventional solutions for high and low temperature techniques. The heat demand and supply and return water temperature of the local system were given as functions over a period of one year.

Kohoner (1984) [23] studied intermittent heating of public buildings both theoretically and experimentally. Thermal behaviors of building under intermittent heating operation were analyzed based on the heat balance method and simplified models. A practical realization of the optimal strategy for intermittent heating was to stop heating totally at the end of the occupied period and to use the maximum heat output of the heating system for preheating. The measured seasonal energy savings compared with the continuous heating were 20%~40% depending on the heating and ventilating system, the massiveness, and the heating control system of the buildings. Some recommendations

for the planning and application of intermittent heating systems were suggested. For a single building, intermittent heating control could be used based on weather conditions and internal loads, but for large district heating system, the approach is not practical.

House and Smith (1995) [9] described a system approach for optimal control of HVAC and building systems and presented optimal control responses that demonstrated the system approach for a large-scale system with multiple state and control variables. The methodology utilized a system approach to the optimal control problem, wherein the interactive nature of the HVAC components, the building system, and their associated variables was accounted for, and an optimal control solution was sought. Four cases were examined. The system-based optimal control approach resulted in energy savings of up to 24% in comparison to a conventional control strategy. Perhaps more important, the system-based optimal control approach had the capacity to accommodate a variety of system conditions, including time-varying loads and occupancy schedules, system constraints, and different set points in different zones, and, in so doing, minimized the operating cost for the system. However, the humidity effects, transient and spatial effects, and heat losses and gains were neglected in the governing equations.

Martin and Oughton (1995) [20] studied a heating system with optimum-start, plus a conventional heating controller. The optimum-start control served to delay the start time of a heating system until the latest possible time to give the shortest preheat period, normally at full output, which would achieve the desired conditions at the start of the occupancy period. The control system monitored the indoor and outdoor air temperature

and considered the thermal response of the building and the system. In addition to optimum-start control, the controller included thermostats to sense outdoor temperature and circulating water flow temperature. By means of a calibrating mechanism, the temperature of water leaving the three-way control valve was adjusted according to the outdoor temperature. The open-loop controller effectively reset the desired temperature set point depending on the outdoor conditions.

Zhang and Nelson (1992) [32] developed a numerical model to simulate a space controlled by a HVAC system. The effects of building system components, including envelope heat transmission, thermal mass of the building enclosure, non-temperature-related heat gains, cooling system capacity, and time delay of thermal effect, were examined. Furthermore, the influence of the control setup, such as the temperature proportional band, minimum throttling rate, PI control, and temperature set point, were studied. First-order linear dynamic model was used to develop a PI controller.

1.2.4 Smith Predictor control design

Smith Predictor (SP) is well known as an effective method in dealing with long time delay compensation. This technique uses a model-based approach. Although Smith [18] developed the concept first, it was not widely employed since the implementation of the controller was difficult. Because of the development of computer technology and hardware devices, the SP is used more and more these days, especially in industrial processes and chemical processes. Many studies described the principle of SP design. However, its applications in district heating systems have not been studied.

Liu, Ni, and Yang (1999) [13] developed an analytical model to design a SP based on loop shifting theory for handling large delay in industrial process control. First, the equivalent inner model control of a SP was derived. And then, its stability and performance were analyzed. Lastly, the analytical approach was used to design the SP. The controller could be equivalently transferred into a PID type controller, and the parameters were easily obtained. A first-order model with large delay was presented and simulated. Simulation results showed that the resulted controller was able to achieve good dynamic response as well as robust performance. The equivalent inner model design method was used when the plant process control had a stable transfer function.

Glickman, Kulessky, and Nudelman [27] developed a new method for a PID-control design in which the PID-control loop was represented as an equivalent one to a control loop operating with an optimized PI-controller and a SP in order to achieve optimal control with time-delay compensation. The method was based on the PID-controller transfer function identification, which approximately described dynamical properties of the optimal PI-controller with the SP. In the approach presented the PID controller was tuned as an equivalent PI-controller with an "ideal" SP; then, the PI-controller parameters were calculated as the optimal ones for a process described without the dead-time; finally, the algorithm in which the accurate descriptions of a process and a time-delay were used represented the "ideal" SP. The tuned of PID controller was implemented on a power plant process provided sufficiently good settings of the controller parameters and exemplified industrial application of the approach. On the other hand, the approach

required a close approximation of the process description and a dead-time transfer function.

Deshpande and Ash (1980) [22] presented a control algorithm and simulation of a SP to deal with long time delay process. The process was conceptually split into a pure lag and a pure dead time. A SP moved the dead time outside the control loop. Since there was no delay in the feedback signal, the response of the system was greatly improved. In addition, an example of applying the SP algorithm for automatic control of a distillation column was presented. The experimental responses of the system to a step change in set point and load were presented. These results clearly showed the superior performance of the SP algorithm compared with the digital PI controller without dead time compensation. This approach requires that the model parameters must be known to a high degree of accuracy in order to be assured of success.

Tzafestas and Pal (1991) [26] developed an approach for time delay compensation. The time delay was common in the process industries due to recycle loop, distance-velocity lags in fluid flow and the "dead time" inherent in many composition analysis. A block diagram of the discrete form of a SP with a zero order hold was shown. The feedback loop around the digital controller contained a block whose output represented the difference between two model outputs: the responses of a system without and with time delay. The process model was considered as a first-order model with time delay. The algorithm required a high accuracy of the model without time delay.

Draganović, Stojić, and Matijević (2001) [25] proposed a new SP for controlling a

process with an integrator and long dead times. The structure comprised the classical SP, in the main control loop, and the disturbance estimator, in the local minor loop. The methods based upon the use of M circle and pole placement procedure were applied for parameter setting according to the desired set point response and speed of disturbance rejection. All tuning parameters, the single parameter of main controller and parameters of disturbance estimator, had clear physical meanings. Several experimental results were present to illustrate the design procedure and to demonstrate the efficiency of the control structure in disturbance rejection. The modified SP was expressed by Laplace transfer function.

From the above, we can group the literature review into three themes: (i) design methods, (ii) dynamic models and optimization, and (iii) control design methods including those involving a Smith Predictor.

It is apparent that most studies on DHS are related to design using steady state methods. Dynamic models for control analysis and operation have not been adequately addressed. Furthermore, the issue of compensating the large transport delay in DHS has not been addressed.

To this end, the contributions of this thesis are described in the following.

1.3 Contributions and summary

The main contributions of the thesis are listed below:

(1) Steady state design models of the DHS are developed.

(2) Important parameters impacting heating system operation are determined.

(3) Full-order dynamic models are developed in order to analyze and simulate the responses of the DHS. The DDHS dynamic model includes 66 nodes and 44 dynamic equations, while the IDHS dynamic model includes 70 nodes and 59 dynamic equations.

(4) An optimization methodology is used to obtain optimal set points for energy efficient operation of the DHS.

(5) A reduced-order model is described and used for the design of a Smith Predictor in order to improve the system performance, especially disturbance rejection.

(6) A control strategy for energy-optimal operation of a typical DDHS is developed.

(7) Optimal set point algorithms are developed so as to reduce the fluctuation of indoor air temperature by internal loads.

The thesis, which includes six chapters, is organized as follows:

In Chapter 2, the steady state models of the DHS are designed. Related design parameters that will be used in the development of dynamic models are given. Also, simulations based on parameter changes are studied in order to find which parameters are most important affecting the heating system operation.

In Chapter 3, the dynamic models of the DHS are developed. Open loop tests are used to evaluate the dynamic models.

In Chapter 4, an optimization methodology is described for the DHS in order to attain optimal parameters that can be used as optimal set points for energy efficient

operation.

In Chapter 5, a Smith Predictor is designed to compensate the larger transport time delay. Several energy saving strategies are studied by considering combinations of optimal set points of supply water temperature and internal loads.

Finally, in Chapter 6, summary and the conclusions of the thesis together with suggestions for future work are given.

Chapter 2 System Design and Performance Evaluation

2.1 Introduction

Two types of the DHS, namely DDHS and IDHS, will be designed and their steady state performance will be studied in this chapter. First, the physical models of the DHS are described, and then the design procedures for design the two types of the DHS are introduced. After that, simple examples of design procedures for the DHS are shown. Finally, steady state performance is evaluated in order to identify the important parameters affecting the heating system operation. In addition, the detail data about the DHS design are given in Appendix.

2.2 Physical models of the DHS

2.2.1 Physical model of the DDHS

The schematic diagram of the DDHS is shown in Figure 2.1. The DDHS consists of a heat source, the distribution system, and user systems. The main components of the heat source include the boiler, circulating water pumps, and the makeup water system that maintains the constant pressure at the return water pressure set point. The distribution system has the supply water piping network and direct-return return water piping network. User systems include terminal heaters and indoor piping network. The circulating water brings the heat generated by the boiler and passes through the supply water piping network to each user, and then goes back to the boiler by means of return

water piping network. The circulating pumps are utilized to operate the loop continuously.

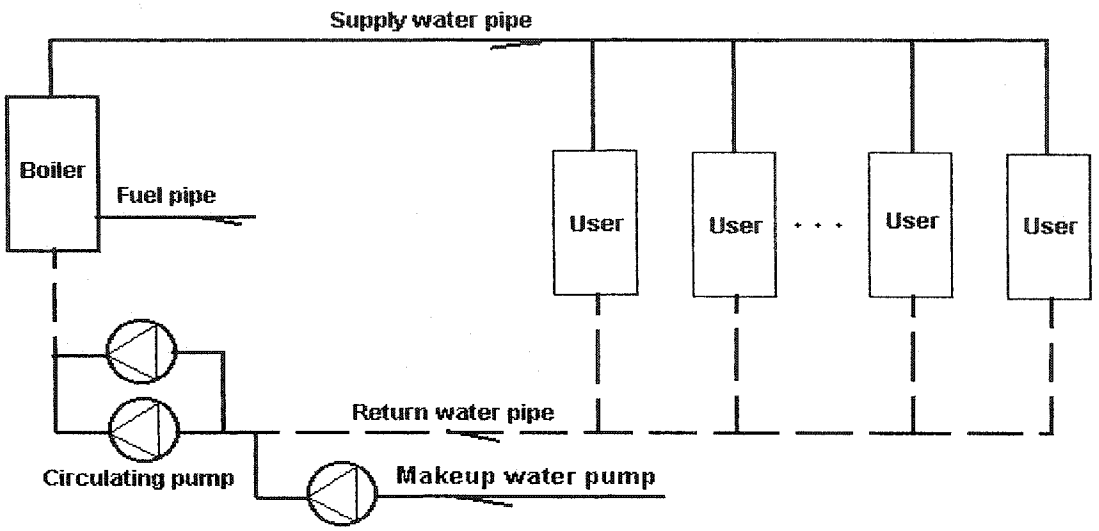

Figure 2.1 Schematic diagram of the DDHS

The typical layout of the DDHS is presented in Figure 2.2. The designed heating system has 30 buildings with total heated floor area 100137m^2 and total design heating load of 6.23Mw. The heated floor area of the two types of buildings namely commercial and residential buildings, are 27326m^2 and 72811m^2 respectively. The elevation of the buildings (sea level) ranges from 32.25m to 35.23m. The height of the buildings ranges from 1-floor to 7-floors. In addition, the distribution system has three branches such as B-B4, C-C6, and C-D-D2. The outdoor piping network is 5146m in length, and the nominal dimension of the outdoor distribution system ranges from 50mm to 250mm. The velocity of the piping network is under 1.4m/s. The heat capacity of the boiler is 7Mw, and it has two circulating water pumps. One of the pumps is operated normally; the other is a standby pump. The design circulating water flow rate is 214.29t/h. The nominal water

flow rate, pressure head, shaft work, and efficiency of each circulating pump are 200t/h, 50m (H_2O column), 36.3kw, and 75% respectively.

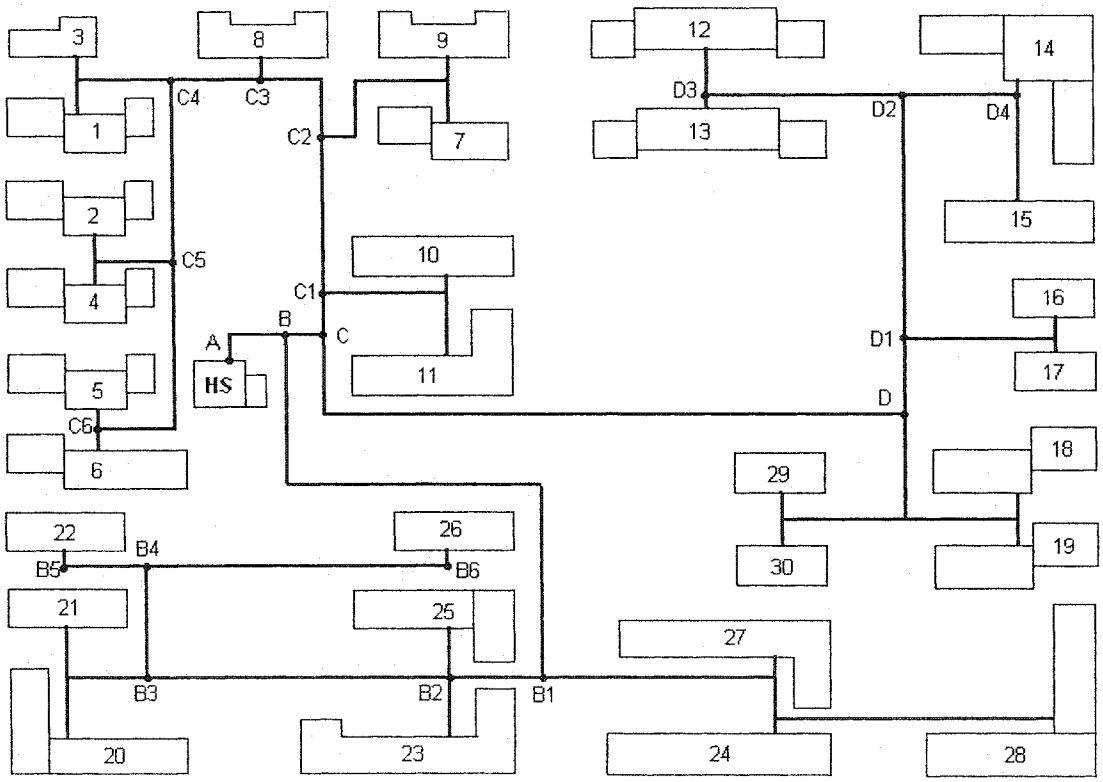

Figure 2.2 Layout of the DDHS

The symbols in Figure 2.2 are explained below.

15: building number. For instance, it expresses the 15th building in the DDHS.

B, D3: nodes of piping network. For instance, "B" indicates the intersection of pipe segment AB and BB1 in the DDHS, and D3 indicates the end of piping line D2D3.

HS: position of the heat source in the DDHS.

Moreover, the configuration of each user system (each building) is depicted in Figure 2.3. There is a self-action ΔP control valve in the entrance of each building. In each indoor heating system, the hot water is supplied from upper supply water pipe

segment to each terminal heater. The amount of heat released to indoor air is controlled by thermostat. And then, water returns back to the boiler.

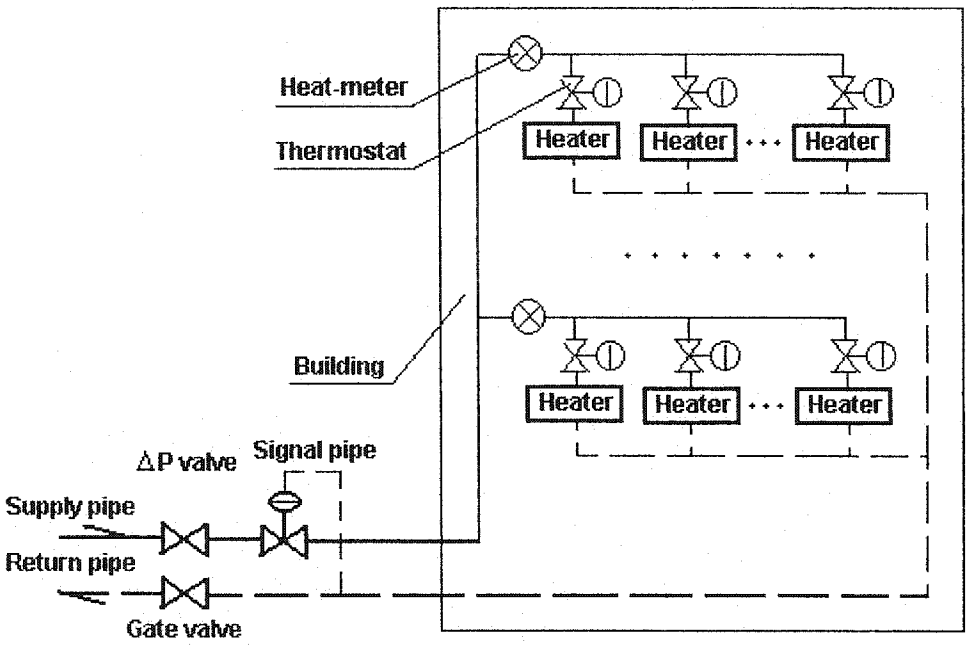

Figure 2.3 Configuration of the user system

2.2.2 Physical model of the IDHS

The typical schematic diagram of the IDHS is presented in Figure 2.4. It includes the heat source, the distribution system, heat exchange stations, and terminal systems. It can be seen from the figure that the distribution system is divided into two sections, which are called the primary system and the secondary system. The major purpose of the primary system is to generate the required heat and transport it to the secondary system. The main purpose of the secondary system is to distribute the heat to each terminal heater. The heat exchanger separates the two closed subsystems in the IDHS. The purpose of heat exchange stations is to transfer heat from primary side to secondary side. An IDHS can have many secondary systems based on the conditions of the whole district heating

system although only one is shown in Figure 2.4. In some large IDHSs, for example, more than 100 heat exchange stations are employed.

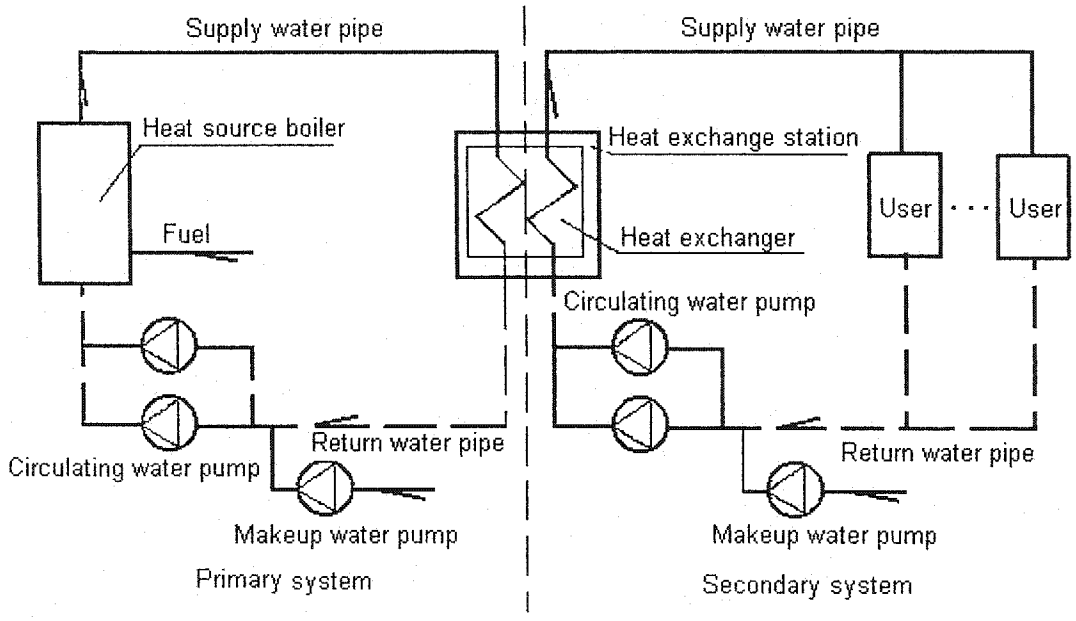

Figure 2.4 Schematic diagram of an IDHS

The typical layout of the IDHS is presented in Figure 2.5. The designed heating system includes 10 heat exchange stations with the total heated floor area of 851031m^2 and total design heating load of 51.47Mw. The heated floor areas of the heat exchange stations vary from 25641m^2 to 250495m^2. In addition, the primary distribution system has two branches named as B-H-I and B-D-G. The length of outdoor piping network is 12040m, and the nominal diameter of the outdoor distribution pipe range between 200mm to 500mm. The heat capacity of the boiler is 58Mw. The design circulating water flow rate is 885t/h. The nominal water flow rate, pressure head, horsepower, and efficiency of each circulating pump are 1260t/h, 75m (H_2O column), 314kw, and 82% respectively.

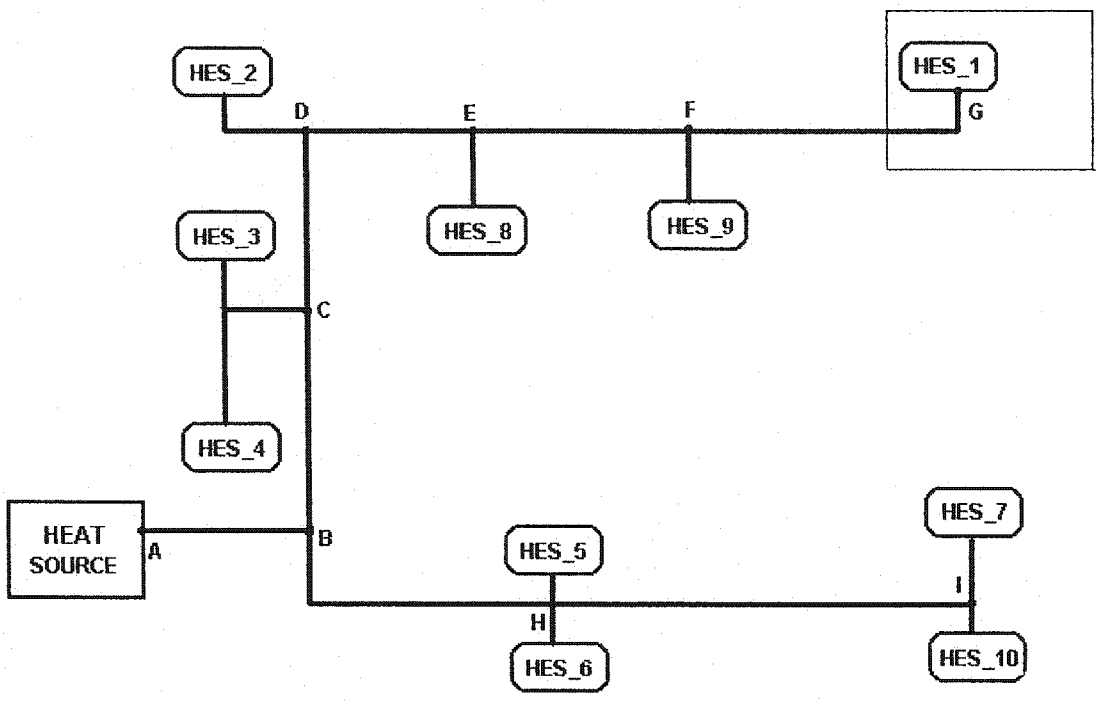

Figure 2.5 Layout of the IDHS

In Figure 2.5 HES_i expresses the i^{th} heat exchange station and letter B denotes the nodal designation.

2.3 DHS design procedure

2.3.1 Design heating load

For a DHS design, several factors have to be considered properly. For example, the heating load of each building should be estimated as accurately as possible. However, since some parameters in buildings vary with time and usage patterns, actual measured heating load data is often utilized as the design heating load instead of original designed heating load. The measured heating load data as a function of design conditions is presented in Figure 2.6 for two types of buildings: commercial and residential buildings.

These are assumed load profiles based on operating experience. In addition, for pipe sizing, water velocity is limited to 1.4m/s [1, 4, 8, 15, 16, 19]. Furthermore, the heat source and heat exchanger design are based on methods given in references [14, 15].

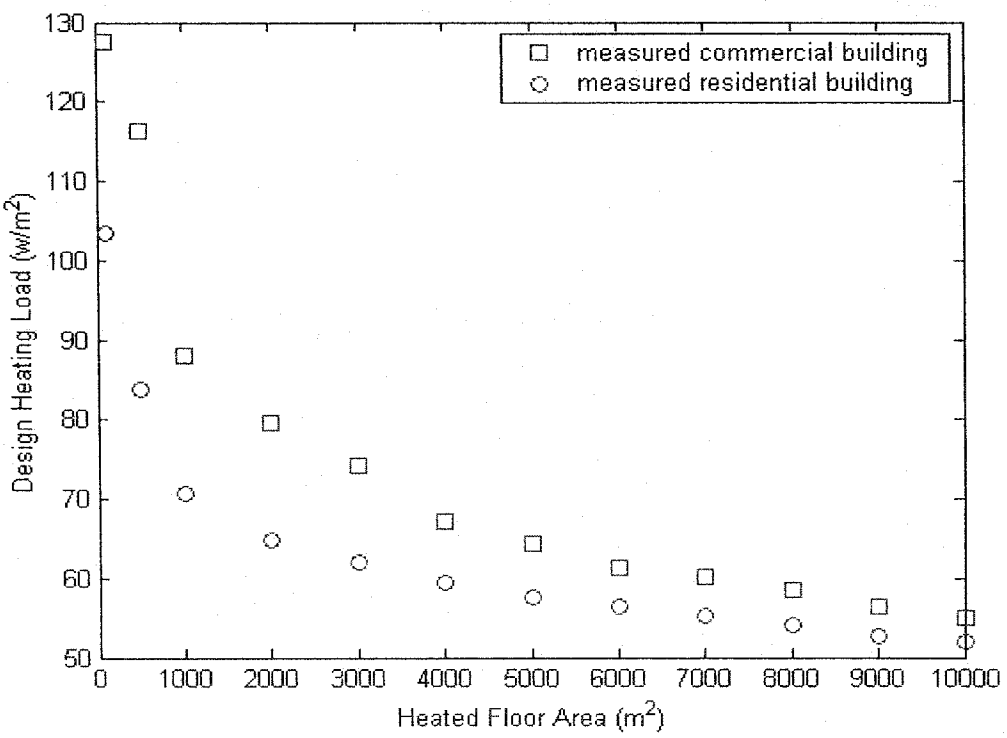

Figure 2.6 Actual design heating load curves in the DHS

Moreover, some design parameters have to be assumed in order to design the entire DHS. These are given in Table 2.1. The values are based on experience and local design guidelines.

Table 2.1 Design parameters of the DHS

Symbol	Item	Unit	Data
T_{bd}	Design supply water temperature of primary system	°C	130
T_{re1d}	Design return water temperature of primary system	°C	80
T_{hd}	Design supply water temperature of secondary system	°C	95
T_{re2d}	Design return water temperature of secondary system	°C	70
T_{sw}	Makeup water temperature of primary system	°C	60
T_{sw2}	Makeup water temperature of secondary system	°C	5
T_{zd}	Design indoor air temperature	°C	18
T_{od}	Design outdoor air temperature	°C	-11
hv	Heat value of the fuel ($6^{\#}$ heavy oil)	MJ/kg	43.35
T_{soil}	Under ground soil temperature 1 m in depth	°C	5
D_p	Days of heating season	Day	137
c_w	Specific heat capacity of water	J/kg°C	4180
d_w	Water density	kg/m^3	975
c_z	Specific heat capacity of air	J/kg°C	1000
d_z	Air density	kg/m^3	1.2

2.3.2 Design procedure of the DDHS

The design approach of the DDHS is described as follows:

(1) Select a layout of the piping system

To determine the layout of the piping system, several factors should be taken into account. First of all, the existing buildings and the buildings that will be built in the future have to be considered. Second, the shortest path layout of the piping system that can be connected to each building should be chosen, and the boiler has to be located as centrally as possible in order to save the first cost as well as to balance circulating water flow resistance easily. After that, the piping system should pass through a region that has a smooth ground soil, lower underground water level, and better soil quality. Then, the piping system should be installed along roads rather than passing through major street frequently. Moreover, appropriate distance among the heating system pipes and other public piping systems should be maintained. Lastly, the heating load in each branch of

the distribution system should be closed so as to balance the flow resistance. Following these principles, the layout of the DDHS presented in Figure 2.2 was chosen.

(2) Estimation of design heating load q_{di} for each building

Design heating load can be estimated by two methodologies. One is the steady state method; the other is called floor area based method.

Steady state method:

$$q_{di} = \sum_{i=1}^{N_b} [(U_{ij} A_{ij} + \frac{c_z d_z ACH_{ij} V_{ij}}{3600})(T_{zdij} - T_{od})] \tag{2.1}$$

Floor area based method:

When a heated floor area of a building is known, the heating load per m^2 can be interpolated by selecting two neighborhood points (A_1, A_2) from Figure 2.6 as follows

$$q_{di} = [\bar{q}_{d1} + \frac{\bar{q}_{d2} - \bar{q}_{d1}}{A_2 - A_1}(A_i - A_1)]A_i \tag{2.2}$$

Note that, for accuracy, the measured data shown in Figure 2.6 is used to calculate the design heating load depending on different types of buildings.

(3) Estimation of design circulating water flow rate G_{di} for each building is calculated from

$$G_{di} = \frac{q_{di}}{c_w (T_{hd} - T_{re2d})} \tag{2.3}$$

(4) The circulating flow rate G_{ci} for each building is estimated from

$$G_{ci} = f_g G_{di} \tag{2.4}$$

Note that the safety factor f_g is selected based on the heat losses caused by pipe insulation and water leakage, and it ranges from 1.07 to 1.25.

(5) Pipe sizing

(a) Calculation of circulated water flow rate G_{ck} in each pipe segment is given by

$$G_{ck} = \sum_{k=1}^{N_{pk}} (G_{ci}) \tag{2.5}$$

(b) Determination of the range of water velocity V_e in the outside pipe system

Depending on economic and technological comparison and local design standard, the water velocity should be limited from 0.5m/s to 1.5m/s.

(c) Determination of pipe dimension d_k in each pipe segment

First, water velocity is assumed to be within the selected range. Then, pipe dimension is computed from

$$d_k = 1.128\sqrt{\frac{G_{ck}}{d_w V_e}} \tag{2.6}$$

and adjusted to nominal pipe dimension.

(d) Determination of friction rate R_{rk} in each pipe segment

When nominal pipe dimension $d_k \geq 0.04$m and water velocity ≥ 0.5m/s, the friction factor λ_k and friction rate R_{rk} can be calculated from [16]

$$\lambda_k = 0.11\left(\frac{K_a}{d_{\text{int}\,k}}\right)^{0.25} \tag{2.7}$$

$$R_{rk} = 0.626\frac{\lambda_k G_{ck}^{\ 2}}{d_w d_{\text{int}\,k}^{\ 5} g} \tag{2.8}$$

In addition, both economic analysis and experience show that friction rate in main pipe should be limited from 30Pa/m to 100Pa/m; while in branches it should be range from 60Pa/m to 250Pa/m in outside piping systems.

(e) The friction resistance R_k in each pipe segment is determined from

$$R_k = L_k(1+\beta_k)R_{rk} \tag{2.9}$$

Equivalent length factor β_k is a function of pipe dimension as shown in Figure 2.7. Table 2.2 shows nominal diameters and wall thickness of commercially available pipes.

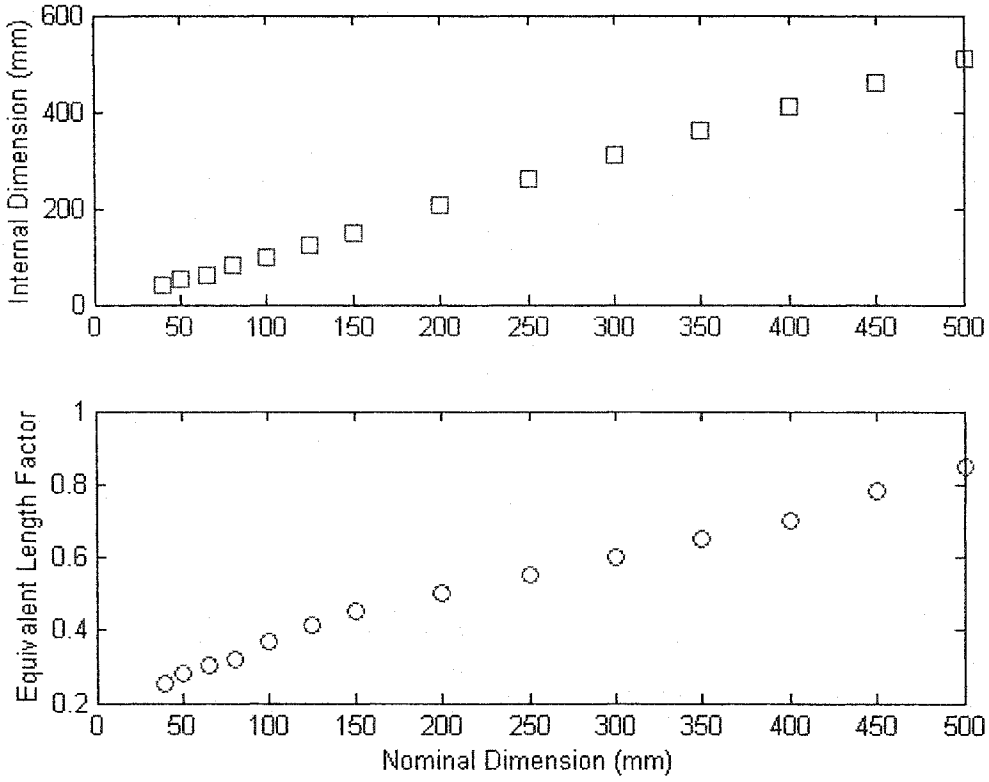

Figure 2.7 Equivalent length factors of local friction resistance and internal dimension

Table 2.2 Relationship between internal dimension and nominal dimension (mm)

External dimension x thickness	45x3	57x3	76x3.5	89x3.5	108x4	133x4	159x4.5
Nominal dimension	40	50	65	80	100	125	150
Internal dimension	39	50	65	80	100	125	150
External dimension x thickness	219x6	273x7	325x7	377x8	426x8	477x8	529x9
Nominal dimension	200	250	300	350	400	450	500
Internal dimension	207	259	311	361	410	461	511

(6) Selection of circulating pump

Estimation of circulating water flow rate G_t and pressure head ΔP is given by

$$G_t = f_f \sum G_{ci} \tag{2.10}$$

$$\Delta P = f_r (\sum_{m=1}^{N_l} R_m)_{\max} \tag{2.11}$$

Note that safety factor of water flow rate f_f ranges from 1.05 to 1.15, and safety factor of water friction resistance f_r ranges from 1.1 to 1.2.

In addition, for each loop, both friction resistance of pipes and the equipment that includes the boiler, the filter, throttling devices, and the terminal heater resistance have to be considered. The pump selection is not only related to the circulating flow rate and its friction resistance but also related to its efficiency e_p. In the other words, the efficiency of the selected pump should be as high as possible.

By comparing several characteristic figures of pumps, the circulating pump is selected, and it has to satisfy all the requirement of G_t, ΔP, and e_p.

(7) Balancing of water flow

The balancing requirement is that the water resistance difference between the largest resistance loop and other loops should be less than 10%. Otherwise, either adjusting the pipe dimension again or the use of throttling device has to be considered.

(8) Selection of the boiler

Estimation of the design heating load of the boiler is made using the following:

$$Q = f_g \sum_{i=1}^{N_b} q_{di} \tag{2.12}$$

When the design heating load of the boiler is calculated, this value sometimes should be adjusted according to available capacity of the existing boiler series.

In addition to the consideration of the heating load of the boiler, other factors related to the boiler selection such as water circulating resistance, working pressure, efficiency, type of fuel, and characteristics of heating load should be considered in order to choose the suitable boiler.

(9) Selection of makeup water system

The makeup water flow rate G_{sw} is estimated from

$$G_{sw} = f_{sw2} G_t \tag{2.13}$$

The makeup water pressure set point P_{sp} is given by

$$P_{sp} = f_{sp} P_m \text{, valid between limits } P_{\min} f_{sp\min} \le P_{sp} \le \frac{P_{\max}}{f_{sp\min}}. \tag{2.14}$$

Makeup water rate f_{sw2} ranges from 1% to 3% of design circulating water flow rate, while safety factor of makeup water pressure set point f_{sp} ranges from 1.05 to 1.2.

Makeup water pressure, minimum makeup water pressure, and maximum makeup water pressure should be computed based on several situations such as elevation of buildings, circulating resistance of pipe and equipment, exact point of makeup water into the circulating system, operating and adjusting methods, vaporizing pressure, highest permitted pressure of terminal heaters, the highest point of the whole system, and the lowest permitted inlet pressure of circulating pumps.

Note that the makeup water pump has to be selected based on: the normal makeup water flow and the accident makeup water flow. As a result, two same sizes of pumps are chosen generally. One is operated as running pump, while the other is held in standby mode.

(10) Other considerations

Although the main design procedures related to the thesis are presented above, other processes that are not mentioned here are also essential for designing complete direct heating systems. Those parts include calculation of heat compensation system, selection of adjusting valves, selection of fans, water treatment system, ventilation of pipe system, discharge water system, and so forth.

2.3.3 DDHS design example

A simple example showing the DDHS design procedure is presented. At the beginning, heating loads and circulating flow rates are calculated for a branch in detail. Then, circulating water resistance in the branch is computed. Moreover, main equipment

such as the circulating pump and the boiler is selected. Finally, the makeup water system is chosen for the DDHS.

(1) Layout of the piping system

Based on the principles mentioned before, the layout of the DDHS piping system is shown in Figure 2.2. Calculations are shown for the branch D-D4.

(2) Estimation of design heating load for buildings 12~19, 29, and 30

The heated floor area of the building 12 is 5632m^2. The floor areas and heating load standard of the two point 1 and 2 are: A_1=5000m^2, $\bar{q}_{d1} = 57.5w/m^2$, A_2=6000m^2, and $\bar{q}_{d2} = 56.25w/m^2$. Therefore, the design heating load of building 12:

$$q_{d12} = [\bar{q}_{d1} + \frac{\bar{q}_{d2} - \bar{q}_{d1}}{A_2 - A_1}(A_{12} - A_1)]A_{12} = [57.5 + \frac{56.25 - 57.5}{6000 - 5000}(5632 - 5000)]5632 = 319390w$$

By using the same principle, the heating loads of q_{d13}, q_{d14}, q_{d15}, q_{d16}, q_{d17}, q_{d18}, q_{d19}, q_{d29}, and q_{d30} are 318768, 256696, 79621, 84931, 84931, 151812, 151812, 84390, and 84390w respectively.

(3) Estimation of design circulating water flow rate G_{di}

For building 12, the design circulating water flow rate G_{d12} is

$$G_{d12} = \frac{q_{d12}}{c_w(T_{hd} - T_{re2d})} = \frac{319390}{4180(95 - 70)} = 3.056kg/s = 11t/h.$$

Also, others circulating flow rates of buildings in this branch are computed as G_{d13}=10.97, G_{d14}=8.84, G_{d15}=2.74, G_{d16}=G_{d17}=2.92, G_{d18}=G_{d19}=5.23, and G_{d29}=G_{d30}=2.9t/h.

(4) Estimation of calculated circulating flow rate G_{ci}

With a safety factor f_g of 1.1, the calculated circulating flow rate of building 12 is $G_{c12} = 12.1t/h$.

In addition, other water flow rates are G_{c13}=12.07, G_{c14}=9.72, G_{c15}=3.01, G_{c16}=G_{c17}=3.21, G_{c18}=G_{c19}=5.75, and G_{c29}=G_{c30}=3.19t/h.

(5) Pipe sizing of the branch D-D4

(a) Calculation of circulating water flow rate G_{ck}

Circulating water flow rate G_{cD2D3}:

$$G_{cD2D3} = \sum_{k=1}^{2}(G_{ci}) = G_{c12} + G_{c13} = 12.1 + 12.07 = 24.17t/h.$$

Similarly, G_{cD2D4}=12.73, G_{cD1D2}=36.9, and G_{cDD1}=43.32t/h.

(b) Determination of the range of water flow velocity

The water velocity in the branch D-D2-D3-D4 is assumed to be 1m/s.

(c) Determination of pipe dimension d_k

Dimension of pipe D2D3:

$$d_{D2D3} = 1.128\sqrt{\frac{G_{cD2D3}}{d_w V_e}} = 1.128\sqrt{\frac{24.17\dfrac{1000}{3600}}{1000\times 1}} = 0.09m$$

Then, the calculated dimension is adjusted to nominal pipe dimension equal to 100mm. Likewise, d_{D2D4}=65, d_{D1D2}=125, and d_{DD1}=125mm.

(d) Determination of friction rate R_{rk}

The absolute roughness of all outside pipe system is assumed as 0.0005m. Since the internal dimension of pipe is $d_{intD2D3}$=0.1m, the friction factor in D2D3 is:

$$\lambda_{D2D3} = 0.11(\frac{K_a}{d_{\text{int } D2D3}})^{0.25} = 0.11(\frac{0.0005}{0.1})^{0.25} = 0.0293$$

The fiction rate in pipe D2D3 is:

$R_{rD2D3} = 0.626\frac{\lambda_{D2D3} G_{cD2D3}^{\ 2}}{d_w d_{\text{int } D2D3}^{\ 5} g} = 0.626\frac{0.0293\times 24.17^2}{975\times 0.1^5 \times 9.81} = 112 Pa/m$. In a similar manner, we have R_{rD2D4}=240.3, R_{rD1D2}=83.2, and R_{rDD1}=112.3Pa/m.

(e) Determination of friction resistance R_k

Friction resistance R_{D2D3} can be calculated as follows

$R_{D2D3} = L_{D2D3}(1+\beta_{D2D3})R_{rD2D3} = 63(1+0.37)\times 112 = 9.7 KPa$. Other values are R_{D2D4}=25, R_{D1D2}=14.1, and R_{DD1}=9KPa.

(6) Selection of circulating pump

With a safety factor f_f of 1.1, the circulating flow rate of the pump is

$G_t = f_f \sum G_{ci} = (1.05 \sim 1.15)(214.29) = 1.1\times 214.29 = 236 t/h$.

Moreover, the loop that has the largest resistance is A-B-B4-B5, and the highest value is 108.8KPa per single pipe. Therefore, with f_r equal to 1.1, the pressure head ΔP can be calculated as follows

the resistance of the outside pipe network: 108.8x2=217.6KPa;

the assumed resistance in the indoor circulating system: 50KPa;

the assumed resistance of the filter: 30KPa;

the boiler resistance: $120(\frac{236}{250})^2 = 106.9 KPa$. The nominal resistance and circulating flow rate are 120KPa and 250t/h.

$$\Delta P = f_r(\sum_{m=1}^{N_l} R_m)_{\max} = 1.1(217.6+106.9+50+30) = 445KPa = 44.5m \text{ } (H_2O \text{ column})$$

Based on the circulating flow rate and pressure head, the pump that has highest efficiency is selected. The nominal parameters of circulating flow rate, pressure head, efficiency, and shaft work of the pump are 200t/h, 50m(H_2O column), 75%, and 36.3Kw respectively.

(7) Balancing of circulating system resistance

The largest resistance loop is A-B-B5, which has the flow resistance of 108.8KPa per single pipe. Also, in branches A-B-C-C6 and A-B-C-D-D4, the resistances are 108.3KPa and 105KPa respectively. Consequently, the difference in resistances is 0.5% and 3.5%.

(8) Selection of the boiler

When the factor f_g is assumed as 1.1, the calculated heating load of the boiler is

$$Q = f_g \sum_{i=1}^{N_b} q_{di} = 1.1 \times 6.23 = 6.85Mw.$$

Hence, an oil-fired boiler with nominal heat capacity 7Mw is suitable for the DDHS.

(9) Selection of makeup water system

The makeup water flow rate is computed below

$$G_{sw} = f_{sw2} G_t = 3\% \times 214.29 = 6.4t/h.$$

By means of analyzing the whole pressure conditions of the heating system, the maximum makeup water pressure and the minimum makeup water pressure are 290KPa

and 180KPa respectively. As a result, the pressure set point can be chosen as P_m=220KPa, and the makeup water pressure set point P_{sp} satisfying the constraints, is

$$P_{sp} = f_{sp} P_m = 1.1 \times 220 = 240 KPa$$

Therefore, the nominal parameters of the makeup water pump are: water flow rate=12.5t/h, pressure head=200KPa, and shaft work=1.13Kw.

2.3.4 Design procedure of the IDHS

The design procedure of the IDHS is similar to the design approach of the DDHS. However, there are two major differences between the design procedures. One of them is the selection of plate heat exchanger. First, total calculated heating load of each heat exchange station is estimated based on calculated heating load of each building in the station. Then, Logarithmic Mean Temperature Difference (LMTD) of the heat exchanger is computed. Lastly, area of the heat exchanger is obtained by considering a fouling factor.

Selection of heat exchanger in each heat exchange station

Calculation of LMTD:

$$LMTD = \frac{T_{bd} - T_{hd} - T_{re1d} + T_{re2d}}{\ln(\frac{T_{bd} - T_{hd}}{T_{re1d} - T_{re2d}})} \tag{2.15}$$

Estimation of transfer area of each heat exchanger A_j for j^{th} heat exchange station:

$$A_j = \frac{f_g(\sum_{i=1}^{N_b} q_{dij})}{nKf_{foul} LMTD} \tag{2.16}$$

Note that, for plate heat exchanger, the value K ranges from 2500 to 4500w/m^2°C, and for design case, f_{foul} can be assumed as 0.8.

The other difference is concerned about makeup water system. Two kinds of makeup water systems should be considered: the primary makeup water system and secondary makeup water system. Makeup water system in secondary pipe should be designed for each secondary system, which is similar as the design procedure mentioned before. The primary makeup water system is chosen according to considering the vapor pressure of the highest supply water temperature and permissible inlet pressure of the circulating water pump. Moreover, note that the water circulating resistance of the heat exchanger should be added in the pressure loss calculations.

2.3.5 Example of designing the IDHS

Due to the fact that the design procedure for the IDHS is similar to it for the DDHS, only the selection of heat exchanger is shown here.

Calculation of the LMTD:

$$LMTD = \frac{T_{bd} - T_{hd} - T_{re1d} + T_{re2d}}{\ln(\frac{T_{bd} - T_{hd}}{T_{re1d} - T_{re2d}})} = \frac{130 - 80 - 95 + 70}{\ln(\frac{130 - 80}{95 - 70})} = 19.96°C$$

Estimation of transfer area of the heat exchanger in HES_1:

When the factor f_g and the conductance K of the plate heat exchanger are assumed as 1.1 and 3000w/m^2°C, the transfer area of each of the two exchangers is:

$$A_1 = \frac{f_g(\sum_{i=1}^{N_b} q_{di1})}{nKf_{foul}LMTD} = \frac{1.1(6.23\times10^6)}{2\times3000\times0.8\times19.96} = 67.4m^2$$

Finally, adjusting the heat transfer area to standard series, the heat transfer area of each heat exchanger is 80m^2 respectively.

2.3.6 Some useful design parameters

Some important design parameters of DHS are listed in Tables 2.3 and 2.4.

Table 2.3 Design parameters of the DDHS

Symbol	Item	Unit	Data
A_{zi}	Heated floor area	m^2	100137
q_{zdi}	Heating load	Mw	6.23
G_{2d}	Design circulating water flow rate	t/h	214
V_b	Water capacity of the boiler	m^3	6.5
V_p	Water capacity of external piping network	m^3	36.7
V_u	Water capacity of user side	m^3	102.1
f_{sw2}	Ratio of makeup water	%	1
e_{bmax}	Maximum efficiency of the boiler	%	91.2
e_2	Piping network efficiency	%	91.74
U_t	Conductance of the envelope	w/°C	214670
af	Conductivity multiplying heat transfer area of terminal heaters	w/°C	27571

Table 2.4 Design parameters of the IDHS

Symbol	Item	Unit	Data		
			A_z (m^2)	q_{zd} (Mw)	G_{1d} (t/h)
A_{z1}, q_{zd1}, G_{1d1}	Heated floor area, heating load, and circulating water flow rate of HES_1		100137	6.23	107
A_{z2}, q_{zd2}, G_{1d2}	Heated floor area, heating load, and circulating water flow rate of HES_2		250495	14.76	254
A_{z3}, q_{zd3}, G_{1d3}	Heated floor area, heating load, and circulating water flow rate of HES_3		35485	2.16	37
A_{z4}, q_{zd4}, G_{1d4}	Heated floor area, heating load, and circulating water flow rate of HES_4		110361	6.70	115
A_{z5}, q_{zd15}, G_{1d5}	Heated floor area, heating load, and circulating water flow rate of HES_5		53682	3.28	56
A_{z6}, q_{zd6}, G_{1d6}	Heated floor area, heating load, and circulating water flow rate of HES_6		95232	5.91	102
A_{z7}, q_{zd7}, G_{1d7}	Heated floor area, heating load, and circulating water flow rate of HES_7		73528	4.45	77
A_{z8}, q_{zd8}, G_{1d8}	Heated floor area, heating load, and circulating water flow rate of HES_8		25641	1.57	27
A_{z9}, q_{zd9}, G_{1d9}	Heated floor area, heating load, and circulating water flow rate of HES_9		55417	3.37	58
A_{z10}, q_{zd10}, G_{1d10}	Heated floor area, heating load, and circulating water flow rate of HES_10		51053	3.05	52
A_z, q_{zd}, G_{1d}	Total heated floor area, heating load, and circulating water flow rate of the IDHS		851031	51.47	885
h_w	Convection heat transfer coefficient of water inside pipe	$w/m^{2\circ}C$	350		
k_{ins}	Thermal conductivity of pipe insulation	$w/m^{\circ}C$	0.03		
$LMTD_{exd}$	Design logarithmic mean temperature difference	$^{\circ}C$	19.96		
V_b	Water content of the heat source boiler	m^3	42		
V_{op}	Total water content of external piping network	m^3	669		
V_{ex1}	Total water content of the exchanger in primary side	m^3	20		
V_{ex2}	Total water content of the exchanger in secondary side	m^3	40		
f_{sw}	Ratio of makeup water in the IDHS	%	0.3		
e_{bmax}	Maximum efficient of heat source boiler	%	91.3		
e_1	Efficiency of the piping network	%	97.51		

2.4 Aggregate steady state performance evaluation

Under design conditions the supply and return water temperature in secondary system are 95°C and 70°C respectively and in primary system they are 130°C and 80°C at design outdoor air temperature of -11°C. When the heating system operates at off-design conditions, the operating parameters such as supply water temperature return water temperature, and indoor air temperature change based on weather conditions. To study the impact under off-design conditions, aggregate steady state models of the DHS are required. Also, the aggregate steady state models can be used to determine which parameters are more important in the system operation and to evaluate the performance of the system under parameter changes.

2.4.1 Measured weather data

Real weather data obtained from a climate measuring station is used for analysis and simulation. The weather station is located at latitude 38.7N and longitude 121.9E. The measured data is from November 15th, 2000 to March 31st, 2001 for a total of 137 days with 1-hour time interval. The measured outdoor air temperature data is used not only in the steady state tests but also in the dynamic simulations.

2.4.2 Aggregate model and steady state performance of the DDHS

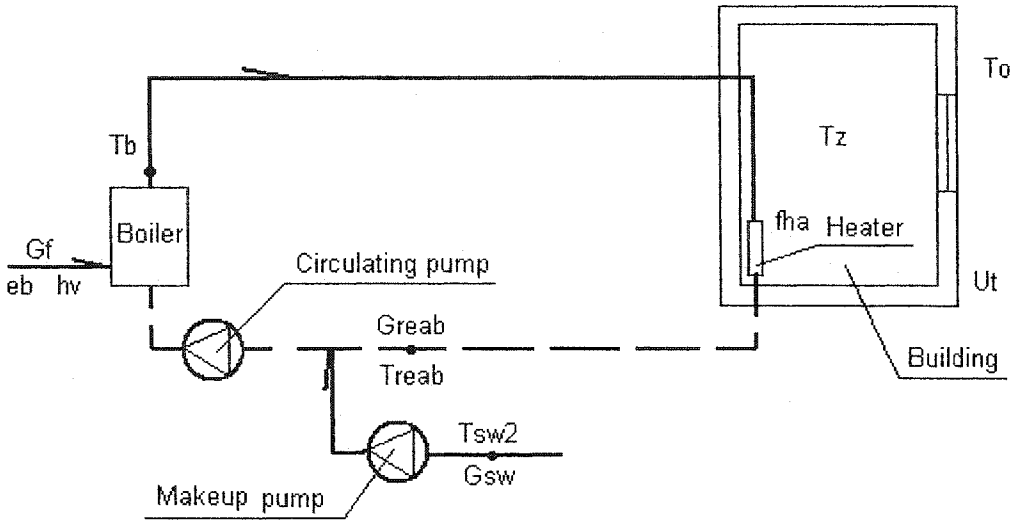

Figure 2.8 Simplified schematic diagram of DDHS

In order to assess the steady state performance of DDHS, aggregate energy balance equations consisting of important parameters of DDHS as shown in Figure 2.8 are written. For the DDHS the aggregate model equations are

$$G_f e_b hv = c_w G_{reab}(T_b - T_{reab}) + c_w G_{sw}(T_b - T_{sw2}) \tag{2.17}$$

$$c_w G_{reab}(T_b - T_{reab}) e_2 = f_{ha} a f_1 (0.5T_b + 0.5T_{reab} - T_z)^{1+bh} \tag{2.18}$$

$$f_{ha} a f_1 (0.5T_b + 0.5T_{reab} - T_z)^{1+bh} = U_t (T_z - T_o) \tag{2.19}$$

The equations above describe the interaction of energy from the boiler to the terminal heater. For example, in Equation (2.17), net heat input from the fuel is utilized to heat return water and makeup water. In Equation (2.18), heat losses from piping network and water leakage are taken into account by introducing an effectiveness factor e_2. In Equation (2.19), the heat transferred by terminal heaters is used to heat indoor air temperature. From these equations, the supply and return water temperatures and mass

flow rate can be determined. These are

$$T_b = T_z + [\frac{U_t(T_z - T_o)}{f_{ha} a f_1}]^{\frac{1}{1+bh}} + \frac{U_t(T_z - T_o)}{2e_2 c_w G_{reab}} \tag{2.20}$$

$$T_{reab} = T_z + [\frac{U_t(T_z - T_o)}{f_{ha} a f_1}]^{\frac{1}{1+bh}} - \frac{U_t(T_z - T_o)}{2e_2 c_w G_{reab}} \tag{2.21}$$

$$G_f = \frac{c_w[(G_{reab} + G_{sw})T_b - G_{reab}T_{reab} - G_{sw}T_{sw2}]}{e_b hv} \tag{2.22}$$

The relationships among the parameters, design condition, and actual operations were studied by carrying out simulations. The simulation results are depicted from Figures 2.9 to 2.13.

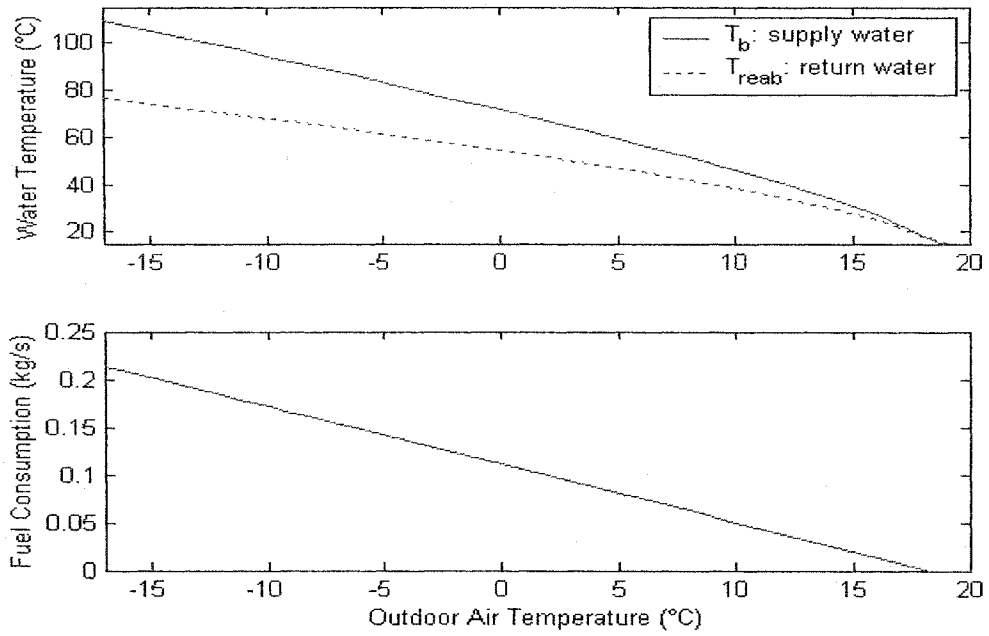

Figure 2.9 Design operation curves of the DDHS

From Figure 2.9, it is noted when outdoor temperature reaches design outdoor air temperature, the supply, return water temperature, and fuel consumption were 96.31℃, 68.96℃, and 0.177kg/s respectively. On the other hand, when outdoor air temperature

T_o=5℃, which means at the beginning of the heating season normally, the supply, return water temperature, and fuel consumption were 59.02℃, 46.68℃ and 0.08kg/s. In addition, the relationship between supply water temperature and outdoor air temperature is approximately linear. Note that the supply water temperature is greater than 95℃ at design outdoor air temperature because of the heat losses other than space heating load.

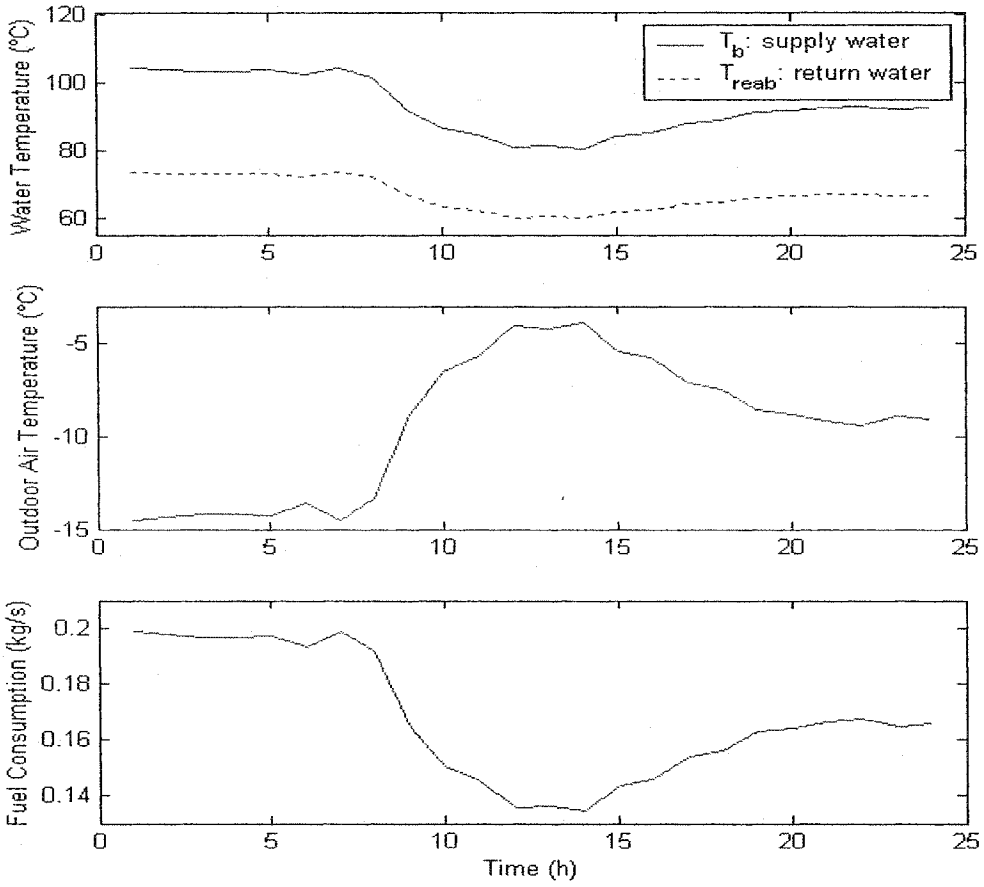

Figure 2.10 Actual operation curves of the DDHS

Off-design operation results are presented in Figure 2.10. When outdoor air temperature increases, the supply, return water temperature, and fuel consumption of the boiler decrease as shown in the figure. Note that the supply water temperature is above

95°C between 1:00 to 8:00 hours. It means that the supply water temperature has already exceeded the maximum temperature limitation of the boiler, and it should not be above this point. In this case the design zone air temperature must be decreased to bring the supply water temperature within prescribed limits.

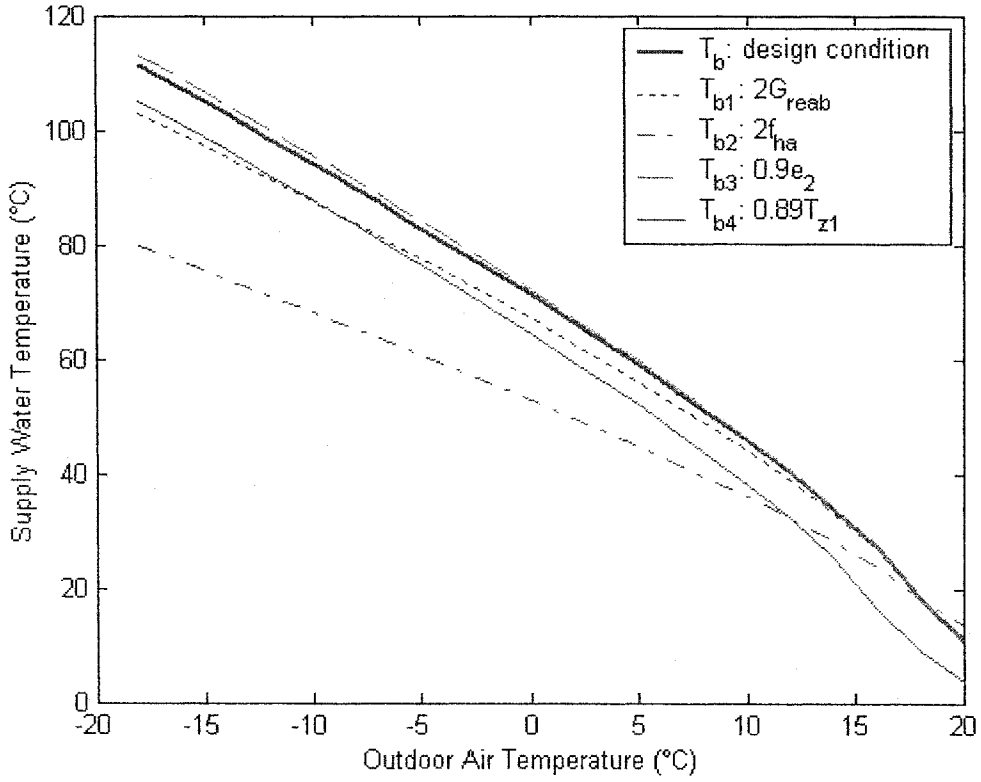

Figure 2.11 Influences of parameter changes in the DDHS

The influences of several design parameters were examined as shown in Figure 2.11. The assumed conditions are: decreasing the effectiveness e_2 by 10%, increasing the circulating water flow rate by 100%, reducing the design indoor air temperature to 16°C, and increasing heat transfer area of terminal heater by 100%. It can be seen that decreasing zone air temperature has the biggest effect on supply water temperature. However, one does not wish to decrease indoor air temperature in winter, as such

decreasing indoor air temperature will not be considered. Hence, both added transfer area of terminal heater and increased circulating water flow rate are more important factors affecting supply water temperature.

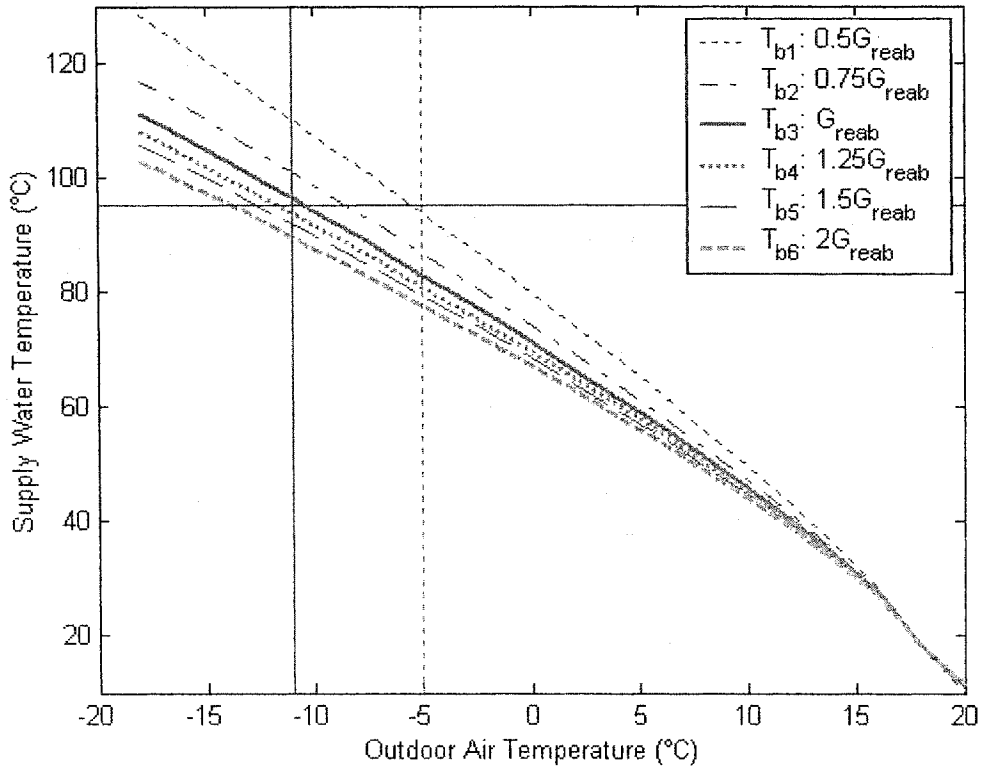

Figure 2.12 Relationship between T_b and G_{reab}

However, circulating water flow rate is more important parameter than heat transfer area of terminal heaters because of its ability to control the rate of heat transfer. The influence is illustrated in Figure 2.12. For example, if outdoor air temperature equals to –5°C, the supply water temperature changes from 93.39°C to 77.32°C when the actual circulating water flow rate increases from 50% to 100% of the design value.

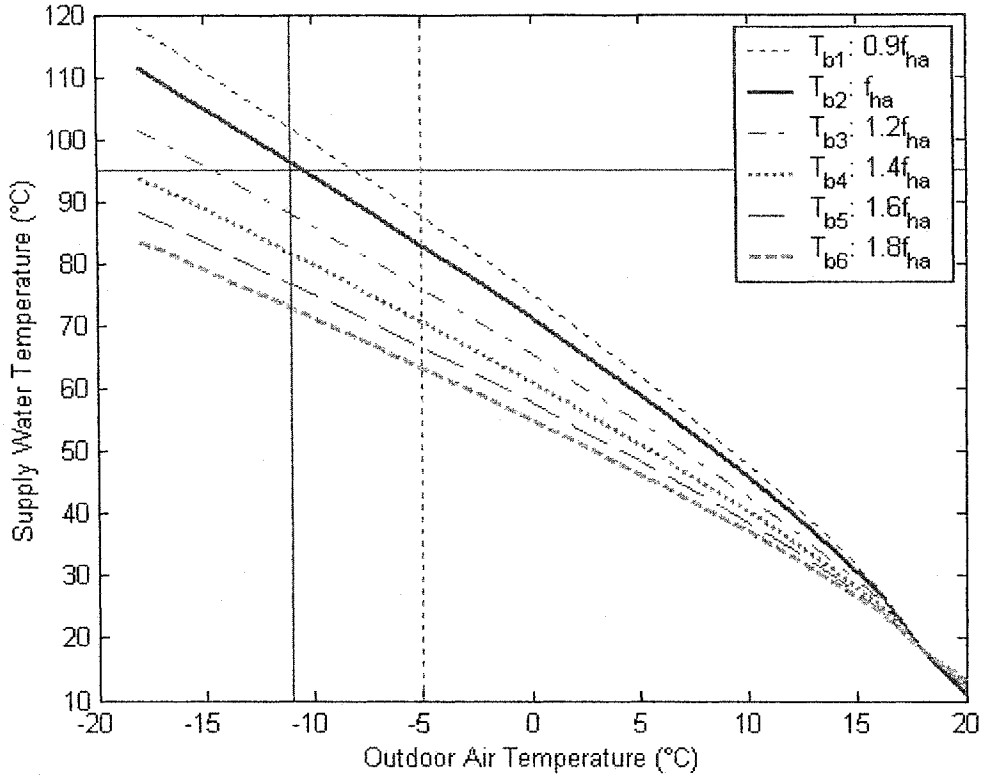

Figure 2.13 Relationship between T_b and f_{ha}

The influence of changing heat transfer area of terminal heater is presented in Figure 2.13. At outdoor air temperature equals to –5°C, supply water temperature of the boiler changes from 87.24°C to 63.03°C when area of heater is changed from 10% to 80% of the design value. It is not convenient to change this area because terminal heaters once installed have a fixed area. Nevertheless, the result is important in design optimization.

2.4.3 Steady state model and responses of the IDHS

A simplified IDHS schematic diagram for the purpose of developing an aggregate IDHS model is shown in Figure 2.14. The aggregate steady state model equations of IDHS are given in the following.

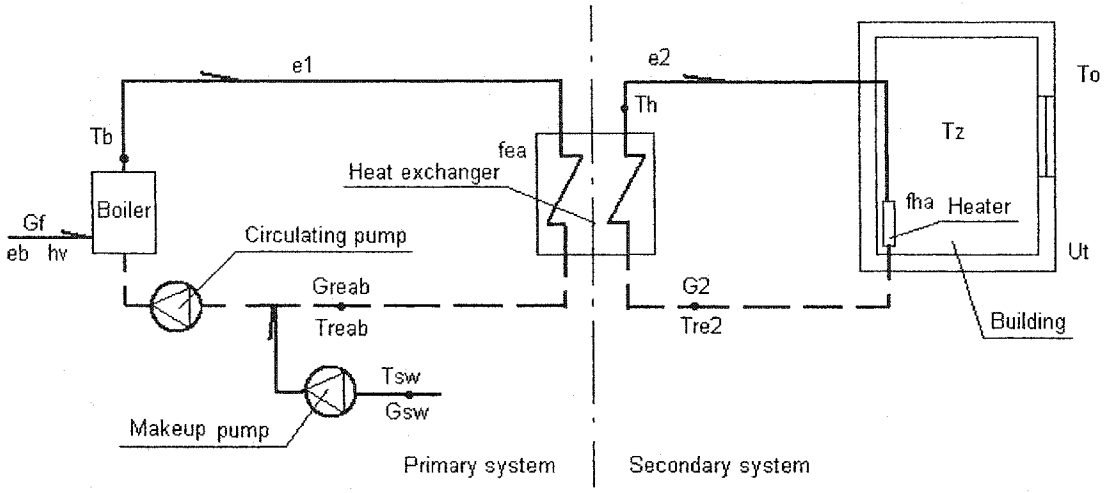

Figure 2.14 Simplified schematic diagram of IDHS

$$G_f e_b hv = c_w G_{reab}(T_b - T_{reab}) + c_w G_{sw}(T_b - T_{sw}) \tag{2.23}$$

$$c_w G_{reab}(T_b - T_{reab})e_1 = \frac{f_{ea} KF(T_b - T_h - T_{reab} + T_{re2})}{\ln \dfrac{T_b - T_h}{T_{reab} - T_{re2}}} \tag{2.24}$$

$$c_w G_{reab}(T_b - T_{reab})e_1 = c_w G_2(T_h - T_{re2}) \tag{2.25}$$

$$c_w G_2(T_h - T_{re2})e_2 = f_{ha} af(0.5T_h + 0.5T_{re2} - T_z)^{1+bh} \tag{2.26}$$

$$c_w G_2(T_h - T_{re2})e_2 = U_t(T_z - T_o) \tag{2.27}$$

A computer program is used to solve the above equations. Simulation results of the IDHS are presented in Figures 2.15 to 2.19.

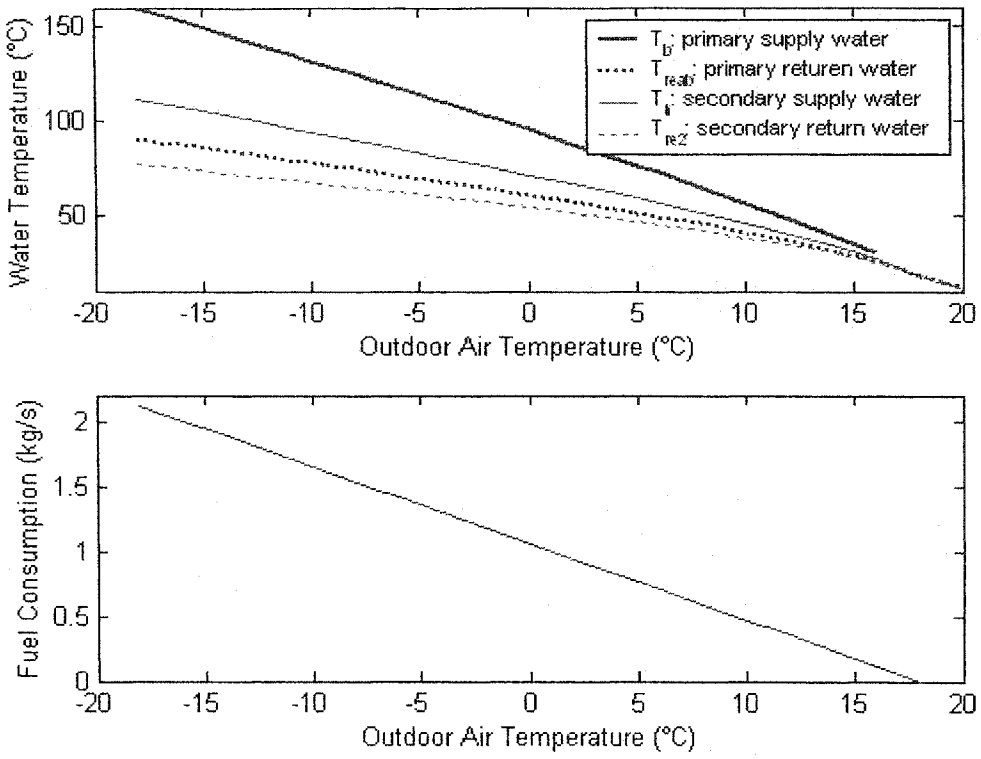

Figure 2.15 Design operation curves of the IDHS

At design outdoor air temperature, the fuel consumption, supply and return water temperature of the boiler, and supply and return water temperature of heat exchanger are 1.651kg/s, 133.67°C, 95.94°C, and 69.06°C respectively.

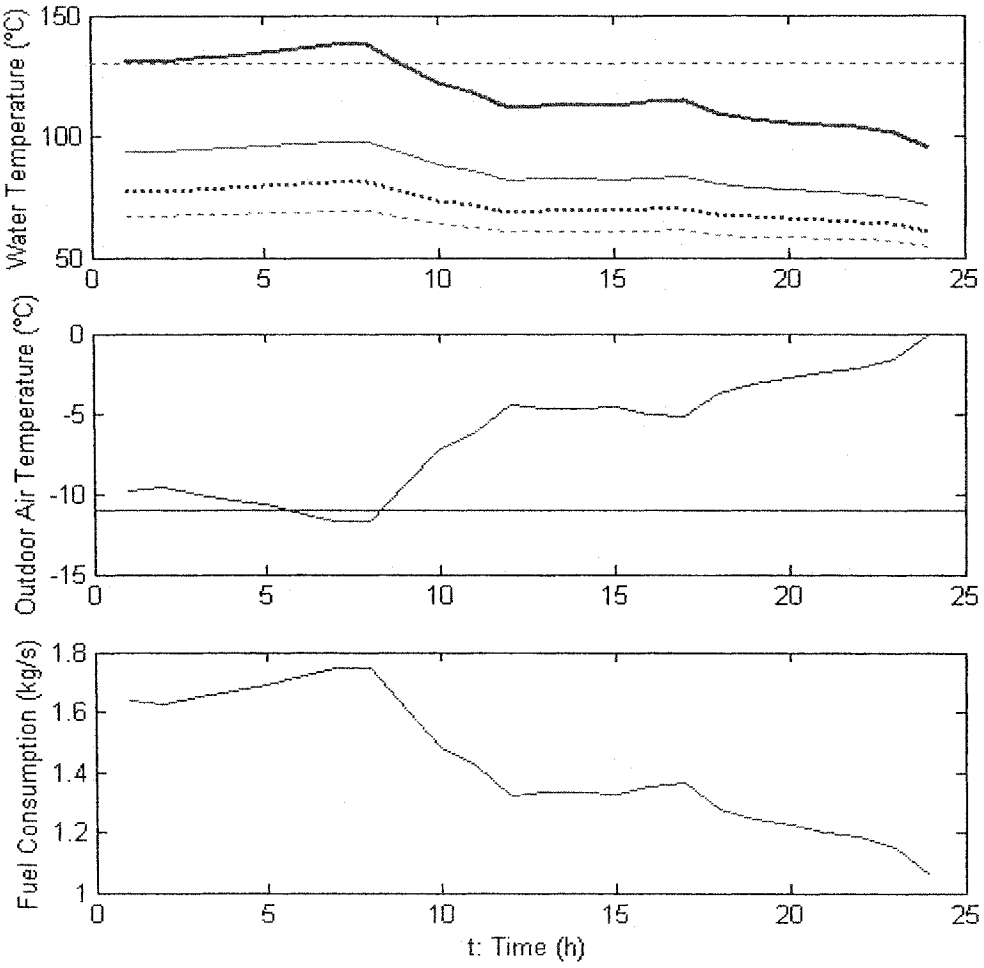

Figure 2.16 Actual operation curves

Steady state simulation results for one day are shown in Figure 2.16. When outdoor air temperature increases, supply and return water temperature and fuel consumption of the IDHS decrease. Moreover, when outdoor air temperature is below –10°C, supply water temperature of the boiler is greater than 130°C. This case should be avoided because of the constraint on the boiler supply water temperature.

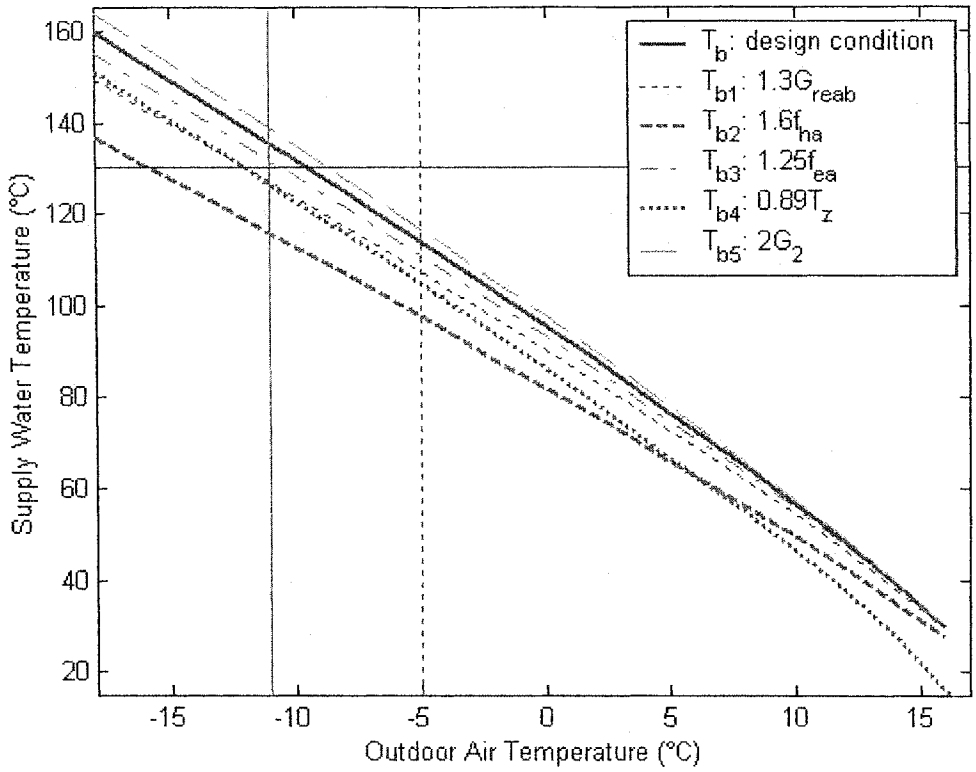

Figure 2.17 Influences of parameters changes in the IDHS

The influences of several different parameters on boiler water temperature are depicted in Figure 2.17. For comparing supply water temperature of the boiler, several cases are taken into account: increasing by 30% the circulating water flow rate in primary side, 25% increase in heat transfer area of heat exchangers, 100% increase in circulating water flow rate in secondary side, 60% increase in heat transfer area of terminal heater, and 2°C decrease in indoor air temperature. These cases usually happen in practical DHSs. It can be seen from this figure that increasing heat transfer area of terminal heater and decreasing indoor air temperature have greater influence on T_b than others. When the outdoor air temperature equals to -5°C, the largest range of the boiler supply water

temperature is about 16.37°C compared with the design condition at the same outdoor temperature. Heat transfer area of terminal heater is the most important parameter.

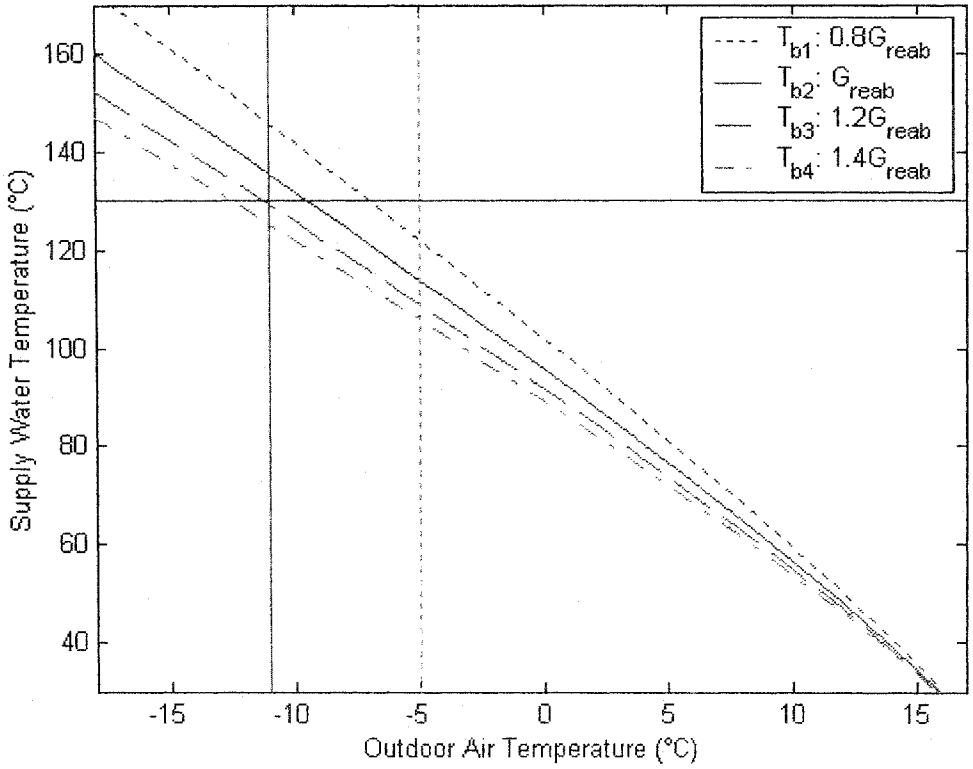

Figure 2.18 Relationship between T_b and G_{reab} in primary side

The impact of changing circulating water flow rate in primary side is illustrated in Figure 2.18. When outdoor air temperature equals to –5°C, for instance, the supply water temperate decreases from 122.1°C to 105.8°C when the circulating water flow rate is increased from 80% to 140% of the design value.

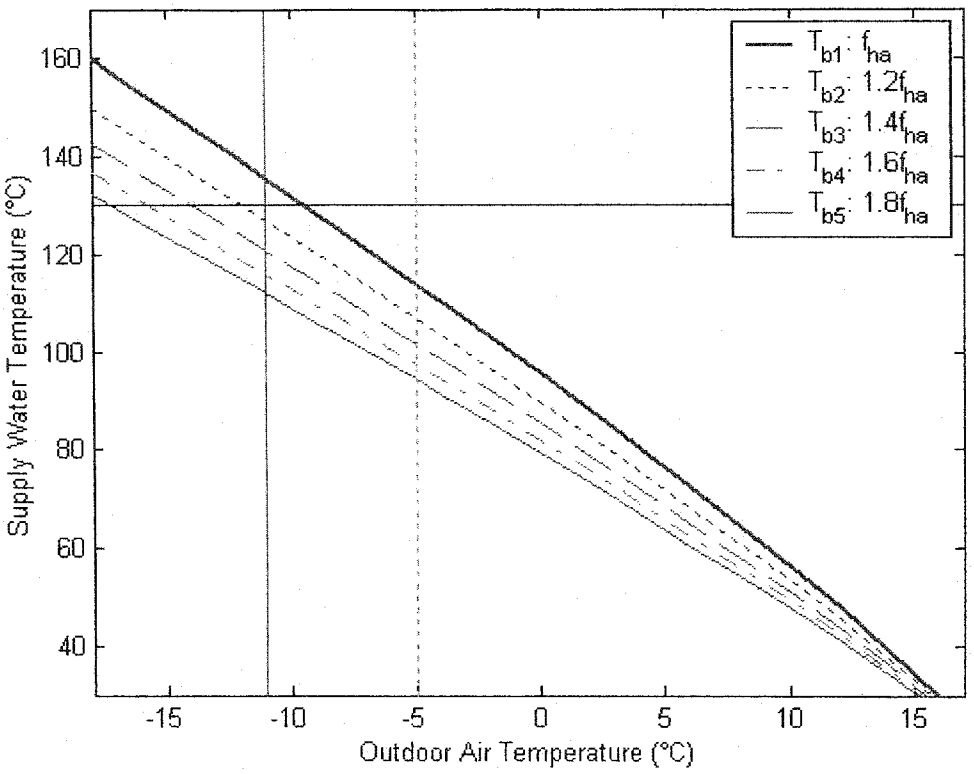

Figure 2.19 Relationship between T_b and f_{ha} in the IDHS

The effect of increasing the heat transfer area of terminal heater on T_b is shown in Figure 2.19. When outdoor air temperature equals to –5°C, supply water temperate of the boiler decreases from 113.9°C to 94.27°C as the heat transfer area of terminal heaters is increased from 100% to 180%. Comparing with Figure 2.18, it is clear that decreasing T_b by changing heat transfer area of the terminal heaters is more effective than that of changing circulating water flow rate in primary side. These results are useful in the design stage as well as in optimization of system operation.

Chapter 3 Dynamic Models of District Heating Systems

3.1 Introduction

In this chapter, dynamic models of a direct district heating system (DDHS) and an indirect district heating system (IDHS) are developed. First, the system layout, the nodal arrangement of the two models is described. Then, dynamic models are developed in order to simulate the performance. Finally, open loop tests are depicted to show the time response characteristics.

Several researchers [5, 15] have developed dynamic models of HVAC systems. These models were used for specific components or small systems. Some specific parameters should be considered if one wants to build dynamic models of large DHS. In addition, solar radiation effects [2] were taken into account for developing the models.

3.2 Physical model of a DDHS

A typical physical model of a DDHS is shown in Figure 2.1. The district heating system includes 30 buildings with total heated floor area of 100137m^2. It is connected with three branch circuits and the heat source. Depending on the distance from the heat source, the buildings were grouped in a simplified configuration consisting of three zones. Zone 1 included buildings 20~28; zone 2 included buildings 12~19 and 29~30; zone 3 included the buildings 1~11, shown in Figure 2.2. The buildings in branches B and C were grouped and represented by node B1 and C, while the buildings in branch D

were grouped and represented as node D. Thus, the simplified block diagram and its nodes are displayed in Figure 3.1.

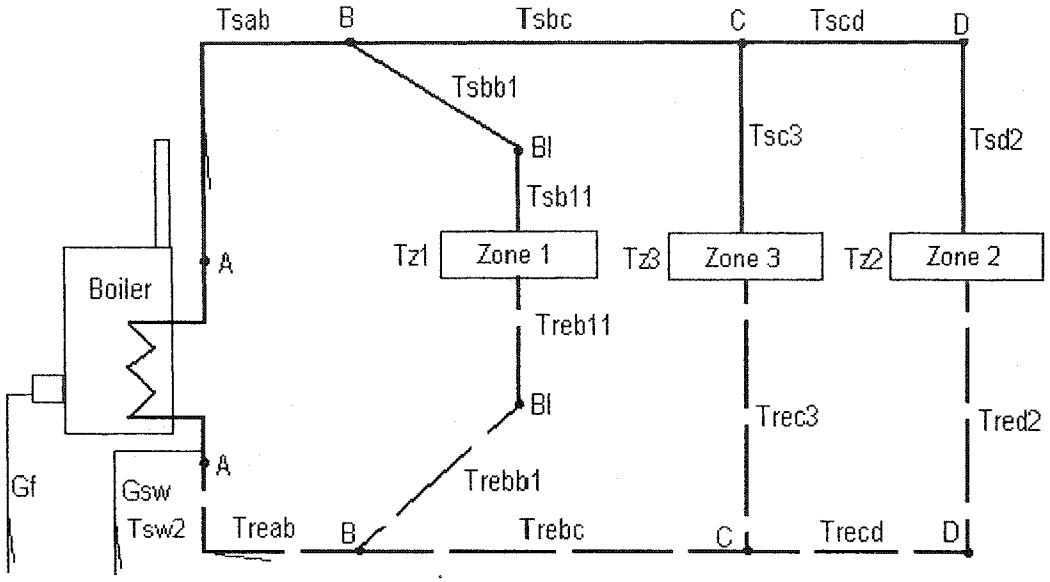

Figure 3.1 Schematic diagram of nodes in DDHS

3.3 Analytical model of the DDHS

By applying the energy balance principle, an analytical model of the DDHS was developed. The underlying assumption made in the model development is that the temperature distribution remained uniform and is represented by the respective nodal temperature. The heat losses from pipe insulation and leakage of water caused by users were included in the dynamic model. The underground soil temperature and the insulation of the embedded piping network were computed using the method given in reference [1]. The design parameters are shown in Table 2.1 and 2.2 in Chapter 2. From the design and actual field operating conditions of DDHSs, the magnitude of makeup water was chosen as 1% of the design value in the system. The analytical models

included several subsystem models such as the equivalent building model, boiler model, piping network model, and terminal heater model. There are 66 nodes in the model. For each node, the energy balance equations are written.

3.3.1 Equivalent building model

All buildings were grouped into three equivalent buildings (three zones) in order to simplify the model. Subscript " i " is used to express the parameters of zone1, 2, and 3. The layout, cross section details, and nodal arrangement of the equivalent building are shown in Figures 3.2 and 3.3.

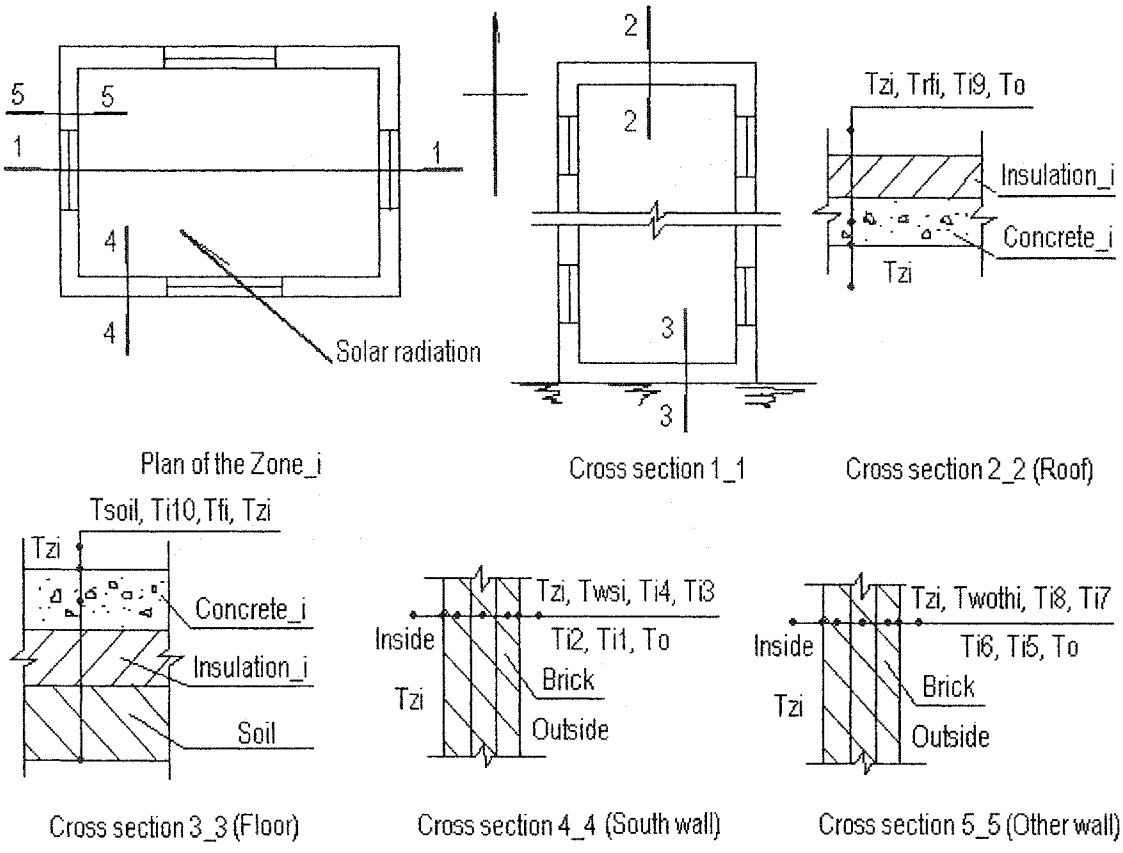

Figure 3.2 Layout and cross-sections of the equivalent building

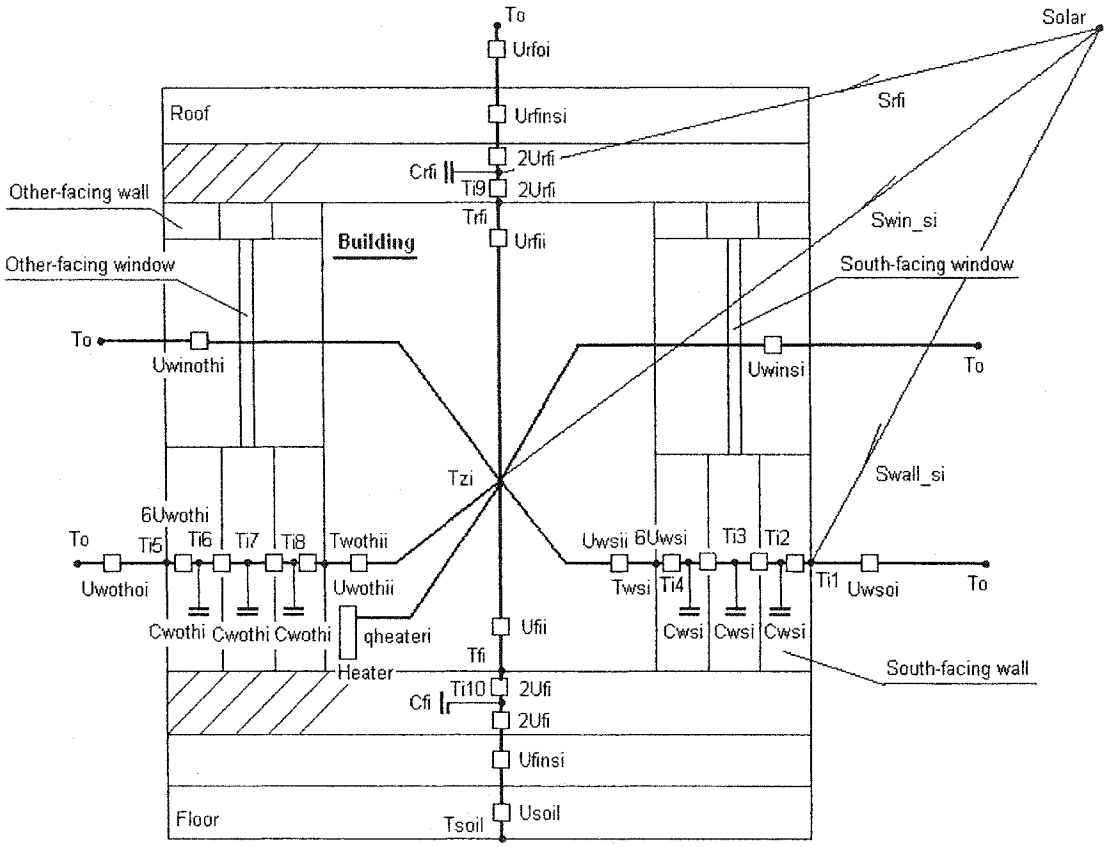

Figure 3.3 Node diagram of the equivalent building

Sets of energy balance equations were written as shown below. The symbols used are defined in the nomenclature.

For a three node south-facing wall

$$T_{i1} = \frac{6U_{wsi}T_{i2} + U_{wsoi}T_o + S_{wall\_si}}{6U_{wsi} + U_{wsoi}} \tag{3.1}$$

$$C_{wsi}\frac{d(T_{i2})}{dt} = 3U_{wsi}(T_{i3} - T_{i2}) + 6U_{wsi}(T_{i1} - T_{i2}) \tag{3.2}$$

$$C_{wsi}\frac{d(T_{i3})}{dt} = 3U_{wsi}(T_{i4} - T_{i3}) + 3U_{wsi}(T_{i2} - T_{i3}) \tag{3.3}$$

$$C_{wsi}\frac{d(T_{i4})}{dt} = 6U_{wsi}(T_{wsi} - T_{i4}) + 3U_{wsi}(T_{i3} - T_{i4}) \tag{3.4}$$

$$T_{wsi} = \frac{6U_{wsi}T_{i4} + U_{wsii}T_{zi}}{6U_{wsi} + U_{wsii}} \tag{3.5}$$

Three node walls facing other orientations

$$T_{i5} = \frac{6U_{wothi}T_{i6} + U_{wothoi}T_{o}}{6U_{wothi} + U_{wothoi}} \tag{3.6}$$

$$C_{wothi}\frac{d(T_{i6})}{dt} = 3U_{wothi}(T_{i7} - T_{i6}) + 6U_{wothi}(T_{i5} - T_{i6}) \tag{3.7}$$

$$C_{wothi}\frac{d(T_{i7})}{dt} = 3U_{wothi}(T_{i8} - T_{i7}) + 3U_{wothi}(T_{i6} - T_{i7}) \tag{3.8}$$

$$C_{wothi}\frac{d(T_{i8})}{dt} = 6U_{wothi}(T_{wothi} - T_{i8}) + 3U_{wothi}(T_{i7} - T_{i8}) \tag{3.9}$$

$$T_{wothi} = \frac{6U_{wothi}T_{i8} + U_{wothii}T_{zi}}{6U_{wothi} + U_{wothii}} \tag{3.10}$$

The roof

$$C_{rfi}\frac{d(T_{i9})}{dt} = 2U_{rfi}(T_{rfi} - T_{i9}) + U_{rf1i}(T_{o} - T_{i9}) + S_{rfi} \tag{3.11}$$

$$T_{rfi} = \frac{U_{rfii}T_{zi} + 2U_{rfi}T_{i9}}{U_{rfii} + 2U_{rfi}} \tag{3.12}$$

Where U_{rf1i} is the total value of U_{rfoi}, U_{rfinsi}, and $2U_{rfi}$.

The floor

$$C_{fi}\frac{d(T_{i10})}{dt} = 2U_{fi}(T_{fi} - T_{i10}) + U_{f1i}(T_{soil} - T_{i10}) \tag{3.13}$$

$$T_{fi} = \frac{U_{fii}T_{zi} + 2U_{fi}T_{i10}}{U_{fii} + 2U_{fi}} \tag{3.14}$$

Where U_{f1i} is the total value of U_{soil}, U_{finsi}, and $2U_{fi}$.

Heating load of each zone

For each zone i:

$$q_{zi} = h_i[(T_{zi} - T_{wsi})A_{wall\_si} + (T_{zi} - T_{wothi})A_{wothi} + (T_{zi} - T_{rfi})A_{roofi} + (T_{zi} - T_{fi})A_{floori}] + \frac{A_{win\_si} + A_{othwini}}{R_{win}}(T_{zi} - T_o) + \frac{c_z V_{zi} d_z ACH}{3600}(T_{zi} - T_o) \quad (3.15)$$

Total heating load

$$q_z = \sum q_{zi} \quad (3.16)$$

Steady state energy balance principle is used to develop Equations (3.1), (3.5), (3.6), (3.10), (3.12), and (3.14). In Equation (3.2), the rate of heat stored in node T_{i2} is equated to the heat flow from the node T_{i3}, plus the heat flow from the node T_{i1}. The other dynamic equations express the heat fluxes in and out of the nodes. Equation (3.15) describes heating load of each equivalent building is equated to the heat flow transferred to interior surfaces of the equivalent building and windows, and infiltration component as well. Equation (3.16) expresses that total heating load which is the sum of heating load of three equivalent buildings.

3.3.2 Zone model

Indoor air temperatures of the three equivalent zones are referred to as T_{z1}, T_{z2}, and T_{z3} respectively. Energy balance equations are shown below.

$$C_{zi}\frac{d(T_{zi})}{dt} = q_{heateri} - q_{zi} + S_{win\_si} \quad (3.17)$$

In Equation (3.17), the rate of heat stored in zone i is equated to the heat supplied by the terminal heaters and solar radiation, minus the rate of heat transferred by windows and inside surfaces.

3.3.3 Boiler model

A steady state design is presented in reference [21]. However, an accurate dynamic model of a boiler is very complex. To simplify the dynamic model of the boiler, some operating data from in field operation is used. For example, the excess air factor, the exhaust flue temperature, and heat loss owing to radiation and natural convection of combustion are expressed as the ratio of heating load of the boiler. Therefore, the boiler model is developed as follows.

$$r_Q = \frac{U_b G_{f\max} hv}{Q_{boiler}} \tag{3.18}$$

$$\alpha = 4.7321 r_Q^{\ 2} - 9.7036 r_Q + 6.32 \tag{3.19}$$

$$T_{ou} = 3.5714 r_Q^{\ 2} + 26.2857 r_Q + 137.6 \tag{3.20}$$

$$q_2 = 0.01[f_m + f_n \alpha (1 - 0.01 q_4)](T_{ou} - T_e) \tag{3.21}$$

$$q_5 = 11.8029 r_Q^{\ 2} - 20.3514 r_Q + 9.126 \tag{3.22}$$

$$e_b = 1 - 0.01(q_2 + q_3 + q_4 + q_5 + q_6) \tag{3.23}$$

$$Q_f = e_b U_b G_{f\max} hv \tag{3.24}$$

$$Q_{f1} = 0.8 Q_f \tag{3.25}$$

$$Q_{f2} = 0.16 Q_f \tag{3.26}$$

$$Q_{f3} = 0.04 Q_f \tag{3.27}$$

$$C_{b1} \frac{d(T_{b1})}{dt} = Q_{f1} - c_w G_{reab} (T_{b1} - T_{reab}) - c_w G_{sw} (T_{b1} - T_{sw2}) \tag{3.28}$$

$$C_{b2} \frac{d(T_{b2})}{dt} = Q_{f2} + c_w (G_{reab} + G_{sw})(T_{b1} - T_{b2}) \tag{3.29}$$

$$C_{b3}\frac{d(T_b)}{dt} = Q_{f3} + c_w(G_{reab} + G_{sw})(T_{b2} - T_b) \tag{3.30}$$

U_b is the normalized fuel flow rate corresponding to the burner capacity. The heat transfer from the boiler is divided into three segments. The temperature of each internal pipe segment is named as T_{b1}, T_{b2}, and T_b. In Equation (3.28), the rate of heat stored in lower pipe segment of the boiler is equated to the net energy input to the water, minus the rate of heat supplied to the middle segment and the heat loss by makeup water in the primary system. The efficiency of the boiler is expressed by Equation (3.23).

3.3.4 Supply and return water temperature nodal model

In the DDHS, both the supply water pipe network and return water network are divided into seven segments (Figure 3.1). Energy balance equations can be used to describe the dynamics for these nodes.

Supply water nodes

$$C_{ab}\frac{d(T_{sab})}{dt} = c_w G_{sab}(T_b - T_{sab}) - U_{insab}(T_{sab} - T_{soil}) - c_w G_{swab}(T_{sab} - T_{sw2}) \tag{3.31}$$

$$C_{bc}\frac{d(T_{sbc})}{dt} = c_w G_{sbc}(T_{sab} - T_{sbc}) - U_{insbc}(T_{sbc} - T_{soil}) - c_w G_{swbc}(T_{sbc} - T_{sw2}) \tag{3.32}$$

$$C_{bb1}\frac{d(T_{sbb1})}{dt} = c_w G_{sbb1}(T_{sab} - T_{sbb1}) - U_{insbb1}(T_{sbb1} - T_{soil}) - c_w G_{swbb1}(T_{sbb1} - T_{sw2}) \tag{3.33}$$

$$C_{cd}\frac{d(T_{scd})}{dt} = c_w G_{scd}(T_{sbc} - T_{scd}) - U_{inscd}(T_{scd} - T_{soil}) - c_w G_{swcd}(T_{scd} - T_{sw2}) \tag{3.34}$$

$$C_{opd2}\frac{d(T_{sd2})}{dt} = c_w G_{sz2}(T_{scd} - T_{sd2}) - U_{insd2}(T_{sd2} - T_{soil}) - c_w G_{swz2}(T_{sd2} - T_{sw2}) \tag{3.35}$$

$$C_{opc3}\frac{d(T_{sc3})}{dt} = c_w G_{sz3}(T_{sbc} - T_{sc3}) - U_{insc3}(T_{sc3} - T_{soil}) - c_w G_{swz3}(T_{sc3} - T_{sw2}) \tag{3.36}$$

$$C_{opb11}\frac{d(T_{sb11})}{dt}=c_wG_{sz1}(T_{sbb1}-T_{sb11})-U_{insb11}(T_{sb11}-T_{soil})-c_wG_{swz1}(T_{sb11}-T_{sw2}) \quad (3.37)$$

Return water nodes

$$C_{bb1}\frac{d(T_{rebb1})}{dt}=c_wG_{rebb1}(T_{reb11}-T_{rebb1})-U_{insbb1}(T_{rebb1}-T_{soil})-c_wG_{swbb1}(T_{rebb1}-T_{sw2}) \quad (3.38)$$

$$C_{cd}\frac{d(T_{recd})}{dt}=c_wG_{recd}(T_{red2}-T_{recd})-U_{inscd}(T_{recd}-T_{soil})-c_wG_{swcd}(T_{recd}-T_{sw2}) \quad (3.39)$$

$$(C_{opc3}+C_{u3})\frac{d(T_{rec3})}{dt}=c_wG_{2dz3}(T_{sc3}-T_{rec3})-q_{heater3} \quad (3.40)$$
$$-U_{insc3}(T_{rec3}-T_{soil})-c_wG_{swz3}(T_{rec3}-T_{sw2})$$

$$(C_{opb11}+C_{u1})\frac{d(T_{reb11})}{dt}=c_wG_{2dz1}(T_{sb11}-T_{reb11})-q_{heater1} \quad (3.41)$$
$$-U_{insb11}(T_{reb11}-T_{soil})-c_wG_{swz1}(T_{reb11}-T_{sw2})$$

$$(C_{opd2}+C_{u2})\frac{d(T_{red2})}{dt}=c_wG_{2dz2}(T_{sd2}-T_{red2})-q_{heater2} \quad (3.42)$$
$$-U_{insd2}(T_{red2}-T_{soil})-c_wG_{swz2}(T_{red2}-T_{sw2})$$

$$C_{bc}\frac{d(T_{rebc})}{dt}=c_wG_{rez3}(T_{rec3}-T_{rebc})+c_wG_{recd}(T_{recd}-T_{rebc}) \quad (3.43)$$
$$-U_{insbc}(T_{rebc}-T_{soil})-c_wG_{swbc}(T_{rebc}-T_{sw2})$$

$$C_{ab}\frac{d(T_{reab})}{dt}=c_wG_{rebb1}(T_{rebb1}-T_{reab})+c_wG_{rebc}(T_{rebc}-T_{reab}) \quad (3.44)$$
$$-U_{insab}(T_{reab}-T_{soil})-c_wG_{swab}(T_{reab}-T_{sw2})$$

In these equations, the rate of heat stored in each pipe segment is equated to the heat supplied by upstream section, minus heat losses through the pipe insulation and due to water leakage.

3.3.5 Terminal heater model

The heat transferred by terminal heaters is shown in Equations (3.45) to (3.47) [16].

$$q_{heater1} = f_{ha} af_1 (0.5T_{sb11} + 0.5T_{reb11} - T_{z1})^{1+bh_1} \quad (3.45)$$

$$q_{heater2} = f_{ha} af_2 (0.5T_{sd2} + 0.5T_{red2} - T_{z2})^{1+bh_2} \quad (3.46)$$

$$q_{heater3} = f_{ha} af_3 (0.5T_{sc3} + 0.5T_{rec3} - T_{z3})^{1+bh_3} \quad (3.47)$$

For instance, the heat transferred by terminal heater 1 in zone1 is equated to the capacity of terminal heater's average temperature minus indoor air temperature. Where f_{ha}, af_1, af_2, af_3, bh_1, bh_2, and bh_3 are factors related zone parameters.

In conclusion, the dynamic model of the typical DDHS consists of 79 energy balance equations, which include 44 dynamic equations. The dynamic model was used to simulate the dynamic responses of the DDHS by writing a computer simulation program in Matlab environment.

3.3.6 Open loop tests

For the open loop tests of the DDHS, several operating conditions such as with or without heat losses, solar radiation, and off-design conditions were simulated. Table 3.1 is presented in order to show the relationship between operating conditions and the respective figures.

Table 3.1 Open loop tests of the DDHS

Operating conditions			Figure
Design condition (U_b=1, f_{ha}=1)	Temperature responses	Without heat losses, T_o=-11°C, no solar radiation	Figure 3.4
		With heat losses, T_o=-11°C, no solar radiation	Figure 3.5
Transient response (U_b=1, f_{ha}=1)		With heat losses, T_o=-11°C, with solar radiation (300 w/m^2)	Figure 3.6
Off design condition (U_b=0.86, f_{ha}=1.57)		With heat losses, T_o=-4.6°C, with solar radiation (200 w/m^2)	Figure 3.7

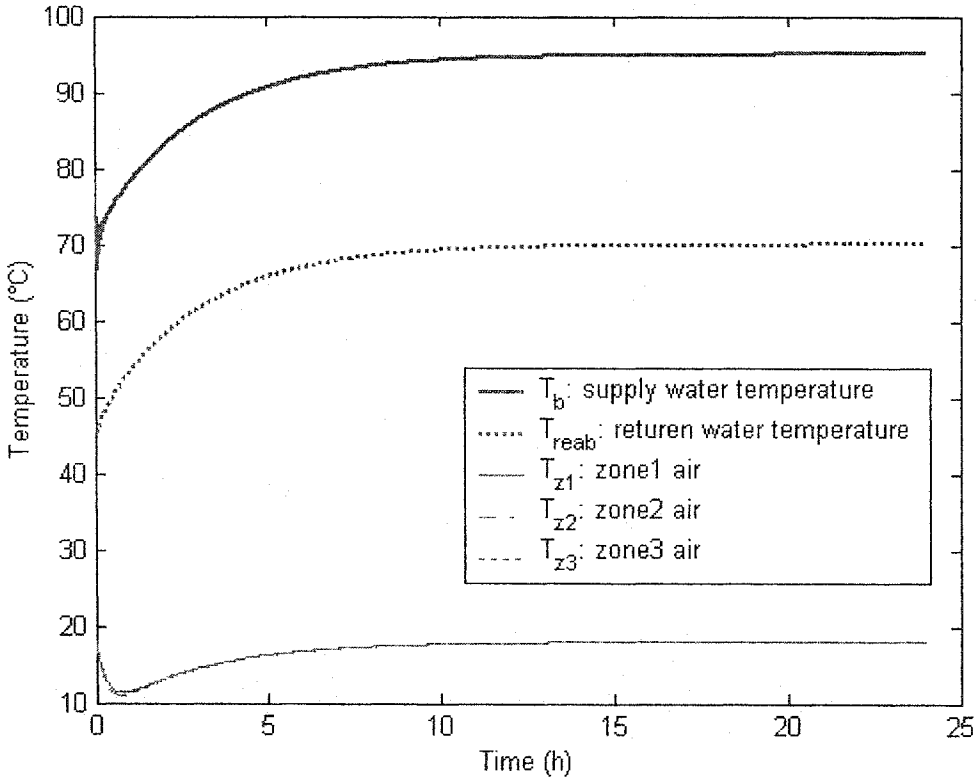

Figure 3.4 OLT: temperature responses without heat losses and solar radiation

The slow temperature response curves in Figure 3.4 are indicative of the thermal capacity of the overall system. These temperatures in the DDHS reach steady state in about 24 hours. Moreover, in the first of five hours, the indoor air temperatures have different responses because the capacity of each equivalent building is different. At 24:00

hours, the temperatures of supply and return water reach 95.02°C and 70.01°C respectively, as well as the temperatures in all zones reach 18°C.

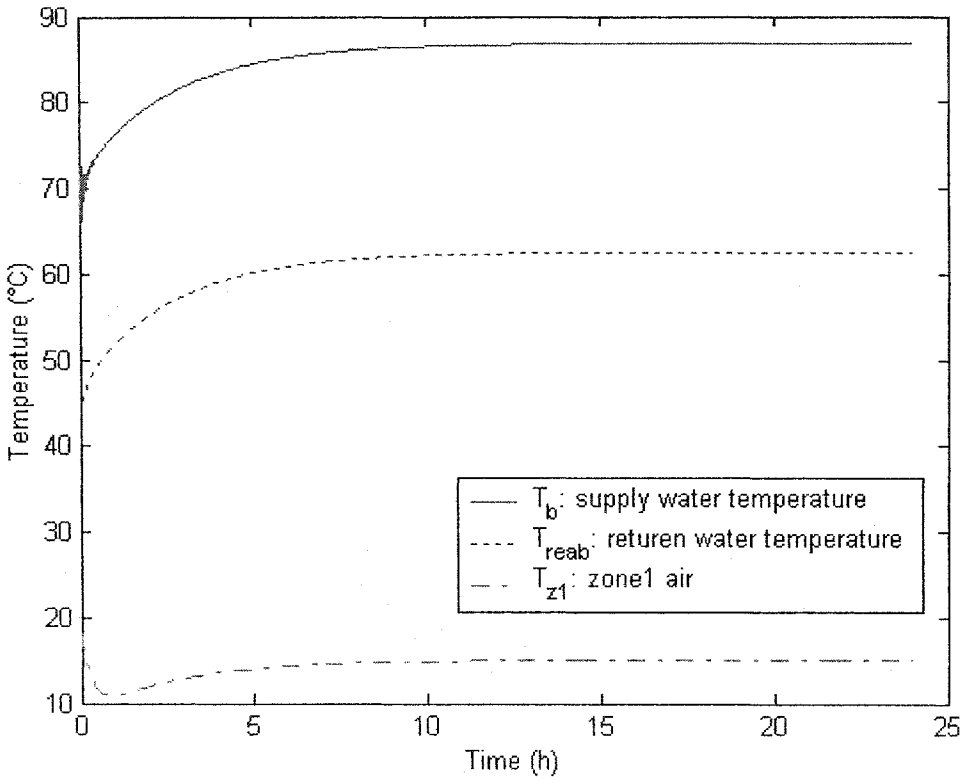

Figure 3.5 OLT: temperature responses with heat losses and without solar radiation

The temperature responses with heat losses are considered in Figure 3.5. The lower temperatures are caused by the heat losses. After 24:00 hours, T_b, T_{reab}, T_{z1} reach the steady state values 86.87°C, 62.56°C, and 15.01°C respectively. In addition, based on the model simulation, the heat loss from water leakage is greater than that of piping insulation.

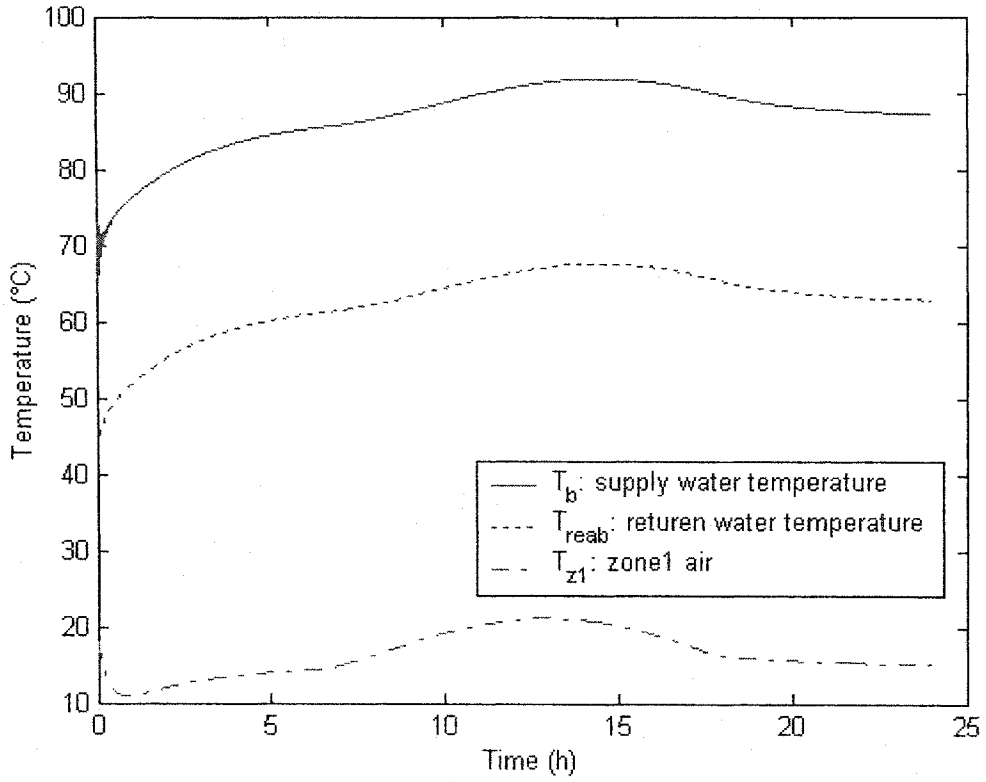

Figure 3.6 OLT: temperature responses with heat losses and solar radiation

Figure 3.6 shows the influence of solar radiation. The increased indoor air temperature is caused by solar radiation during daytime and reaches 21.32℃ at 13:00 hours. This means that the air temperatures should be controlled in a reasonable range because solar radiation can result in larger indoor air temperature swing. If the supply water temperature T_b is above design temperature, it has to be decreased in order to avoid severe overheating.

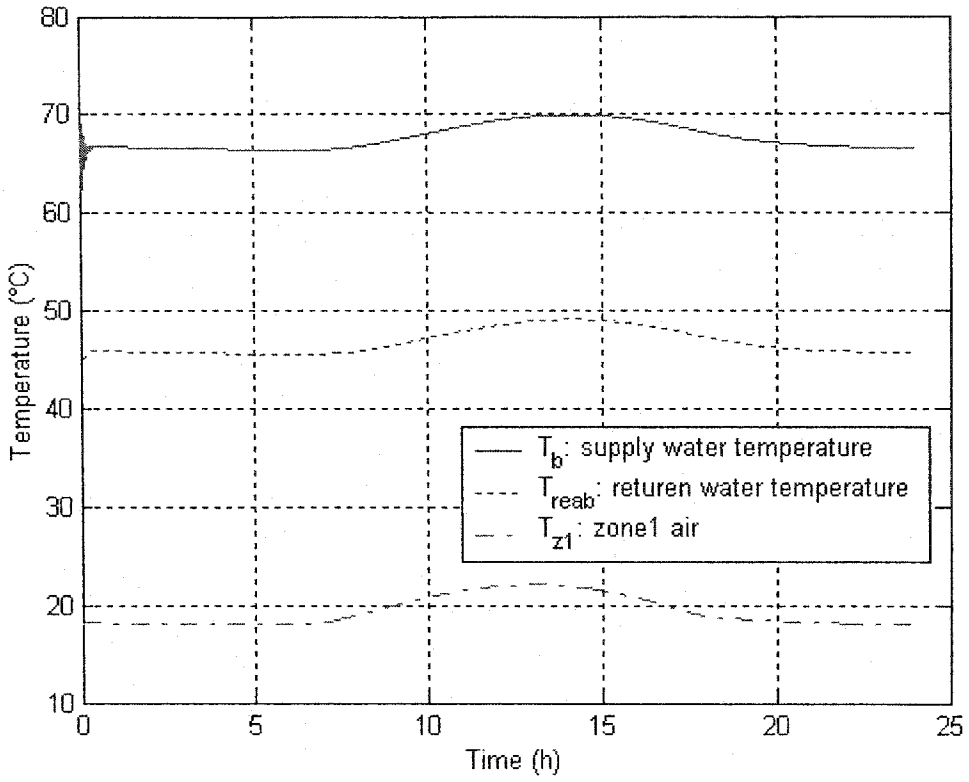

Figure 3.7 OLT: temperature responses in off-design condition

The simulation results in off-design conditions are depicted in Figure 3.7. The off-design conditions considered are U_b=0.86, T_o=-4.6°C, and S_{ol}=200w/m^2. The highest temperatures of the supply water, return water, and zone reach 69.95°C, 49.12°C, and 22.14°C at 14:10 hours, 14:30 hours, and 13:00 hours respectively.

3.4 Physical model of the IDHS

The main difference between an IDHS and a DDHS is that heat exchange stations are added in order to transfer heat from primary side to secondary side. The layout of a typical IDHS is illustrated in Figure 2.5, and its block diagram including nodes is shown in Figure 3.8. The designed IDHS includes ten heat exchange stations. The total designed

heated floor area and heating load are 851031m^2 and 51.47Mw respectively. Note that the heat exchangers in each station are integrated as an equivalent exchanger represented by letter "j".

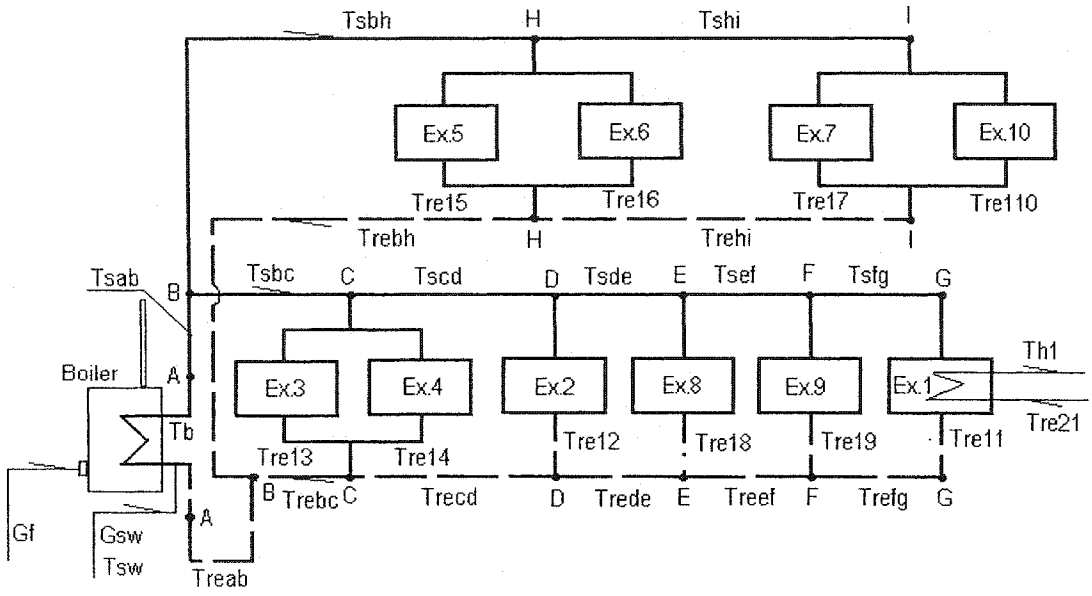

Figure 3.8 Schematic diagram of nodes in IDHS

3.5 Dynamic model of the IDHS

Applying energy balance principle, a dynamic model of the IDHS is developed. The model considers the heat losses from piping insulation and water leakage as well as solar radiation. The analytical models included several subsystem models such as boiler model, piping network model, heat exchanger model, and terminal heater model. There are 70 nodes in the dynamic model. For each node, the energy balance equations were developed.

3.5.1 Boiler model

The boiler model is described by the following equations. Note that the structure of

boiler model remains the same as in DDHS. The difference is in the magnitude of empirical coefficients used in the model.

$$r_Q = \frac{U_b G_{f\max} hv}{Q_{boiler}} \tag{3.48}$$

$$\alpha = 3.3929 r_Q^{\ 2} - 7.4214 r_Q + 5.37 \tag{3.49}$$

$$T_{ou} = 5.3571 r_Q^{\ 2} + 33.9286 r_Q + 127.99 \tag{3.50}$$

$$q_2 = 0.01[f_m + f_n \alpha (1 - 0.01 q_4)](T_{ou} - T_e) \tag{3.51}$$

$$q_5 = 9.6429 r_Q^{\ 2} - 16.9714 r_Q + 8 \tag{3.52}$$

$$e_b = 1 - 0.01(q_2 + q_3 + q_4 + q_5 + q_6) \tag{3.53}$$

$$Q_f = e_b U_b G_{f\max} hv \tag{3.54}$$

$$Q_{f1} = 0.82 Q_f \tag{3.55}$$

$$Q_{f2} = 0.145 Q_f \tag{3.56}$$

$$Q_{f3} = 0.035 Q_f \tag{3.57}$$

$$C_{b1} \frac{d(T_{b1})}{dt} = Q_{f1} - c_w G_{reab}(T_{b1} - T_{reab}) - c_w G_{sw}(T_{b1} - T_{sw}) \tag{3.58}$$

$$C_{b2} \frac{d(T_{b2})}{dt} = Q_{f2} + c_w (G_{reab} + G_{sw})(T_{b1} - T_{b2}) \tag{3.59}$$

$$C_{b3} \frac{d(T_b)}{dt} = Q_{f3} + c_w (G_{reab} + G_{sw})(T_{b2} - T_b) \tag{3.60}$$

3.5.2 Supply and return water temperature nodal model in primary side

In the IDHS, both of the supply water pipe network and return water network in the primary side are divided into eight segments as shown in Figure 3.8. Energy balance equations are used to express the dynamics of these nodes.

Supply water nodes

$$C_{ab}\frac{d(T_{sab})}{dt}=c_wG_{sab}(T_b-T_{sab})-U_{insab}(T_{sab}-T_{soil})-c_wG_{swab}(T_{sab}-T_{sw}) \tag{3.61}$$

$$C_{bc}\frac{d(T_{sbc})}{dt}=c_wG_{sbc}(T_{sab}-T_{sbc})-U_{insbc}(T_{sbc}-T_{soil})-c_wG_{swbc}(T_{sbc}-T_{sw}) \tag{3.62}$$

$$C_{cd}\frac{d(T_{scd})}{dt}=c_wG_{scd}(T_{sbc}-T_{scd})-U_{inscd}(T_{scd}-T_{soil})-c_wG_{swcd}(T_{scd}-T_{sw}) \tag{3.63}$$

$$C_{de}\frac{d(T_{sde})}{dt}=c_wG_{sde}(T_{scd}-T_{sde})-U_{insde}(T_{sde}-T_{soil})-c_wG_{swde}(T_{sde}-T_{sw}) \tag{3.64}$$

$$C_{ef}\frac{d(T_{sef})}{dt}=c_wG_{sef}(T_{sde}-T_{sef})-U_{insef}(T_{sef}-T_{soil})-c_wG_{swef}(T_{sef}-T_{sw}) \tag{3.65}$$

$$C_{fg}\frac{d(T_{sfg})}{dt}=c_wG_{sfg}(T_{sef}-T_{sfg})-U_{insfg}(T_{sfg}-T_{soil})-c_wG_{swfg}(T_{sfg}-T_{sw}) \tag{3.66}$$

$$C_{bh}\frac{d(T_{sbh})}{dt}=c_wG_{sbh}(T_{sab}-T_{sbh})-U_{insbh}(T_{sbh}-T_{soil})-c_wG_{swbh}(T_{sbh}-T_{sw}) \tag{3.67}$$

$$C_{hi}\frac{d(T_{shi})}{dt}=c_wG_{shi}(T_{sbh}-T_{shi})-U_{inshi}(T_{shi}-T_{soil})-c_wG_{swhi}(T_{shi}-T_{sw}) \tag{3.68}$$

Return water nodes

$$C_{fg}\frac{d(T_{refg})}{dt}=c_wG_{1d1}(T_{re11}-T_{refg})-U_{insfg}(T_{refg}-T_{soil})-c_wG_{swfg}(T_{refg}-T_{sw}) \tag{3.69}$$

$$\begin{aligned}C_{ef}\frac{d(T_{reef})}{dt}&=c_wG_{1d9}(T_{re19}-T_{reef})+c_wG_{refg}(T_{refg}-T_{reef})\\&-U_{insef}(T_{reef}-T_{soil})-c_wG_{swef}(T_{reef}-T_{sw})\end{aligned} \tag{3.70}$$

$$\begin{aligned}C_{de}\frac{d(T_{rede})}{dt}&=c_wG_{1d8}(T_{re18}-T_{rede})+c_wG_{reef}(T_{reef}-T_{rede})\\&-U_{insde}(T_{rede}-T_{soil})-c_wG_{swde}(T_{rede}-T_{sw})\end{aligned} \tag{3.71}$$

$$\begin{aligned}C_{cd}\frac{d(T_{recd})}{dt}&=c_wG_{1d2}(T_{re12}-T_{recd})+c_wG_{rede}(T_{rede}-T_{recd})\\&-U_{inscd}(T_{recd}-T_{soil})-c_wG_{swcd}(T_{recd}-T_{sw})\end{aligned} \tag{3.72}$$

$$C_{bc}\frac{d(T_{rebc})}{dt} = c_w G_{1d3}(T_{re13} - T_{rebc}) + c_w G_{1d4}(T_{re14} - T_{rebc}) + c_w G_{recd}(T_{recd} - T_{rebc}) \quad (3.73)$$
$$-U_{insbc}(T_{rebc} - T_{soil}) - c_w G_{swbc}(T_{rebc} - T_{sw})$$

$$C_{hi}\frac{d(T_{rehi})}{dt} = c_w G_{1d7}(T_{re17} - T_{rehi}) + c_w G_{1d10}(T_{re110} - T_{rehi}) \quad (3.74)$$
$$-U_{inshi}(T_{rehi} - T_{soil}) - c_w G_{swhi}(T_{rehi} - T_{sw})$$

$$C_{bh}\frac{d(T_{rebh})}{dt} = c_w G_{1d5}(T_{re15} - T_{rebh}) + c_w G_{1d6}(T_{re16} - T_{rebh}) + c_w G_{rehi}(T_{rehi} - T_{rebh}) \quad (3.75)$$
$$-U_{insbh}(T_{rebh} - T_{soil}) - c_w G_{swbh}(T_{rebh} - T_{sw})$$

$$C_{ab}\frac{d(T_{reab})}{dt} = c_w G_{rebc}(T_{rebc} - T_{reab}) + c_w G_{rebh}(T_{rebh} - T_{reab}) \quad (3.76)$$
$$-U_{insab}(T_{reab} - T_{soil}) - c_w G_{swab}(T_{reab} - T_{sw})$$

3.5.3 Heat exchanger model

Index "j", which is equals to 1 to 10, is employed to describe the series of heat exchange stations as well as the related zones. Note that the equivalent heat exchanger concept is used to integrate the heat exchangers in each heat exchange station.

Supply water nodes of the secondary side

$$C_{h2j}\frac{d(T_{hj})}{dt} = q_{exj} - c_w G_{2dj}(T_{hj} - T_{re2j}) \quad (3.77)$$

The Equation (3.77) expresses the rate of heat stored in the secondary side of equivalent heat exchanger j is equated to the heat input from the primary side, minus the heat transferred to the secondary side.

Return water nodes of the primary side

$$C_{h11}\frac{d(T_{re11})}{dt} = c_w G_{1d1}(T_{sfg} - T_{re11}) - q_{ex1} \quad (3.78)$$

$$C_{h12}\frac{d(T_{re12})}{dt} = c_w G_{1d2}(T_{scd} - T_{re12}) - q_{ex2} \tag{3.79}$$

$$C_{h13}\frac{d(T_{re13})}{dt} = c_w G_{1d3}(T_{sbc} - T_{re13}) - q_{ex3} \tag{3.80}$$

$$C_{h14}\frac{d(T_{re14})}{dt} = c_w G_{1d4}(T_{sbc} - T_{re14}) - q_{ex4} \tag{3.81}$$

$$C_{h15}\frac{d(T_{re15})}{dt} = c_w G_{1d5}(T_{sbh} - T_{re15}) - q_{ex5} \tag{3.82}$$

$$C_{h16}\frac{d(T_{re16})}{dt} = c_w G_{1d6}(T_{sbh} - T_{re16}) - q_{ex6} \tag{3.83}$$

$$C_{h17}\frac{d(T_{re17})}{dt} = c_w G_{1d7}(T_{shi} - T_{re17}) - q_{ex7} \tag{3.84}$$

$$C_{h18}\frac{d(T_{re18})}{dt} = c_w G_{1d8}(T_{sde} - T_{re18}) - q_{ex8} \tag{3.85}$$

$$C_{h19}\frac{d(T_{re19})}{dt} = c_w G_{1d9}(T_{sef} - T_{re19}) - q_{ex9} \tag{3.86}$$

$$C_{h110}\frac{d(T_{re110})}{dt} = c_w G_{1d10}(T_{shi} - T_{re110}) - q_{ex10} \tag{3.87}$$

From Equations (3.78) to (3.87), the rate of heat stored in the primary side of the equivalent heat exchanger j is equated to the heat supplied by the primary piping network, minus the heat transferred to secondary side.

Logarithmic mean temperature difference of each equivalent heat exchanger is computed from

$$LMTD_{ex1} = \frac{T_{sfg} - T_{h1} - T_{re11} + T_{re21}}{\ln\dfrac{T_{sfg} - T_{h1}}{T_{re11} - T_{re21}}} \tag{3.88}$$

$$LMTD_{ex2} = \frac{T_{scd} - T_{h2} - T_{re12} + T_{re22}}{\ln \frac{T_{scd} - T_{h2}}{T_{re12} - T_{re22}}} \tag{3.89}$$

$$LMTD_{ex3} = \frac{T_{sbc} - T_{h3} - T_{re13} + T_{re23}}{\ln \frac{T_{sbc} - T_{h3}}{T_{re13} - T_{re23}}} \tag{3.90}$$

$$LMTD_{ex4} = \frac{T_{sbc} - T_{h4} - T_{re14} + T_{re24}}{\ln \frac{T_{sbc} - T_{h4}}{T_{re14} - T_{re24}}} \tag{3.91}$$

$$LMTD_{ex5} = \frac{T_{sbh} - T_{h5} - T_{re15} + T_{re25}}{\ln \frac{T_{sbh} - T_{h5}}{T_{re15} - T_{re25}}} \tag{3.92}$$

$$LMTD_{ex6} = \frac{T_{sbh} - T_{h6} - T_{re16} + T_{re26}}{\ln \frac{T_{sbh} - T_{h6}}{T_{re16} - T_{re26}}} \tag{3.93}$$

$$LMTD_{ex7} = \frac{T_{shi} - T_{h7} - T_{re17} + T_{re27}}{\ln \frac{T_{shi} - T_{h7}}{T_{re17} - T_{re27}}} \tag{3.94}$$

$$LMTD_{ex8} = \frac{T_{sde} - T_{h8} - T_{re18} + T_{re28}}{\ln \frac{T_{sde} - T_{h8}}{T_{re18} - T_{re28}}} \tag{3.95}$$

$$LMTD_{ex9} = \frac{T_{sef} - T_{h9} - T_{re19} + T_{re29}}{\ln \frac{T_{sef} - T_{h9}}{T_{re19} - T_{re29}}} \tag{3.96}$$

$$LMTD_{ex10} = \frac{T_{shi} - T_{h10} - T_{re110} + T_{re210}}{\ln \frac{T_{shi} - T_{h10}}{T_{re110} - T_{re210}}} \tag{3.97}$$

The amount of heat transferred is determined from

$$q_{exj} = f_{ea} KF_j LMTD_{exj} \tag{3.98}$$

$$q_{ex} = \sum q_{exj} \tag{3.99}$$

Return water temperature in the secondary side is determined from

$$C_{2j}\frac{d(T_{re2j})}{dt} = e_2 q_{exj} - q_{heaterj} \tag{3.100}$$

The rate of heat stored in the return water segment of the secondary side is equated to the difference between the net heat supplied by the equivalent heat exchanger j and the heat gain by the terminal heaters. Where e_2 means the average efficiency of the secondary side, which is assumed as 0.9.

The terminal heater and zone model equations remain the same as in DDHS.

3.5.4 Open loop tests of the IDHS

Open loop tests are employed to examine the transient response characteristics of IDHS. Several operating conditions showed in Table 3.2 are considered.

Table 3.2 Open loop tests of the IDHS

Operating conditions			Figure
Design condition (f_{ea}=1, f_{ha}=1, U_b=1, T_o=-11°C)	Temperature responses	Without heat losses, e_2=1, no solar radiation	Figure 3.9
		With heat losses, e_2=1, no solar radiation	Figure 3.10
		With heat losses, e_2=0.9, with solar radiation (200w/m^2)	Figure 3.11
Off design condition (f_{ea}=1.15, f_{ha}=1.57, e_2=0.9)	Temperature responses	With heat losses, compare to U_b=1,T_o= -11°C and U_b=1, T_o= -15°C, no solar radiation	Figure 3.12
		With heat losses, compare to U_b=1, T_o=-11°C and U_b=0.778,T_o= -4.6°C, no solar radiation	Figure 3.13

Figure 3.9 below shows that the temperature responses reach the steady state values in about 24 hours. At 24:00 hours, T_b, T_{reab}, T_{h1}, T_{re21}, and T_{z1} reach 129.90, 79.90, 94.90, 69.91, and 17.96°C respectively. When the simulation is made over 48 hours, T_b, T_{reab},

T_{h1}, T_{re21}, and T_{z1} reach 130, 80, 95, 70, and 18°C respectively. Since the thermal capacity of the building is very large, the IDHS needs almost one day to reach the steady state values.

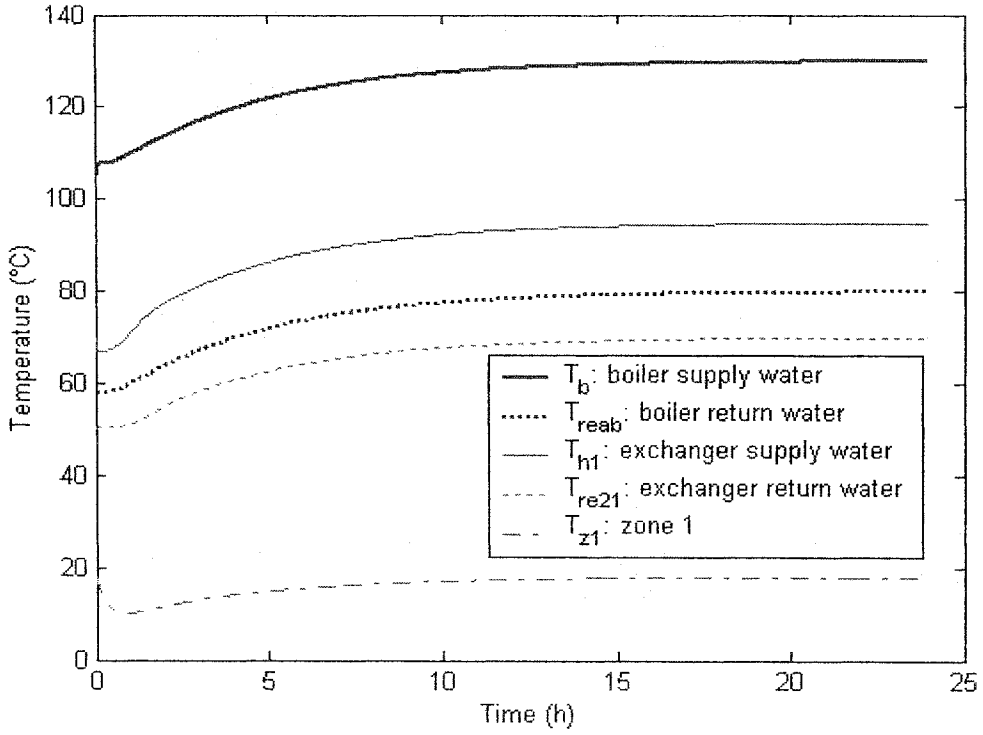

Figure 3.9 OLT: temperature responses without heat losses and solar radiation

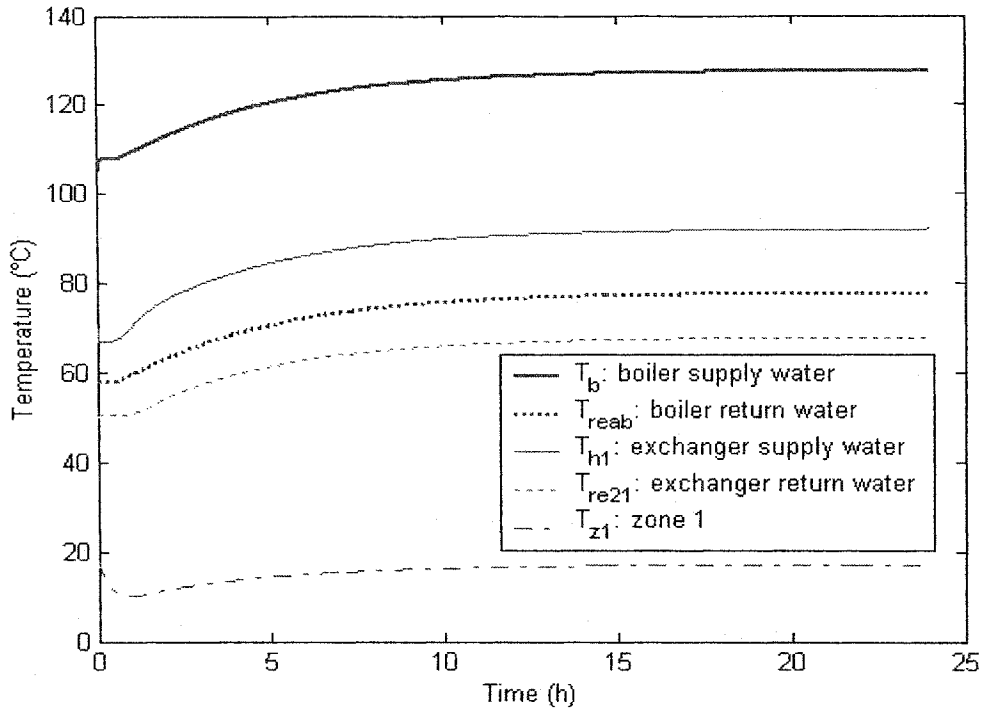

Figure 3.10 OLT: temperature responses with heat losses and without solar radiation

The temperature responses with heat losses in the IDHS system is presented in Figure 3.10. Comparing with Figure 3.9, T_b, T_{reab}, T_{h1}, T_{re21}, and T_{z1} decrease because of the heat losses from piping network insulation and water leakage from the primary system. For example, at 24:00 hours, T_b, T_{reab}, T_{h1}, T_{re21}, and T_{z1} reach 127.60, 77.73, 92.11, 67.89, and 17.08°C respectively.

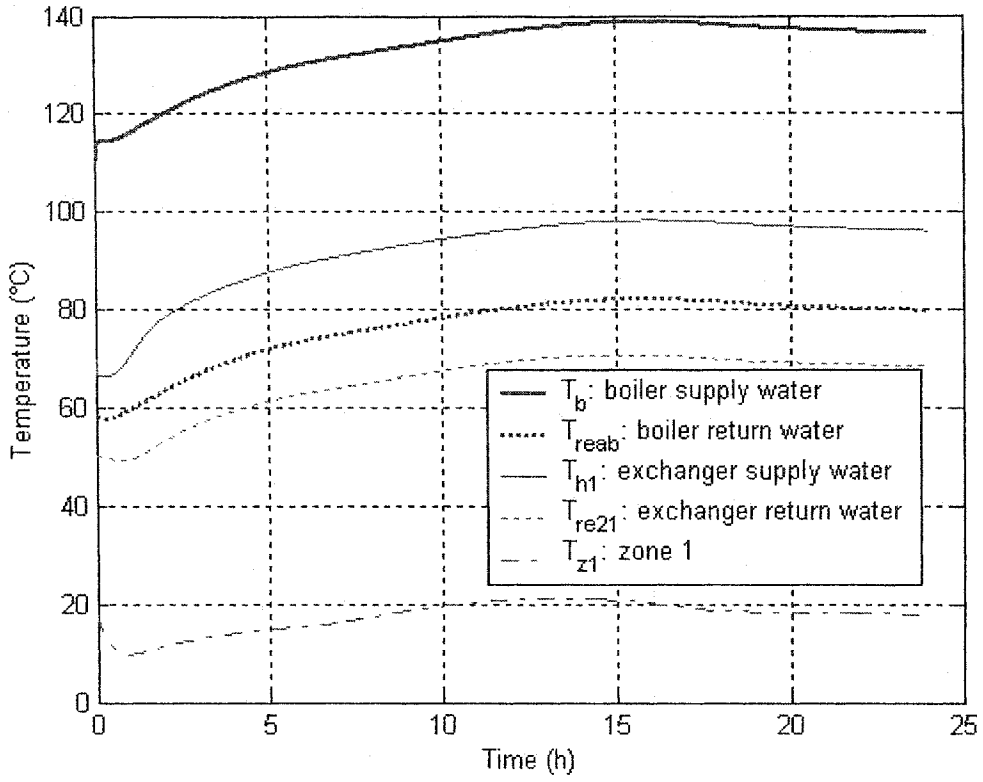

Figure 3.11 OLT: temperature responses with heat losses and solar radiation

The temperature responses affected by solar radiation are depicted in Figure 3.11. The largest value of indoor air temperature appears at 13:00 hours. However, the biggest value of the supply water temperature appears at 16:00 hours because the solar radiation impacts the heat transfer process slowly. In order to compensate the heat losses, the efficiency of the secondary system is taken into account. Therefore, the indoor air temperature reaches 18.14°C at 24:00 hours.

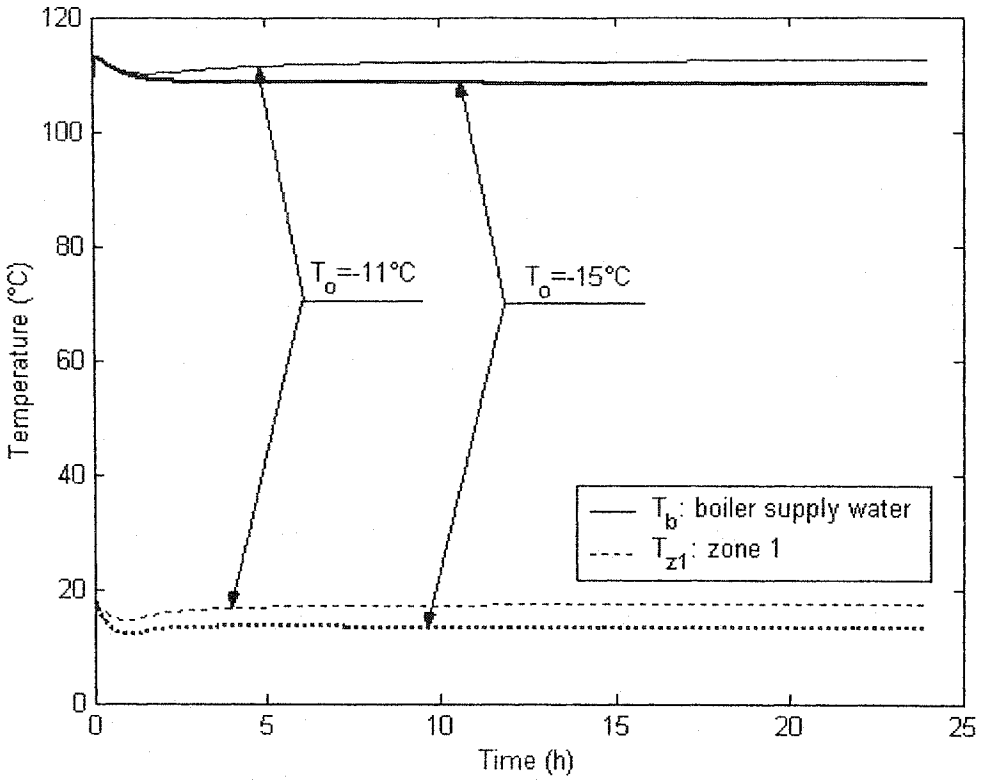

Figure 3.12 OLT: comparison with different outdoor air temperature (T_o=-11°C and T_o=-15°C)

It can be seen clearly from Figure 3.12 that when outdoor air temperature is less than the design outdoor air temperature, indoor air temperature decreases. The case might take place in heating season since the heating system design does not guarantee the designed indoor air temperature for all outdoor air temperature. In this case, for instance, T_b and T_{z1} reach 112.30°C and 17.25°C at T_o=-11°C, while they reach 108.39°C and 13.29°C at T_o=-15°C.

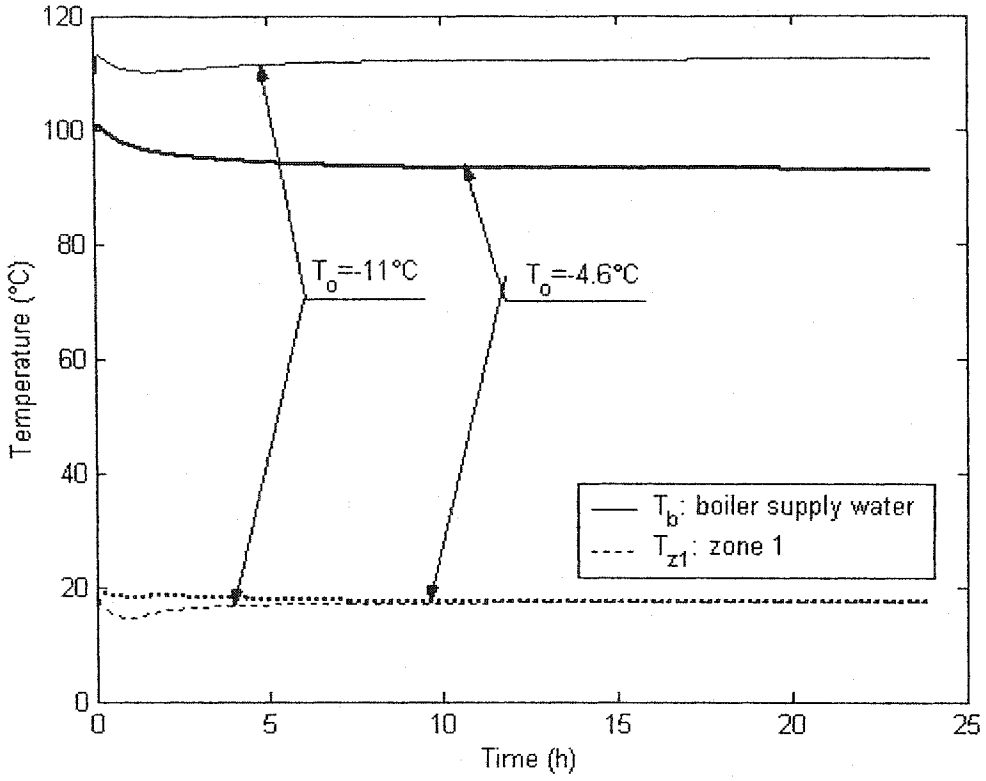

Figure 3.13 OLT: comparison with different outdoor air temperature (T_o= -11°C and T_o= -4.6°C)

In order to obtain the same indoor air temperature, the fuel consumption and the supply water temperature should be different. Figure 3.13 shows this case. The supply temperatures reach 112.3°C and 92.91°C when indoor air temperatures reach the same value 17.25°C with different outdoor air temperature at 24:00 hours. Moreover, the fuel consumption is 77.41% compared to the design outdoor air temperature.

In addition, the heat losses from piping insulation and water leakage in the primary and secondary system are studied in order to find the percentage of component heat losses. The results are presented in Figure 3.14. The pie chart shows heat loss from the makeup water in primary system is the lowest, while heat loss from the makeup water in

secondary system is the largest up to 6.1% except for considering boiler efficiency. Note that effective heat utilization of the system is 78.7%, and total heat losses add up to 21.3%.

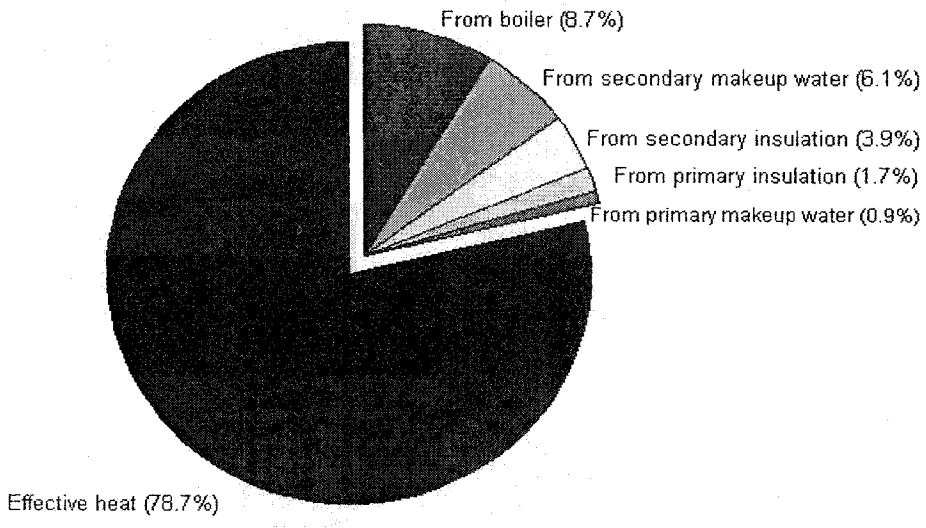

Figure 3.14 Component heat losses and heat utilization efficiency in the IDHS

Chapter 4 Optimization of Operating Parameters

4.1 Introduction

The total energy consumption in a district heating system consists of electrical power for running supply fan, exhaust fan, circulating pump, makeup water pump, and fuel consumed. In general, the electrical power consumption is less than 25% of the total energy consumption.

Researchers addressed several approaches such as using variable speed devices, designing optimal controllers, and optimal control strategies to save energy [5, 30]. These methods are based on air handling systems in buildings. Therefore, it is necessary to study the specific issues relevant to optimal operation of DHS.

Significant energy is consumed by large district heating systems. However, operating the boiler at as high efficiency as possible at the given load and through selecting optimal set points can achieve significant energy savings. To this end, a constrained optimization problem was formulated and solved. The idea behind this is that if the boiler control loop can track an energy optimal set point profile, significant energy savings can be realized. The method of multi-variable constraint optimization is utilized to obtain the optimal set point T_b. The optimization approach consists of defining an objective function and specifying the constraints.

The operating costs of the DHS are function of heating load. In other words, energy consumption (fuel consumption) depends on outdoor weather condition. Also, electricity

consumption by fans and pumps, and water consumption by compensating water leakage are influenced by load. As a result, the objective function in the optimization problem should include the effects of variables such as T_o, G_{cp}, G_{sf}. A multi-variable constraint optimization function was developed to obtain optimal operating set points based on different weather conditions for both DDHS and IDHS.

The optimal operating condition and design operating condition are defined first because they are quoted frequently in the thesis. Optimal operating condition refers to the operating condition that has the minimal operating cost. Design operating condition refers to the operating condition where the circulating water flow rate is constant and equals to the design circulating water flow rate.

4.2 Optimization of DDHS operating parameters

4.2.1 Optimization methodology

The method of multi-variable constraint optimization was used to solve this problem. To begin, the objective function requires establishing the variables that include all of the energy consumption elements. Then, constraints such as linear and nonlinear relationships with equality and inequality should be described. After that, upper bounds, lower bounds, and initial values of these variables should be chosen. A computer program was developed to find the optimal situation.

Thirteen variables such as G_{cp}, G_{sf}, G_{ef}, G_f, T_s, T_{re}, T_{s_d}, T_{re_d}, T_{zup}, T_{zlow}, e_b, r_Q, and α were used in the optimization. The upper and lower bounds of the variables are given in Table 4.1.

Table 4.1 Upper and lower bounds of the variables for the DDHS

Variable	G_{cp}	G_{sf}	G_{ef}	G_f	T_s	T_{re}	T_{s_d}
Uint	kg/s	m^3/s	m^3/s	kg/s	°C		
Lower bounds	8.333	0.833	0	0.01	20	20	20
Upper bounds	83.333	2.778	0	0.5	95	70	95
Variable	T_{re_d}	T_{zup}	T_{zlow}	e_b	r_Q	α	
Uint	°C			%			
Lower bounds	20	17	17	0.3	0.01	0.5	
Upper bounds	70	19	19	0.99	1.1	10	

Objective function

The aim of the optimization is to minimize the objective function in order to fulfill the minimum operating cost. The objective function is defined in Equation (4.1) and simplified in Equation (4.2).

$$J = \int (J_e + J_w + J_f)dt \tag{4.1}$$

$$J_{\min} = \int_0^t [E_p(N_{sf} + N_{ef} + N_{cp} + N_{mp}) + 3.6W_p G_{mp} + 3600O_p G_f]dt \tag{4.2}$$

$$N_{sf} = 1.6489G_{sf}^{\ 2} - 5.6008G_{sf} + 10.6054 \tag{4.3}$$

$$N_{ef} = f_{se}N_{sf} \tag{4.4}$$

$$N_{cp} = 0.0006G_{cp}^{\ 2} + 0.3738G_{cp} + 13.0354 \tag{4.5}$$

$$N_{mp} = 0.4645 f_{sw2} G_{cpd} \tag{4.6}$$

The optimization problem was defined as the minimization of J (Equation (4.2)) subject to steady state constraints for the model Equations (3.1) through (3.47). The

steady state constraint equations were simplified to reduce the number of equations. The resulting equations are given below.

Linear and nonlinear equality constraints are described as follow.

$$A_{eq}X = b_{eq} \tag{4.7}$$

Where

$$X = [G_{cp}, G_{sf}, G_{ef}, G_f, T_s, T_{re}, T_{s\_d}, T_{re\_d}, T_{zup}, T_{zlow}, e_b, r_Q, \alpha]',$$

$$A_{eq} = [0,1,0,\frac{-\alpha V_{air}(273+T_{in})}{273},0,0,0,0,0,0,0,0,0],$$

$$b_{eq} = 0.$$

$$r_Q = \frac{G_f hv}{Q_{boiler}} \tag{4.8}$$

$$\alpha = 4.7321 r_Q^{\ 2} - 9.7036 r_Q + 6.32 \tag{4.9}$$

$$T_{ou} = 3.5714 r_Q^{\ 2} + 26.2857 r_Q + 137.6 \tag{4.10}$$

$$q_2 = 0.01[f_m + f_n \alpha (1 - 0.01 q_4)](T_{ou} - T_e) \tag{4.11}$$

$$q_5 = 11.8029 r_Q^{\ 2} - 20.3514 r_Q + 9.126 \tag{4.12}$$

$$e_b = 1 - 0.01(q_2 + q_3 + q_4 + q_5 + q_6) \tag{4.13}$$

$$T_s = T_z + \frac{(T_{sd} + T_{red} - 2T_{zd})}{2}[\frac{T_z - T_o}{f_{ha}(T_{zd} - T_{od})}]^{\frac{1}{1+bh}} + \frac{G_{cpd}(T_{sd} - T_{red})(T_z - T_o)}{2G_{cp}(T_{zd} - T_{od})} \tag{4.14}$$

$$T_{re} = T_z + \frac{(T_{sd} + T_{red} - 2T_{zd})}{2}[\frac{T_z - T_o}{f_{ha}(T_{zd} - T_{od})}]^{\frac{1}{1+bh}} - \frac{G_{cpd}(T_{sd} - T_{red})(T_z - T_o)}{2G_{cp}(T_{zd} - T_{od})} \tag{4.15}$$

$$T_{s\_d} = T_z + \frac{(T_{sd} + T_{red} - 2T_{zd})}{2}[\frac{T_z - T_o}{f_{ha}(T_{zd} - T_{od})}]^{\frac{1}{1+bh}} + \frac{(T_{sd} - T_{red})(T_z - T_o)}{2(T_{zd} - T_{od})} \tag{4.16}$$

$$T_{re\_d} = T_z + \frac{(T_{sd} + T_{red} - 2T_{zd})}{2}\left[\frac{T_z - T_o}{f_{ha}(T_{zd} - T_{od})}\right]^{\frac{1}{1+bh}} - \frac{(T_{sd} - T_{red})(T_z - T_o)}{2(T_{zd} - T_{od})} \quad (4.17)$$

$$\frac{T_{zup} - T_o}{T_{zd} - T_o} = \left(\frac{T_s - \frac{T_s - T_{re}}{2n} - T_{zup}}{T_{s\_d} - \frac{T_{s\_d} - T_{re\_d}}{2n} - T_{zd}}\right)^{1+bh} \quad (4.18)$$

$$\frac{T_{zlow} - T_o}{T_{zd} - T_o} = \left(\frac{T_{re} + \frac{T_s - T_{re}}{2n} - T_{zlow}}{T_{re\_d} + \frac{T_{s\_d} - T_{re\_d}}{2n} - T_{zd}}\right)^{1+bh} \quad (4.19)$$

$$G_f = \frac{1}{e_b hv}\left[\frac{T_s + T_{re} - 2T_{soil}}{\frac{1}{2\pi r_i L_t h_i} + \frac{\ln(\frac{r_e + d_e}{r_e})}{2\pi k_{ins} L_t}} + c_w G_{cp}(T_s - T_{re}) + c_w G_{mp}(T_s - T_{sw2})\right] \quad (4.20)$$

4.2.2 Simulation results of DDHS

Simulation results showing the optimization process are depicted in Figure 4.1. The results correspond to outdoor air temperature of -7°C.

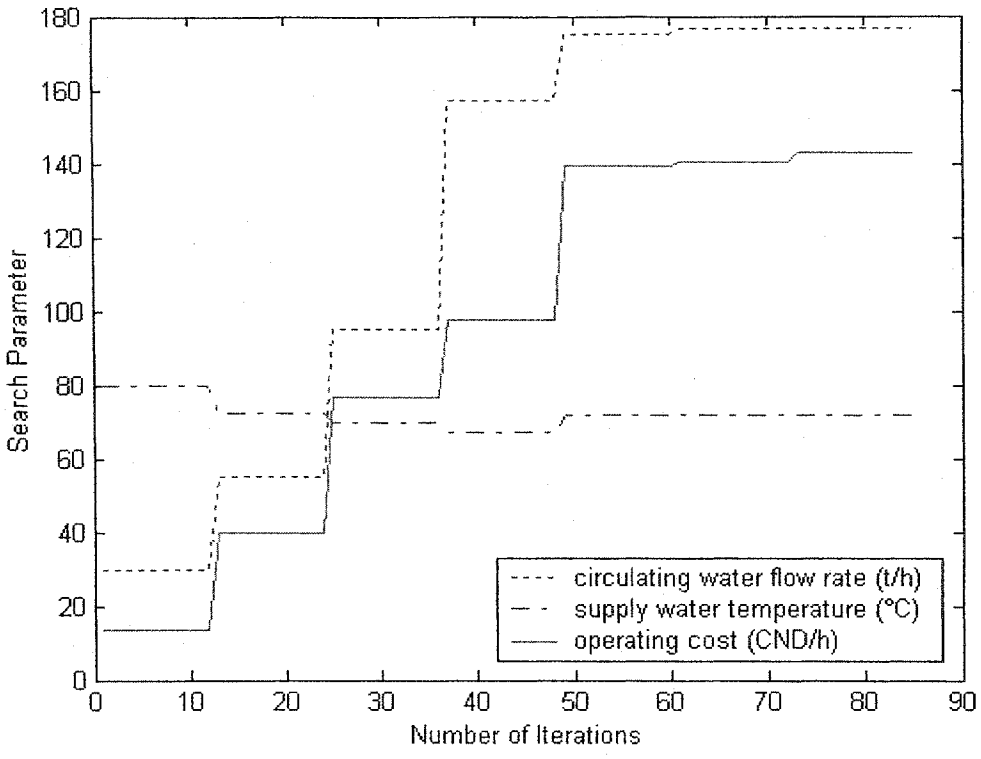

Figure 4.1 Optimizing process at T_o= -7°C

At the beginning, the computer program sets the initial value of each variable, and then tries to find the point that satisfies all of the constraints. After searching 85 times, J, G_{cp}, and T_s reach their optimal values 142.76CND/h, 176.74t/h, and 71.75°C respectively as shown in Figure 4.1.

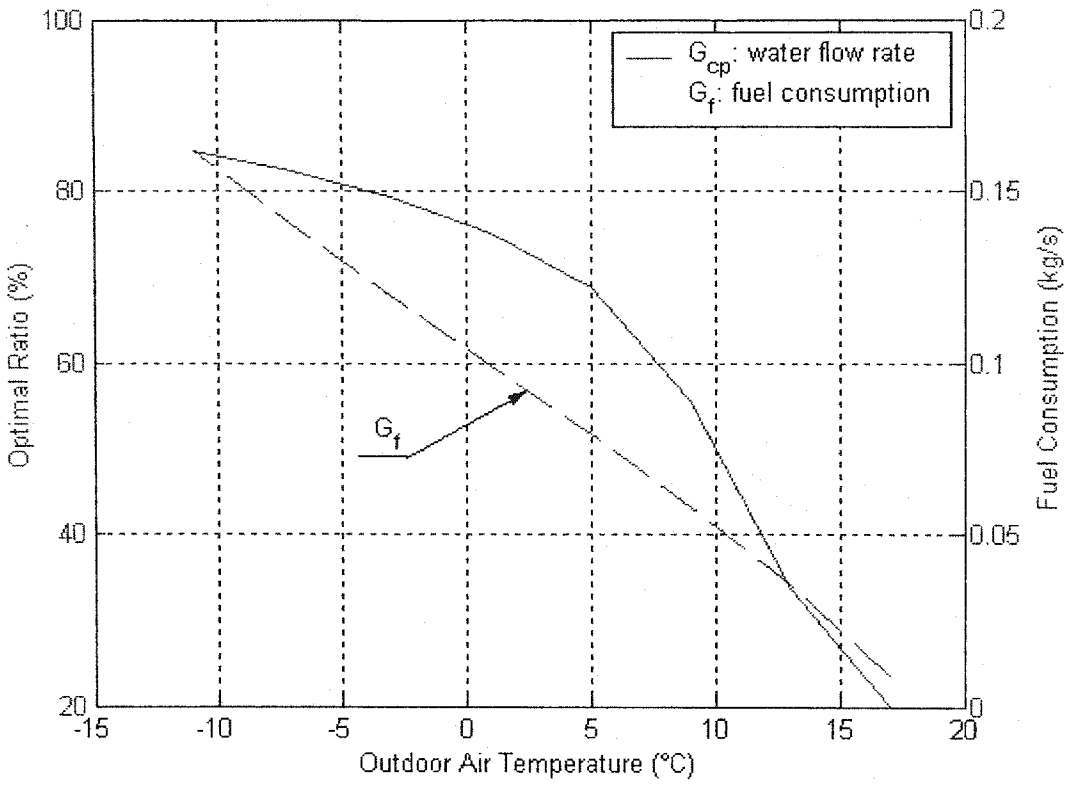

Figure 4.2 Optimal circulating water flow rate and fuel consumption

The optimal circulating water flow rate ratio shown in Figure 4.2 increases from 20.12% to 84.74% compared to the design circulating water flow rate when the outdoor air temperature varies from 17°C to –11°C. Moreover, it has nonlinear relationship between G_{cp} and T_o. Therefore, it is the most economical to vary the speed of circulating water pump to modulate the water flow rate continuously as a function of T_o. Note that the relationship between G_f and T_o is nonlinear because the efficiency of the boiler is a nonlinear function of the ratio of heating load r_Q.

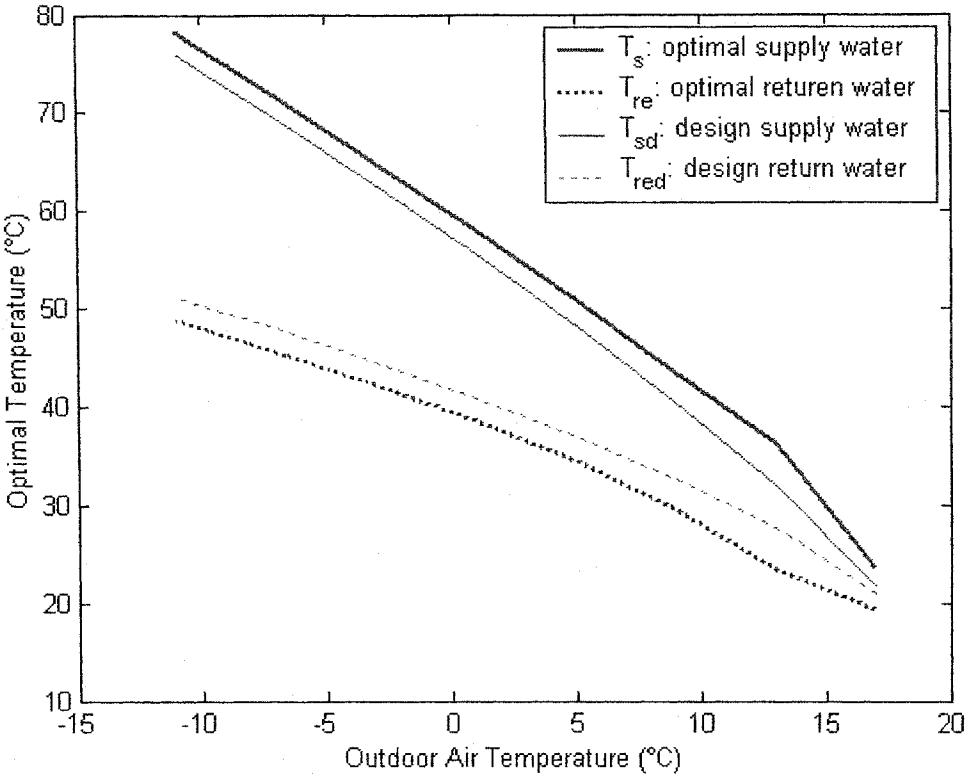

Figure 4.3 Optimal and design operating temperatures

Figure 4.3 shows the optimal operating temperatures and design operating temperatures as a function of T_o. When T_o=-11°C, for instance, T_s, T_{re}, T_{sd}, and T_{red} are 78.34°C, 48.84°C, 76.09°C, and 51.09°C respectively.

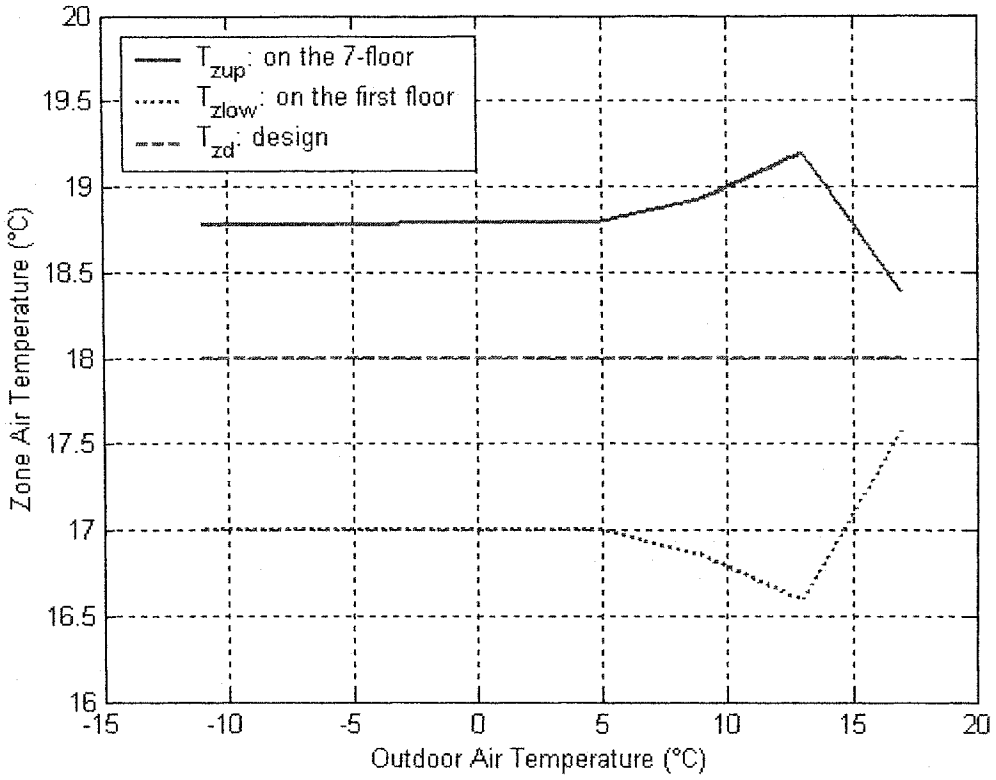

Figure 4.4 Indoor air temperatures with optimal operation

Figure 4.4 depicts the response of the indoor air temperature as a function of outdoor air temperature. When outdoor air temperature is higher than the temperature at the beginning of heating season (5°C), indoor air temperatures on the 7-floor and first floor show opposite trends. When outdoor air temperature is less than 5°C, indoor air temperature on the 7-floor tends to reach the highest temperature (18.78°C), while the temperature on the first floor tends to reach the lowest temperature (17°C). Moreover, although indoor air temperature on the first floor equals to 17°C, indoor air temperature on the highest floor never reach the upper bound temperature. The reason is due to decreased surface temperature of terminal heater caused by the return water. Note that the

constraints are not satisfied at all outdoor temperatures for example, especially when outdoor air temperature is in the 6°C to 14°C range.

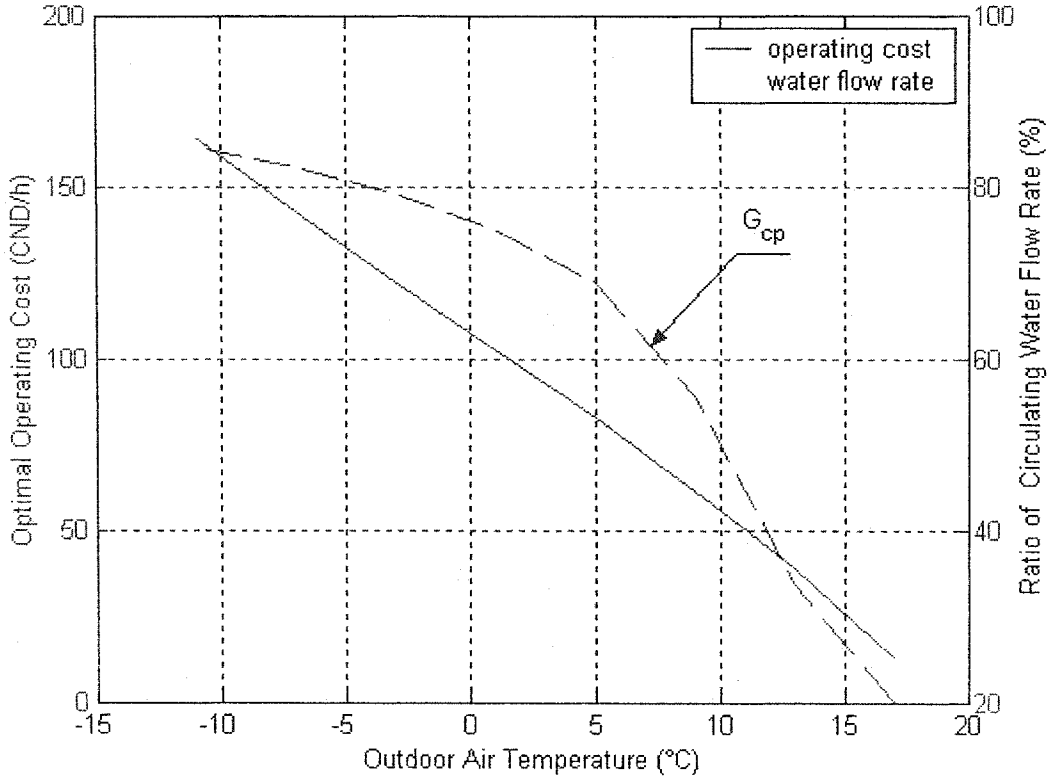

Figure 4.5 J and G_{cp} as a function of outdoor air temperature

Figure 4.5 shows the relationship for optimal operating cost and optimal circulating water flow rate as a function of outdoor air temperature. When T_o decreases, optimal circulating water flow rate and operating cost increase simultaneously. For example, when T_o reduces from 1°C to –3°C, J and G_{cp} reach 102.61CND/h, 122.46CND/h, 75.02%, and 79.31% respectively.

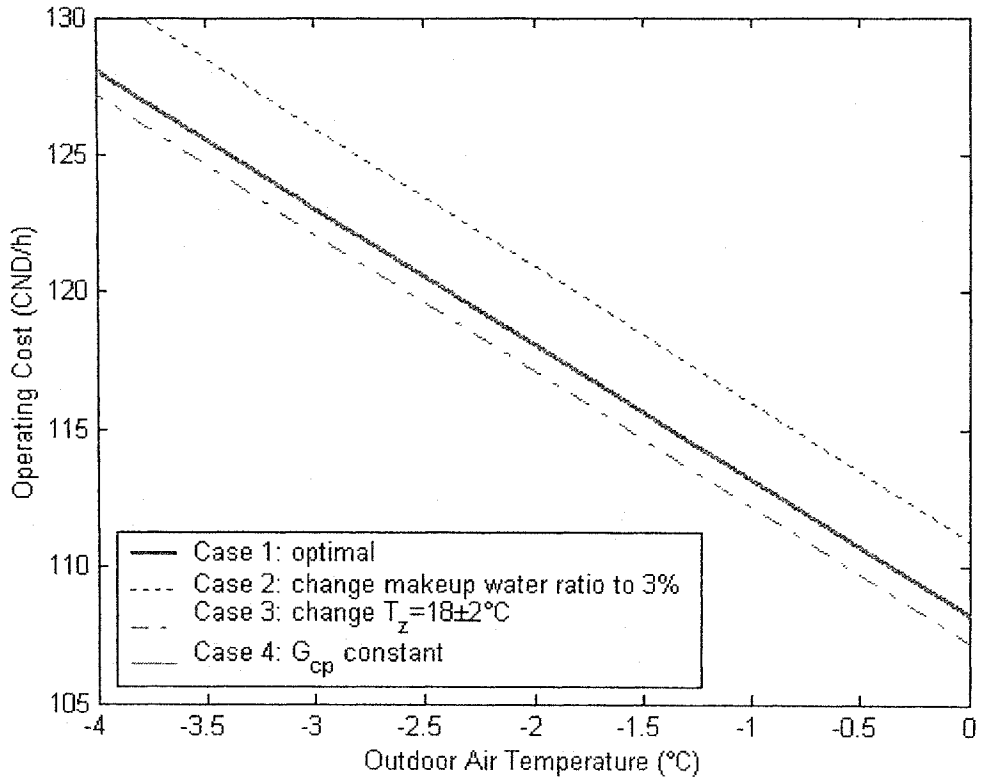

Figure 4.6 Comparison of operating costs with four cases

When the DDHS does not operate under optimal condition, operating cost will be higher. Four cases are considered to make comparisons. These are:

Case 1: optimal operation,

Case 2: increasing makeup water flow rate from 1% to 3%,

Case 3: increasing the range of the indoor air temperature from 18±1°C to 18±2°C, and

Case 4: keeping design circulating water flow rate as actual circulating water flow rate.

The comparisons of operating costs are depicted in Figure 4.6. In Case 3, the operating cost is reduced because of decreasing indoor air temperature. However, this is

not desirable. Largest operating cost occurs in Case 2 because of the operating cost includes not only the amount of makeup water but also the heat loss from water leakage. For example, the operating cost in Case 2 increases by 2.5% compared with the optimal case (Case 1) at –2°C. Case 4 and Case 1 are very similar since the pumping cost account for a small contribution of the total operating cost.

4.3 Optimization of IDHS operating parameters

4.3.1 Optimization methodology

The major deference in the optimization problem between the IDHS and the DDHS is the additional heat transfer process in each heat exchange station. For simplicity, all heat exchangers were aggregated and represented as an equivalent heat exchanger. A computer program was also developed using the constraint optimization methodology.

In the optimization program, eighteen variables were chosen as follows: G_{sf}, G_{ef}, G_1, G_2, G_f, T_b, T_{re1}, T_h, T_{re2}, T_{b_d}, T_{re1_d}, T_{h_d}, T_{re2_d}, T_{zup}, T_{zlow}, e_b, r_Q, and α. The upper and lower bounds of these variables are listed in Table 4.2. The set of Equations describing the optimization problems are given in (4.21) thru (4.52).

Table 4.2 Upper and lower bounds of the variables for the IDHS

Variable	G_{sf}	G_{ef}	G_1	G_2	G_f	T_b	T_{re1}	T_h	T_{re2}
Uint	10^4 m^3/h		t/h		kg/s	°C			
Lower bounds	0.5	0.5	100	100	0.01	20	20	20	20
Upper bounds	9	12	885	2000	2.5	130	80	95	70
Variable	T_{b_d}	T_{re1_d}	T_{h_d}	T_{re2_d}	T_{zup}	T_{zlow}	e_b	r_Q	α
Uint	°C								
Lower bounds	20	20	20	20	17	17	0.3	0.01	1
Upper bounds	130	80	95	70	19	19	0.99	1.2	10

Objective function

The equations of the objective function for the IDHS is presented in Equations (4.21) and (4.22).

$$J = \int (J_{w1} + J_{w2} + J_e + J_f)dt \tag{4.21}$$

$$J_{\min} = \int_0^t [3.6W_p(G_{mp1} + G_{mp2}) + E_p(N_{sf} + N_{ef} + N_{cp1} + N_{cp2} + N_{mp1} + N_{mp2}) + 3600O_p G_f]dt \tag{4.22}$$

$$N_{sf} = -0.3655G_{sf}^{\ 2} + 5.0583G_{sf} + 54.1786 \tag{4.23}$$

$$N_{ef} = -0.6976G_{ef}^{\ 2} + 14.9905G_{ef} + 28.625 \tag{4.24}$$

$$N_{cp1} = 1.5476G_{cp1}^{\ 2} - 15.0595G_{cp1} + 418.8869 \tag{4.25}$$

$$N_{cp2} = 0.4286G_{cp2}^{\ 2} - 6.6143G_{cp2} + 483.2671 \tag{4.26}$$

$$N_{mp1} = 0.1465 f_{sw1} G_{1d} \tag{4.27}$$

$$N_{mp2} = 0.1101 f_{sw2} G_{2d} \tag{4.28}$$

Note that the units of G_{sf}, G_{ef}, G_{cp1}, and G_{cp2} in Equations from (4.23) to (4.26) are $10^{-4}m^3/h$, $10^{-4}m^3/h$, $10^{-2}t/h$, and $10^{-2}t/h$ respectively.

Linear and nonlinear equality constraints

$$A_{eq}X = b_{eq} \tag{4.29}$$

Where

$$X = [G_{sf}, G_{ef}, G_1, G_2, G_f, T_b, T_{re1}, T_h, T_{re2}, T_{b\_d}, T_{re1\_d}, T_{h\_d}, T_{re2\_d}, T_{zup}, T_{zlow}, e_b, r_Q, \alpha]',$$

$$A_{eq} = \begin{bmatrix} 1 & 0 & 0 & 0 & -0.36\alpha V_{air}\frac{273+T_{in}}{273} & 0 & 0 & 0 & 0 & 0 & 0 & 0 & 0 & 0 & 0 & 0 & 0 & 0 \\ -1.5 & 1 & 0 & 0 & 0 & 0 & 0 & 0 & 0 & 0 & 0 & 0 & 0 & 0 & 0 & 0 & 0 & 0 \end{bmatrix},$$

$b_{eq} = [0,0]'$.

The simplified steady state constraints are defined as shown in the following:

$$r_Q = \frac{G_f hv}{Q_{boiler}} \tag{4.30}$$

$$\alpha = 3.3929 r_Q^{\ 2} - 7.4214 r_Q + 5.37 \tag{4.31}$$

$$T_{ou} = 5.3571 r_Q^{\ 2} + 33.9286 r_Q + 127.99 \tag{4.32}$$

$$q_2 = 0.01[f_m + f_n \alpha (1 - 0.01 q_4)](T_{ou} - T_e) \tag{4.33}$$

$$q_5 = 9.6429 r_Q^{\ 2} - 16.9714 r_Q + 8 \tag{4.34}$$

$$e_b = 1 - 0.01(q_2 + q_3 + q_4 + q_5 + q_6) \tag{4.35}$$

$$f_{d1} = \frac{G_{1d}(T_{bd} - T_{re1d})}{T_{zd} - T_{od}} \tag{4.36}$$

$$f_{d2} = \frac{T_{bd} - T_{hd} - T_{re1d} + T_{re2d}}{(T_{zd} - T_{od}) \ln \dfrac{T_{bd} - T_{hd}}{T_{re1d} - T_{re2d}}} \tag{4.37}$$

$$f_{d3} = \frac{G_{2d}(T_{hd} - T_{re2d})}{T_{zd} - T_{od}} \tag{4.38}$$

$$f_{d4} = \frac{(0.5T_{hd} + 0.5T_{re2d} - T_{zd})^{1+bh}}{T_{zd} - T_{od}} \tag{4.39}$$

$$G_1(T_b - T_{re1}) e_1 e_2 = f_{d1}(T_z - T_o) \tag{4.40}$$

$$f_{ea} e_2 \frac{T_b - T_h - T_{re1} + T_{re2}}{\ln \dfrac{T_b - T_h}{T_{re1} - T_{re2}}} = f_{d2}(T_z - T_o) \tag{4.41}$$

$$G_2 e_2 (T_h - T_{re2}) = f_{d3}(T_z - T_o) \tag{4.42}$$

$$f_{ha}(0.5T_h + 0.5T_{re2} - T_z)^{1+bh} = f_{d4}(T_z - T_o) \tag{4.43}$$

$$G_{1d}(T_{b\_d} - T_{re1\_d})e_1 e_2 = f_{d1}(T_z - T_o) \tag{4.44}$$

$$f_{ea} e_2 \frac{T_{b\_d} - T_{h\_d} - T_{re1\_d} + T_{re2\_d}}{\ln \dfrac{T_{b\_d} - T_{h\_d}}{T_{re1\_d} - T_{re2\_d}}} = f_{d2}(T_z - T_o) \tag{4.45}$$

$$G_{2d} e_2 (T_{h\_d} - T_{re2\_d}) = f_{d3}(T_z - T_o) \tag{4.46}$$

$$f_{ha}(0.5T_{h\_d} + 0.5T_{re2\_d} - T_z)^{1+bh} = f_{d4}(T_z - T_o) \tag{4.47}$$

$$\frac{T_{zup} - T_o}{T_{zd} - T_o} = \left(\frac{T_h - \dfrac{T_h - T_{re2}}{2n} - T_{zup}}{T_{h\_d} - \dfrac{T_{h\_d} - T_{re2\_d}}{2n} - T_{zd}} \right)^{1+bh} \tag{4.48}$$

$$\frac{T_{zlow} - T_o}{T_{zd} - T_o} = \left(\frac{T_{re2} + \dfrac{T_h - T_{re2}}{2n} - T_{zlow}}{T_{re2\_d} + \dfrac{T_{h\_d} - T_{re2\_d}}{2n} - T_{zd}} \right)^{1+bh} \tag{4.49}$$

$$q_{ins} = U_{f1}(T_b + T_{re1} - 2T_{soil}) + U_{f2}(T_h + T_{re2} - 2T_{soil}) \tag{4.50}$$

$$q = c_w G_1 (T_b - T_{re1}) + c_w G_{mp1}(T_b - T_{sw1}) + c_w G_{mp2}(T_h - T_{sw2}) + q_{ins} \tag{4.51}$$

$$G_f = \frac{q}{e_b h v} \tag{4.52}$$

4.3.2 Simulation results

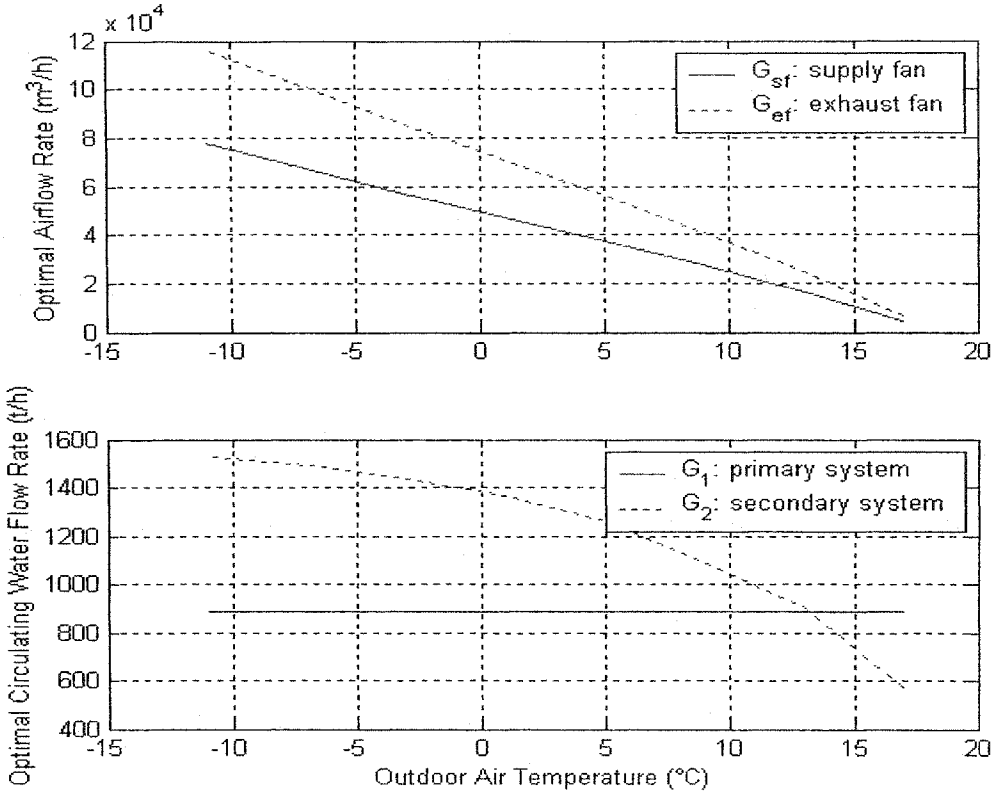

Figure 4.7 Optimal operating flow rates of fans and circulating pumps

Figure 4.7 shows that the optimal operating airflow rates (combustion air) and circulating water flow rates as a function of outdoor air temperature. When T_o= -7°C, for example, the magnitudes of G_{sf}, G_{ef}, G_1, and G_2 are 6555m^3/h, 9861m^3/h, 885t/h, and 1458t/h respectively. The relationship between airflow rate and outdoor air temperature is approximately linear. In addition, this figure also depicts the obvious difference in the optimal operating water flow rates in the primary and secondary system. In the primary system, the optimal circulating water flow rate remains constant and is limited by its upper bound. However, in the secondary system, the optimal circulating water flow rate changes depending on the outdoor air temperature. Moreover, the circulating water flow

rate is 84.76% compared to the design circulating water flow rate at T_o=-11°C. In other words, the circulating water temperature difference in the secondary system should be larger than that in the design case.

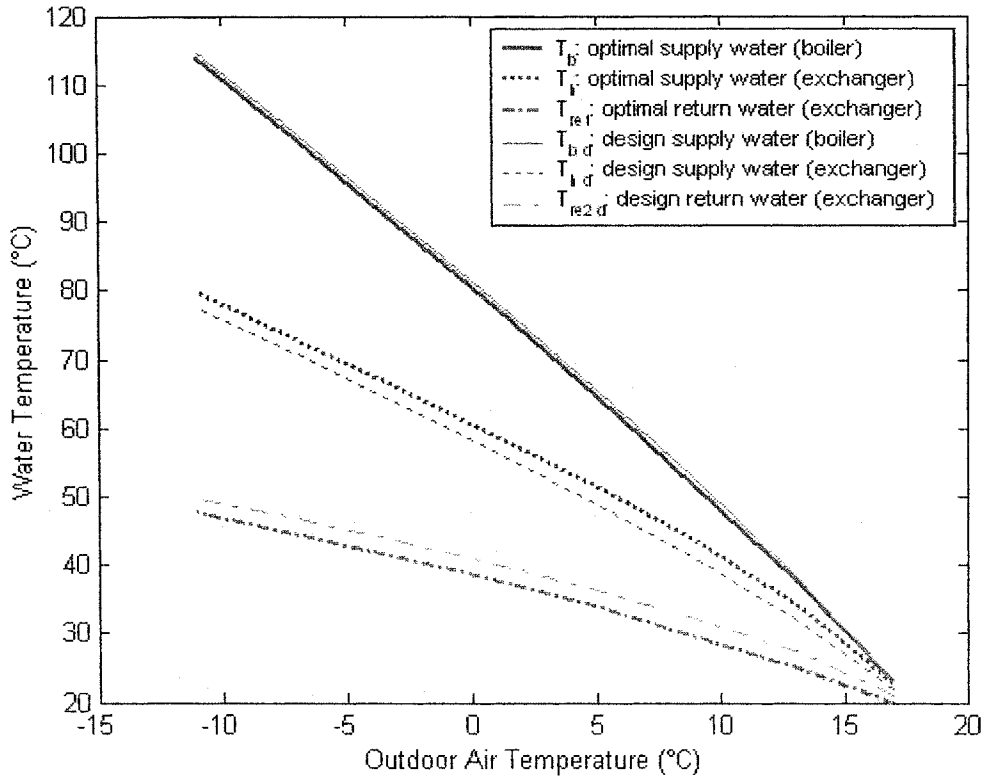

Figure 4.8 Comparison of optimal and design optimal operating supply water temperature

The optimal supply water temperature in the primary system is 0.2°C ~2°C less than that of the design operating condition shown in Figure 4.8. On the other hand, the optimal supply and return water temperature difference in the secondary system is greater than that in design condition because the optimal circulating water flow rate in the secondary system is reduced. Also, the decreased circulating water flow rate can reduce operating cost. The optimal supply water temperature of the boiler can be used as optimal set points to control the system operation.

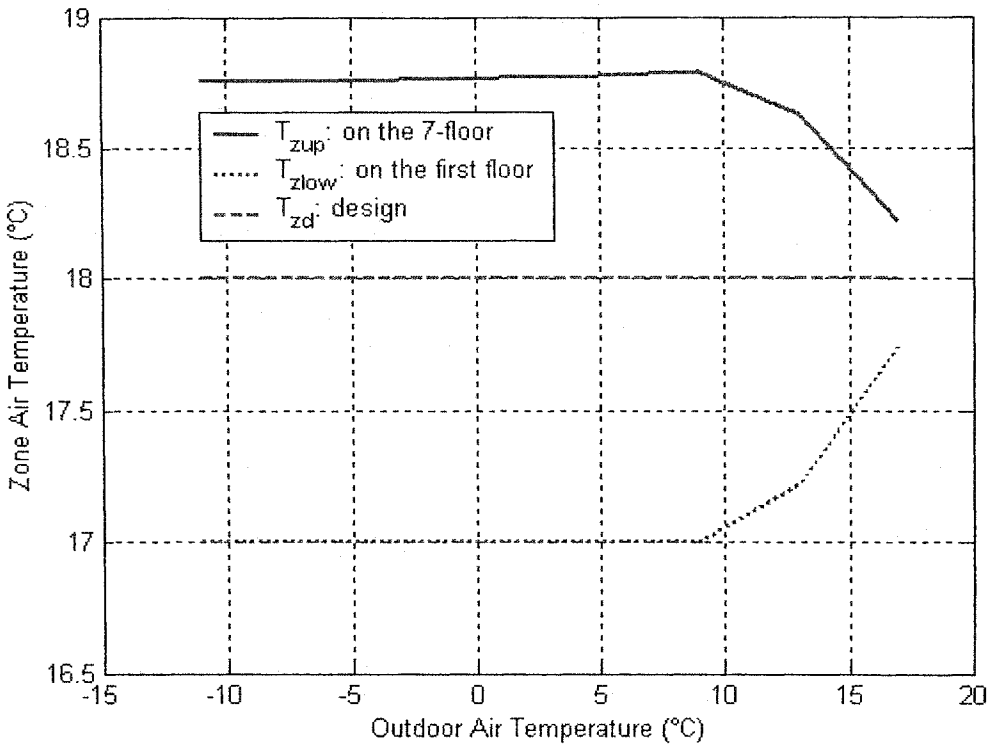

Figure 4.9 Optimal indoor air temperature

Figure 4.9 illustrates the indoor air temperature trends when outdoor air temperature changes. This behavior is similar to the one observed in DDHS.

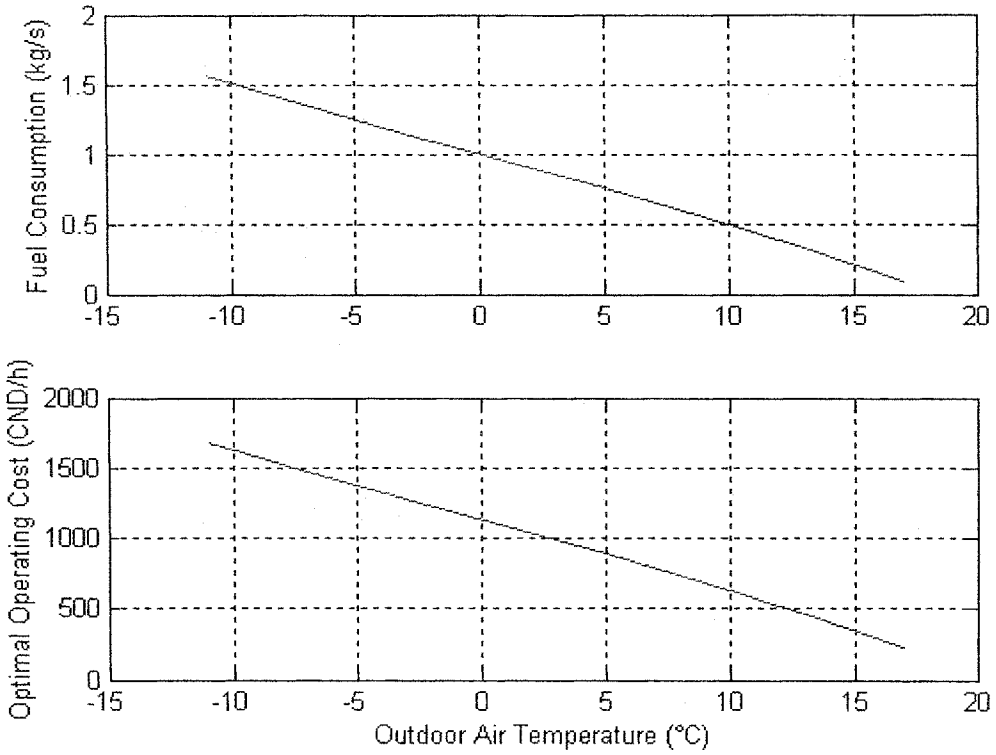

Figure 4.10 Fuel consumption and optimal operating cost

Fuel consumption and operating cost as a function of outdoor air temperature are illustrated in Figure 4.10. The relationship between the optimal operating cost and outdoor air temperature seems like linear although it is nonlinear actually. The reason is that the fuel cost is the largest part of the operating cost. At an outdoor air temperature of -11°C, the fuel consumption and operating cost are 1.54kg/s and 1662CND/h respectively.

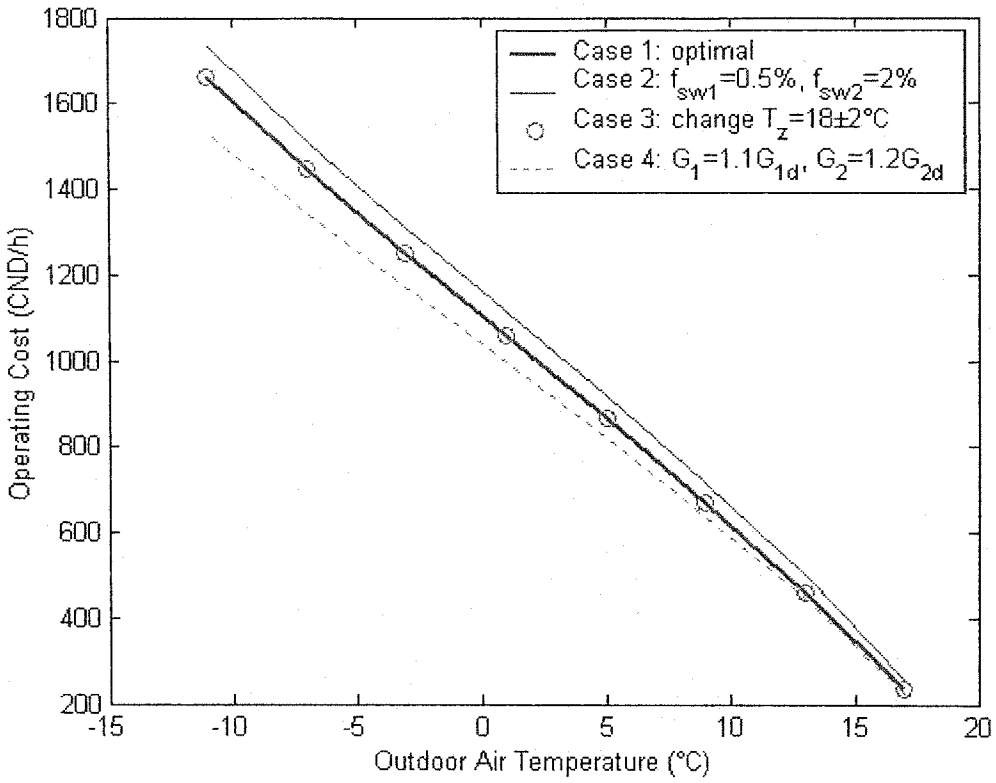

Figure 4.11 Comparison of operating costs with four cases

The effect of varying the operating conditions on cost was examined by carrying out simulation runs. For this purpose four cases were defined.

Case 1: optimal operation,

Case 2: increasing makeup water flow rate of the primary and secondary systems,

Case 3: increasing the range of the indoor air temperature from 18±1°C to 18±2°C, and

Case 4: keeping circulating water flow rate constant.

From the results shown in Figure 4.11 it is noted that, in Case 3, when the range of the indoor air temperature is increased from 18±1°C to 18±2°C, the operating cost shows no change because the average indoor air temperature does not change. In Case 4, when

the circulating water flow rates of the primary and secondary system keep increasing, the operating cost decreases about 2.9%~7.9% compared with Case 1 since the average of indoor air temperature is reduced by about 0.1°C~0.5°C. In Case 2, when the makeup flow rates in the primary and secondary system change from 0.3% and 1% to 0.5% and 2% respectively, the operating cost increases 11.5% and 4.6% compared with Case 1. It is clear that the makeup water ratio plays the most important role in operating cost of IDHS.

4.4 Typical daily and monthly optimal operating costs

Three different days such as warm, cool, and cold day were chosen for simulating typical daily operation. The average outdoor air temperature on these days were 5.12, -1.03, and –6.89°C respectively.

The optimal operating costs for the three days are shown in Figure 4.12 and 4.13. Note that on the cold day, the operating cost of the DHS is constant between 17:00 hours to 21:00 hours because outdoor air temperature at that time is lower than design outdoor air temperature. In other words, the required heat cannot be provided because of the limitations of the heating system, and indoor air temperature may be lower than design temperature. The optimal daily operating costs for the three days are 1950, 2729, and 3416CND for the DDHS, while they are 20497, 27917, and 34641CND for the IDHS, corresponding to warm, cool, and cold day respectively.

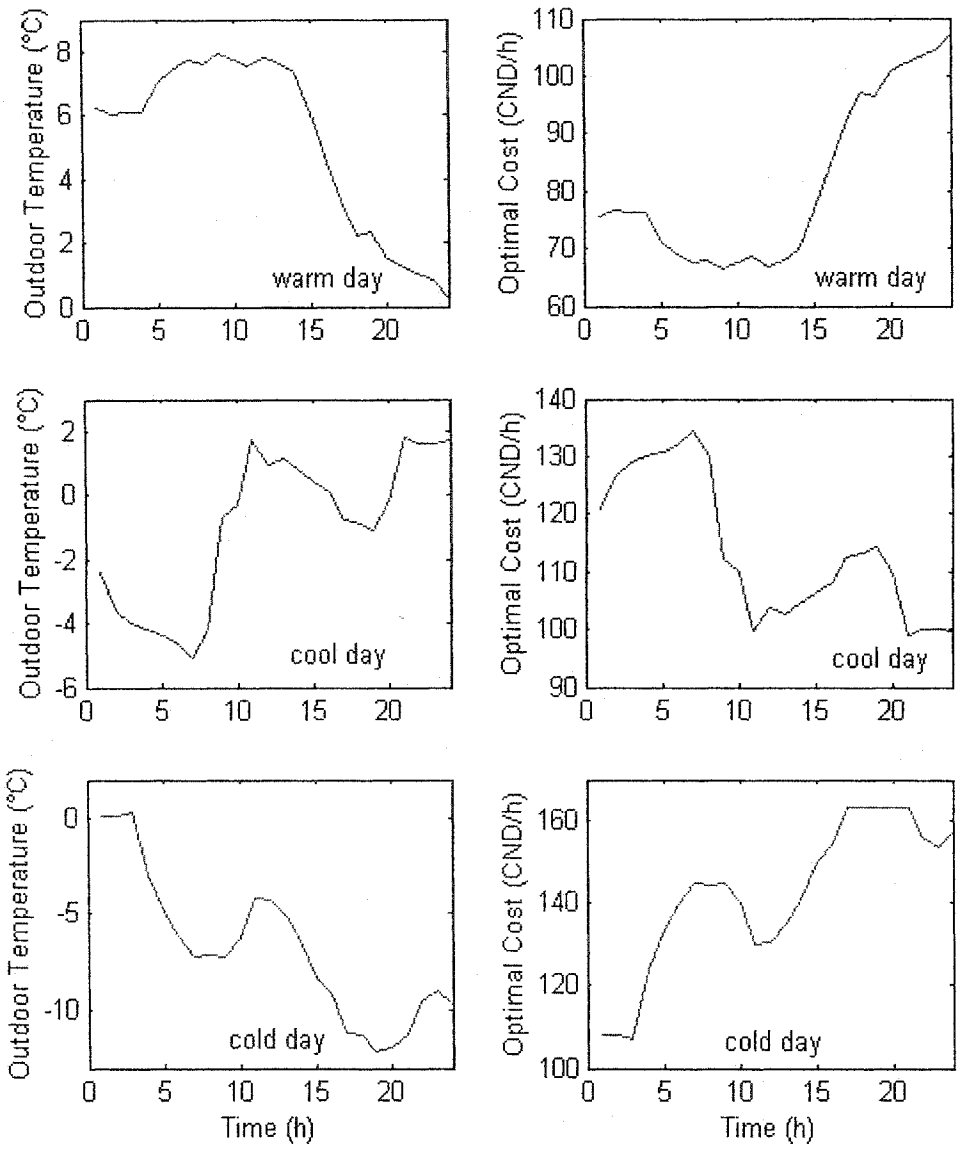

Figure 4.12 Optimal operating costs on warm, cool, and cold day in the DDHS

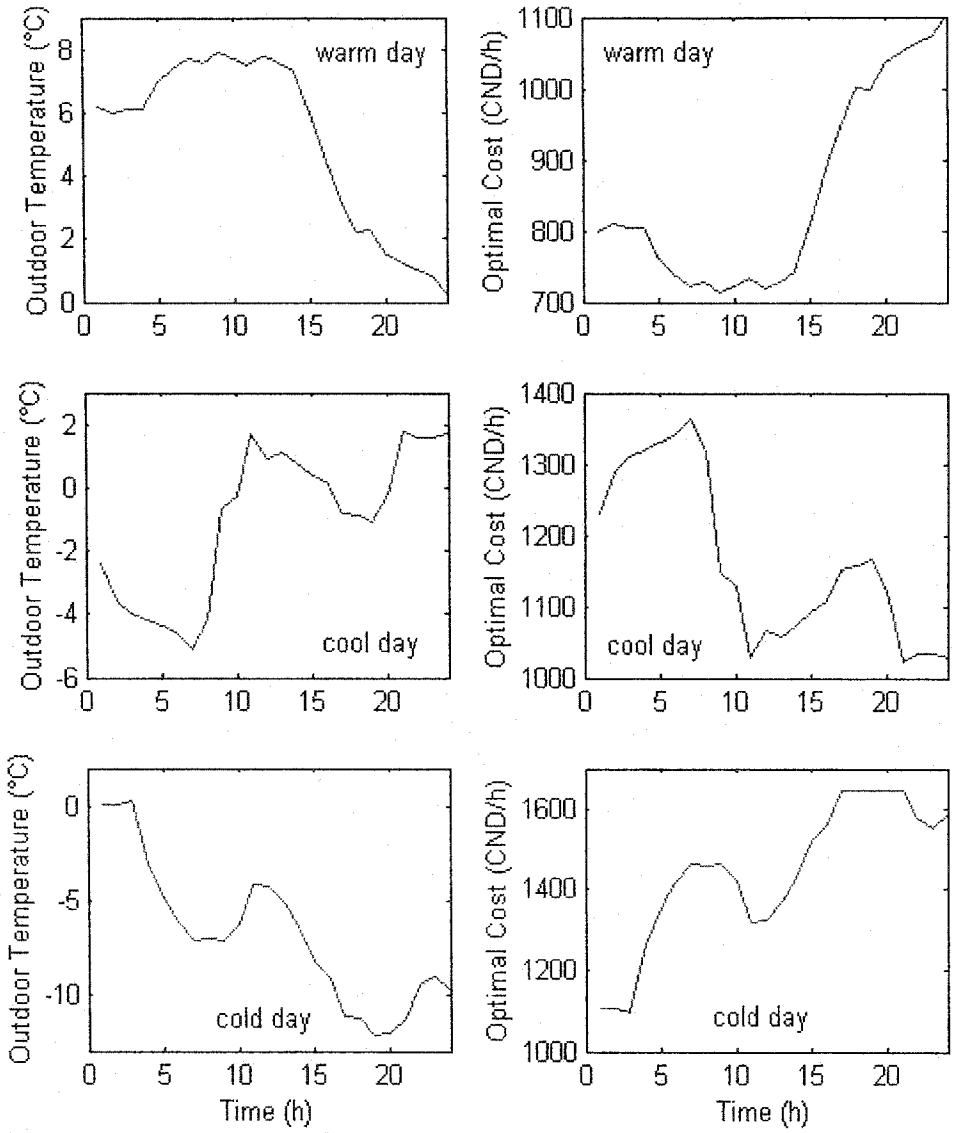

Figure 4.13 Optimal operating costs on warm, cool, and cold day in the IDHS

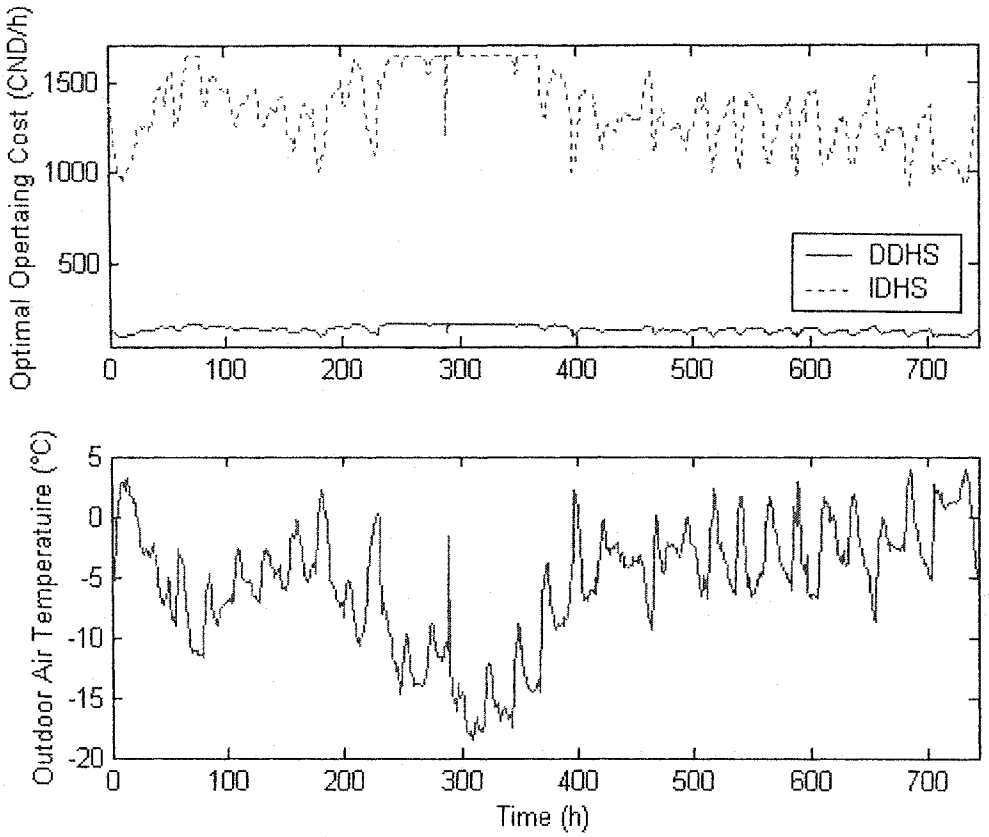

Figure 4.14 Optimal operating cost in Jan. 2001

Figure 4.14 depicts the optimal operating cost for the month of January 2001, for both DDHS and IDHS. Note that outdoor air temperatures on several days are lower than design condition, and they last for about four days. This case is called "no guarantee heating condition". Also, the average outdoor air temperature for this month is –5.4°C, and the monthly operating costs for the DDHS and IDHS are 9.8905×10^4CND and 1.0055 MCND respectively.

Chapter 5 A Control Strategy for Energy-Optimal Operation

5.1 Introduction

Since a DHS has a long transport time delay, special control strategy should be considered in order to improve the temperature response in real time operation. This is achieved by designing a Smith Predictor. The SP takes the transport time delay out of the closed-loop feedback control system. Therefore, the time delay is completely compensated if the system model is relatively accurate. In references [12, 13, 22, 25, 26, 27], the applications and the theory of control systems with time delay were described.

In this chapter, a reduced-order model of the DDHS is described and open-loop responses are presented. Then, a methodology for computing optimal set points of supply water temperature is described. Finally, a control strategy using the SP is designed, and simulation results showing the influences of different parameters and the use of optimal set points in improving energy efficiency are presented. Note that for design of the control strategy, the DDHS was considered. The same methodology can be applied to design the control strategy for the IDHS.

5.2 Reduced-order model of the DDHS

The full-order dynamic model of DDHS developed in Chapter 3 included 44 dynamic equations, which is too large for control design. Therefore, a reduced-order model is developed for the purpose of designing a control strategy. By using steady state approach, the dynamic equations are rewritten as

$$T_{i2} = \frac{T_{i3} + 2T_{i1}}{3} \tag{5.1}$$

$$T_{i3} = 0.5(T_{i4} + T_{i2}) \tag{5.2}$$

$$T_{i4} = \frac{2T_{wsi} + T_{i3}}{3} \tag{5.3}$$

$$T_{i6} = \frac{T_{i7} + 2T_{i5}}{3} \tag{5.4}$$

$$T_{i7} = 0.5(T_{i8} + T_{i6}) \tag{5.5}$$

$$T_{i8} = \frac{2T_{wothi} + T_{i7}}{3} \tag{5.6}$$

$$T_{i9} = \frac{2U_{rfi}T_{rfi} + U_{rf1i}T_o + S_{rfi}}{2U_{rfi} + U_{rf1i}} \tag{5.7}$$

$$T_{i10} = \frac{2U_{fi}T_{fi} + U_{f1i}T_{soil}}{2U_{fi} + U_{f1i}} \tag{5.8}$$

$$C_b \frac{d(T_b)}{dt} = U_b G_{f\max} hv[1 - F_{boiler}(\frac{T_{b\max}}{T_b})^{0.5}] - c_w G_{reab}(T_b - T_{reab}) - c_w G_{sw}(T_b - T_{sw2}) \tag{5.9}$$

$$T_{sab}(t) = \frac{c_w G_{sab} T_b(t - l_{ab}) + U_{insab} T_{soil} + c_w G_{swab} T_{sw2}}{c_w G_{sab} + U_{insab} + c_w G_{swab}} \tag{5.10}$$

$$T_{sbc}(t) = \frac{c_w G_{sbc} T_{sab}(t - l_{bc}) + U_{insbc} T_{soil} + c_w G_{swbc} T_{sw2}}{c_w G_{sbc} + U_{insbc} + c_w G_{swbc}} \tag{5.11}$$

$$T_{sbb1}(t) = \frac{c_w G_{sbb1} T_{sab}(t - l_{bb1}) + U_{insbb1} T_{soil} + c_w G_{swbb1} T_{sw2}}{c_w G_{sbb1} + U_{insbb1} + c_w G_{swbb1}} \tag{5.12}$$

$$T_{scd}(t) = \frac{c_w G_{scd} T_{sbc}(t - l_{cd}) + U_{inscd} T_{soil} + c_w G_{swcd} T_{sw2}}{c_w G_{scd} + U_{inscd} + c_w G_{swcd}} \tag{5.13}$$

$$T_{sd2}(t) = \frac{c_w G_{sz2} T_{scd}(t - l_{z2}) + U_{insd2} T_{soil} + c_w G_{swz2} T_{sw2}}{c_w G_{sz2} + U_{insd2} + c_w G_{swz2}} \tag{5.14}$$

$$T_{sc3}(t) = \frac{c_w G_{sz3} T_{sbc}(t - l_{z3}) + U_{insc3} T_{soil} + c_w G_{swz3} T_{sw2}}{c_w G_{sz3} + U_{insc3} + c_w G_{swz3}} \tag{5.15}$$

$$T_{sb11}(t) = \frac{c_w G_{sz1} T_{sbb1}(t - l_{z1}) + U_{insb11} T_{soil} + c_w G_{swz1} T_{sw2}}{c_w G_{sz1} + U_{insb11} + c_w G_{swz1}} \tag{5.16}$$

$$T_{recd}(t) = \frac{c_w G_{recd} T_{red2}(t - l_{cd}) + U_{inscd} T_{soil} + c_w G_{swcd} T_{sw2}}{c_w G_{recd} + U_{inscd} + c_w G_{swcd}} \tag{5.17}$$

$$T_{rebc}(t) = \frac{c_w G_{rez3} T_{rec3}(t - l_{bc}) + c_w G_{recd} T_{recd} + U_{insbc} T_{soil} + c_w G_{swbc} T_{sw2}}{c_w G_{rec3} + c_w G_{recd} + U_{insbc} + c_w G_{swbc}} \tag{5.18}$$

$$T_{rebb1}(t) = \frac{c_w G_{rebb1} T_{reb11}(t - l_{bb1}) + U_{insbb1} T_{soil} + c_w G_{swbb1} T_{sw2}}{c_w G_{rebb1} + U_{insbb1} + c_w G_{swbb1}} \tag{5.19}$$

Where, l_{ab}, l_{bc}, l_{cd}, l_{bb1}, l_{z1}, l_{z2}, and l_{z3} are equal to 58, 91, 275, 144, 212, 196, and 388sec respectively. In summary, the reduced-order model is described by the above equations together with Equations (3.17), (3.40) to (3.42), and (3.44), and this constitutes an eight order model.

It can be seen that, in Equations (5.10) to (5.19), the transport delay is added to the model. For instance, in Equation (5.10), $T_b(t\text{-}l_{ab})$ means that the present value of $T_{sab}(t)$ is dependent on that value of T_b, which is delayed by 58 seconds. Note that appropriate time delays also exist in return pipe segments in zone 1, 2, and 3, as well as segment AB shown in Figure 3.1.

5.3 Simulation model

The full-order model and the reduced-order models are simulated using the Simulink (Matlab). The Simulink block diagram is depicted in Figure 5.1.

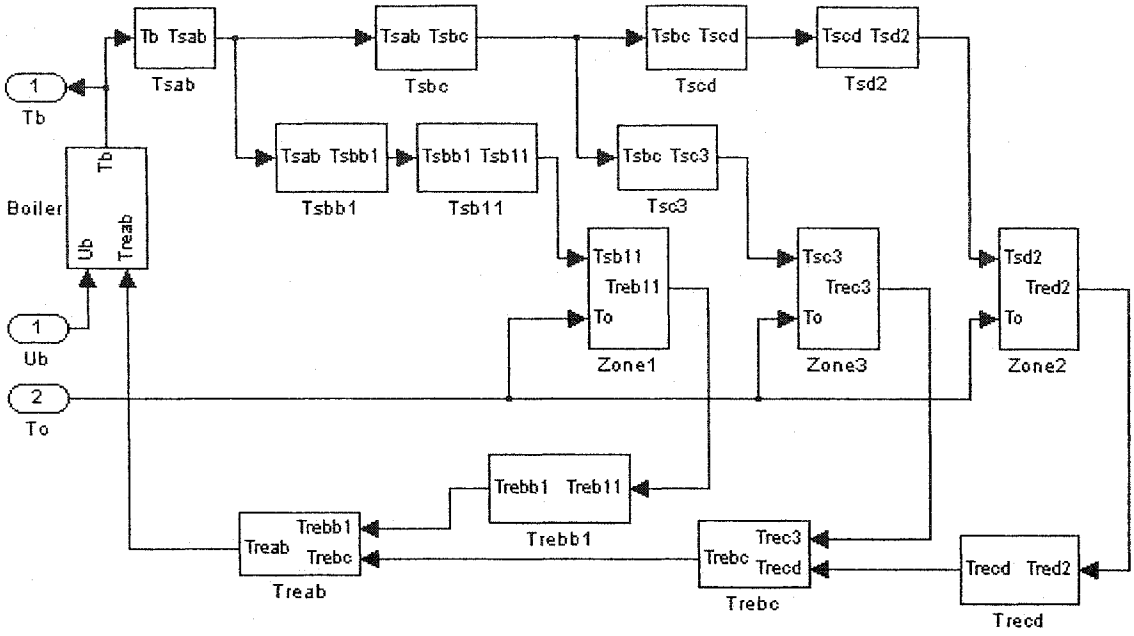

Figure 5.1 Block diagram of the dynamic model

In each block, one or more differential equations are included. Although the block profile of the full-order model is the same as the reduced-order model, the content is different. Input signal U_b and T_o as well as output T_b are represented in this figure. Note that the transport time delays in the piping network are also included in some blocks.

5.4 Open loop simulation results

Open loop simulation runs at constant boiler input and water flow rate are conducted to compare the results from full-order and reduced-order models. The results are depicted in Figure 5.2.

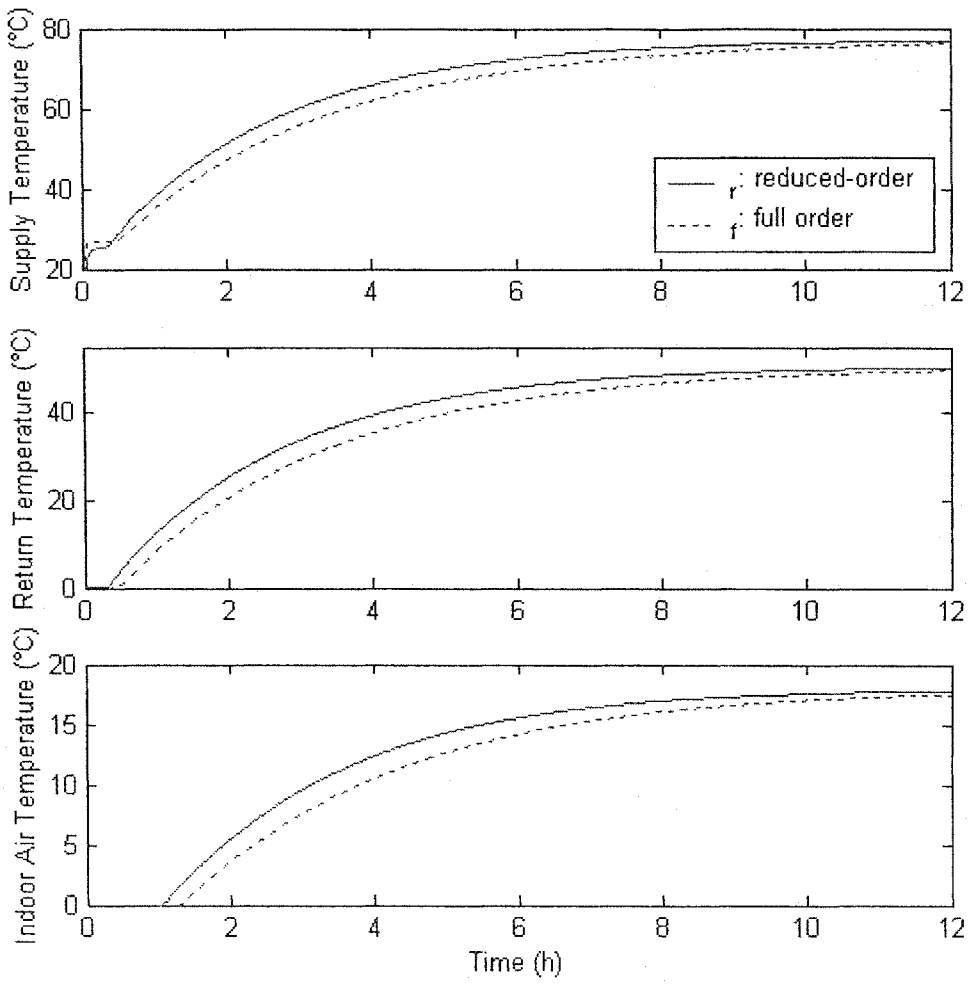

Figure 5.2 OLT: temperature responses under design condition (T_o=-11°C and U_b=1)

The slow temperature response curves in Figure 5.2 are indicative of the transport delay of the piping system and the thermal capacity of the overall system. These temperatures in a typical system reach steady state in about 12 hours. At 12:00 hours, for instance, the temperatures in the reduced-order model T_b, T_{reab}, and T_{z1} reach 76.88, 50.30, and 17.81°C respectively. In fact, the steady state values of these temperatures are 77.29, 50.71, and 18.03°C respectively. The design supply water, return water, and indoor air temperatures are 95, 70, and 18°C respectively. Because of the heat transfer area of

the terminal heaters in actual system is larger than that of the design values, the steady state temperatures cannot reach the design temperatures.

5.5 Optimal set points

Significant energy savings can be achieved by operating the boiler at as high efficiency as possible at the given load. To this end, a constrained optimization problem was formulated and solved in Chapter 4. The idea behind this is that if the boiler control loop can track an energy optimal set point profile, significant energy savings can be realized.

In addition, since the users of the DDHS have different occupancy patterns, the internal loads associated with variable occupancy have to be considered. To this end, the internal load patterns were divided into three groups such as low-energy users, high-energy users, and public building user group. This grouping is based on their function and energy consumption. Indeed, each of these classes may have their own operating parameters because of their different internal loads. The internal loads considered here consist of individuals in room, heat gains from appliances, and solar radiation. These profiles are shown in Figure 5.3. For example, the public buildings have the largest internal load up to $22w/m^2$ around 12:00 hours, while the internal load in the low-energy user group has the lowest value ($15.3w/m^2$). In the lower part of Figure 5.3, it can be seen that the internal load in zone 1 is the greatest than that in other zones since the heating floor area of the public buildings in zone 1 is larger. These internal load patterns in the

DDHS are assumed to occur concurrently. In other words, they occur at identical supply water temperatures and at the same time.

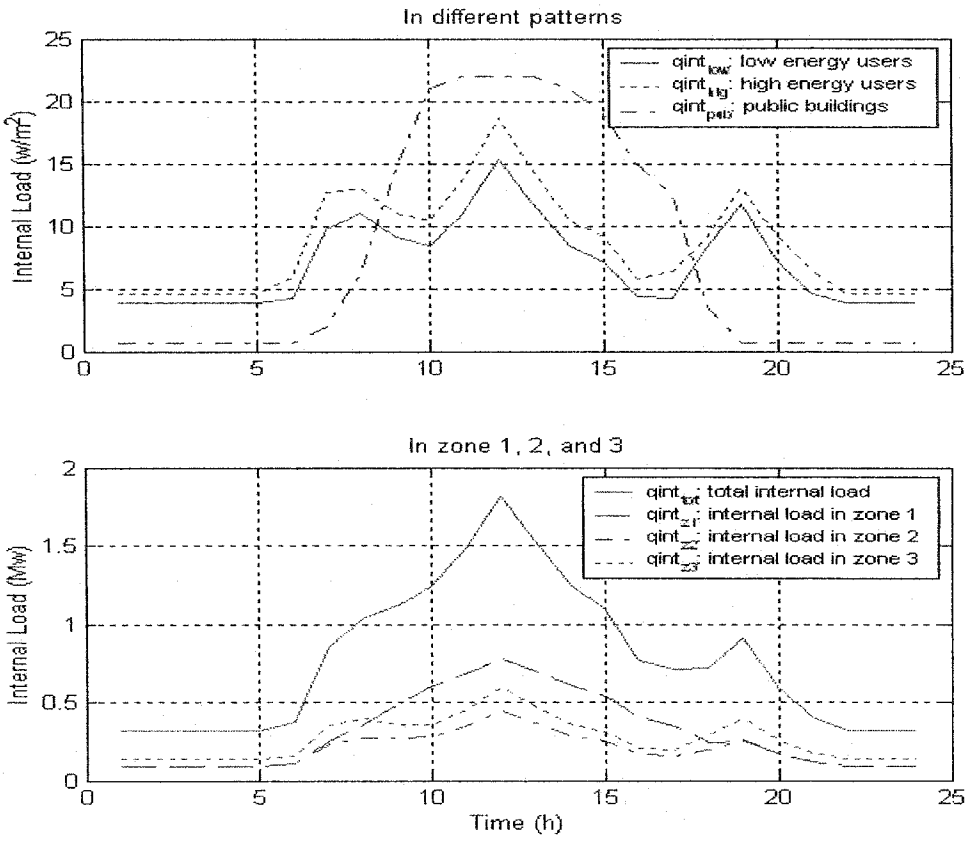

Figure 5.3 Internal load in different patterns and zones

In addition, the equivalent outdoor air temperature is defined as the outside air temperature at which the heat gain from internal loads such as people, appliances, as well as solar radiation that affects buildings is no longer enough to offset heat losses occurring in the space to maintain design room temperature. It is the "theoretical" temperature at which additional heat is needed to maintain the set point temperature.

With this assumption and the concept of equivalent outdoor temperature, an equivalent outdoor temperature T_o' was used to determine the optimal set point T_{bsp}. The

equivalent outdoor temperature is calculated from

$$T_o' = T_o + \frac{q_{\text{int}}}{U_{t1} + U_{t2} + U_{t3}} \tag{5.20}$$

By calculating the equivalent outdoor air temperature T_o' from Equation (5.20), one could use the no internal load set point curve in Figure 5.4 to determine the boiler set point in the presence of internal loads.

The optimal profile curves for each q_{int} in different zone are also obtained according to their respective weighting factors. These are depicted in Figure 5.4. Moreover, the average set point T_{bspavg} curve is also shown in this figure. Note that the case with no internal load gives higher optimal set point T_{bspnil} compared to the cases with internal loads.

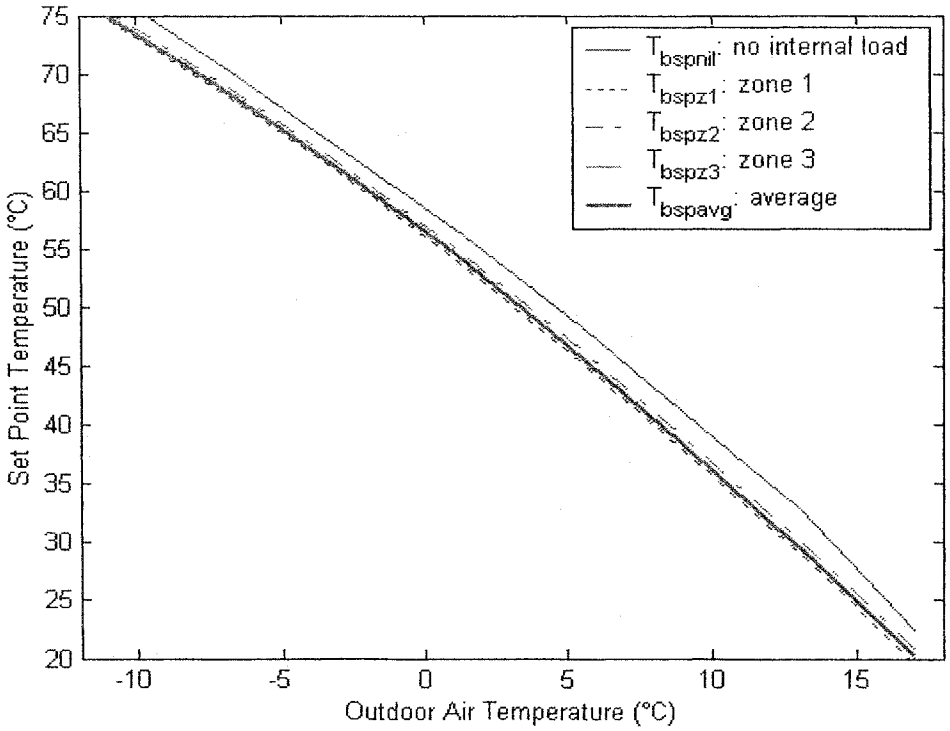

Figure 5.4 Optimal temperature set point profiles for the boiler

5.6 Smith Predictor design for the DDHS

5.6.1 Principle of a Smith Predictor

Since many processes have apparent transport time delay phenomenon, there is considerable incentive to develop advanced control algorithms that can compensate for such kind of time delay. Smith [18] proposed a controller that became well known as the Smith Predictor. Note that the response of the control system is based on the accuracy of the plant model. Since plant models are not completely accurate, some unmodeled dynamics always remain. The use of a PID controller could compensate the effects of these unmodeled dynamics. The SP control scheme is presented in Figure 5.5.

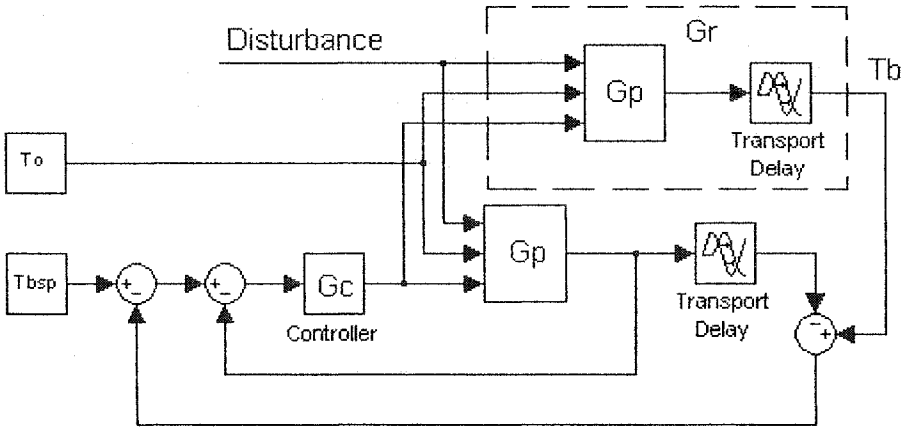

Figure 5.5 The Smith Predictor control scheme

The SP has two control loops: an internal feedback without time delay and an external feedback loop with time delay. The controller operates on two separate models of the plant. If the plant model is accurate and the plant performance is reliable, this control system can provide good control of the real plant.

5.6.2 SP design methodology

A real plant transfer function with transport delay e^{-Ts}, is defined as $G_r(s)= G_p(s)e^{-Ts}$. Since SP attempts to remove the effect of the T second time delay from the closed loop system, the controller can be designed as if there is no time delay. To this end, the overall transfer function of the reduced-order linearized closed loop system is written as

$$G_o(s)=\frac{T_b(s)}{T_{bsp}(s)}=\frac{G_c(s)G_p(s)e^{-Ts}}{1+G_c(s)G_p(s)} \tag{5.21}$$

The SP design consists of two steps. In the first step, a control law for the system without delay is designed; the second step consists of directly calculating an equivalent controller for the system with delay as shown below.

$$\frac{G_{csp}(s)G_p(s)e^{-Ts}}{1+G_{csp}(s)G_p(s)e^{-Ts}}=\frac{G_c(s)G_p(s)e^{-Ts}}{1+G_c(s)G_p(s)} \tag{5.22}$$

$$G_{csp}(s)=\frac{G_c(s)}{1+(1-e^{-Ts})G_c(s)G_p(s)} \tag{5.23}$$

The equivalent plant concept is used to obtain equivalence between Equation (5.21) and the SP controller that is described in Equation (5.22).

The design method is explained briefly. The linearized plant transfer function $G_p(s)$ of the reduced-order DDHS is obtained as in Equation (5.24).

$$G_p(s)=\frac{\begin{array}{l}0.05411s^7+0.001082s^6+3.392\times10^{-6}s^5+4.718\times10^{-9}s^4\\+3.544\times10^{-12}s^3+1.499\times10^{-15}s^2+3.373\times10^{-19}s+3.15\times10^{-23}\end{array}}{\begin{array}{l}s^8+0.02949s^7+0.0002526s^6+6.134\times10^{-7}s^5+6.859\times10^{-10}s^4\\+4.02\times10^{-13}s^3+1.228\times10^{-16}s^2+1.676\times10^{-20}s+5.145\times10^{-25}\end{array}} \tag{5.24}$$

The specifications for nominal controller design are chosen such that (i) position error =0. (ii) overshoot ≤5%. (iii) settling time <1000sec. (iiii) rise time as small as

possible.

Consider a PI controller $G_c(s)$ for the nominal controller design, and let $k_i=0.05k_p$.

Then, $G_c(s)=\frac{k_p(s+0.05)}{s}$ and $G_1(s)=\frac{s+0.05}{s}$.

The root locus transfer function is given by $G_{rls}(s)=G_1(s)G_p(s)$. From the trajectory of $G_{rls}(s)$ in s-plane, the pole P_o (-0.095,0) satisfies all of the above specifications. Therefore, the corresponding value of the proportional gain k_p is found to be 3.3358.

In the controller design with the SP, the transport time delay e^{-Ts} is approximated by $G_e(s)=\frac{-2728s+2}{2728s+2}$, where T=2728sec. Thus, using Equation (5.23), the SP controller was designed and reduced to the form: $G_{csp}(s)=\frac{0.2034s+5.987\times10^{-6}}{s}$. For this plant with SP, the designed parameters of PI controller are $k_p=0.2$, $k_i=0.002$.

5.7 Simulation results

5.7.1 Control system configuration

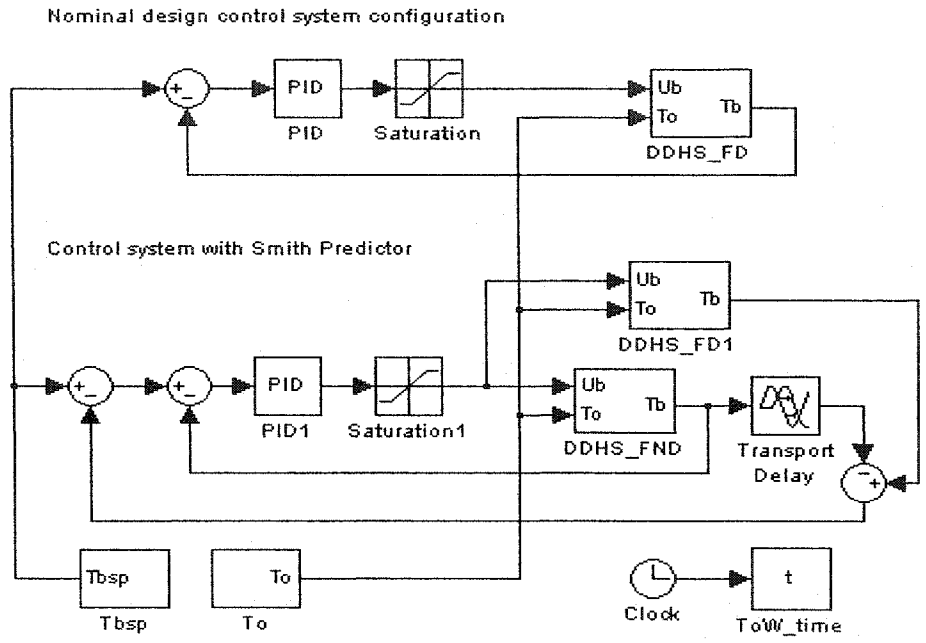

Figure 5.6 Control system configurations

Figure 5.6 displays two control blocks: the upper part shows the nominal controller and lower part depicts the SP controller. The block "DDHS_FD" is the full-order model, while the block "DDHS_FND" refers to the model without time delay. The block "Transport Delay" is the total transport time delay, which is set equal to 2728sec. Note that in "DDHS_FD" block, there are 14 time delays corresponding to the transport delay of pipe segments AB, BC, CD, BB1, and the supply and return piping network of each zone (Figure 3.1).

5.7.2 The effect of set point changes

The simulation of step change in T_{bsp} set point is shown in Figure 5.7. In this figure, the set point changes from 40°C to 60°C at 12:00 hours, and from 60°C to 30°C at 24:00

hours. Other than the influence of initial condition, the T_{bsp} response with SP is faster than that of the system without SP. For example, in the set point increase phase, the control system with SP reaches the new set point 3 hours faster compared to the case without SP. Also, the fluctuations in indoor air temperature in each zone are smaller than that in the control system without SP.

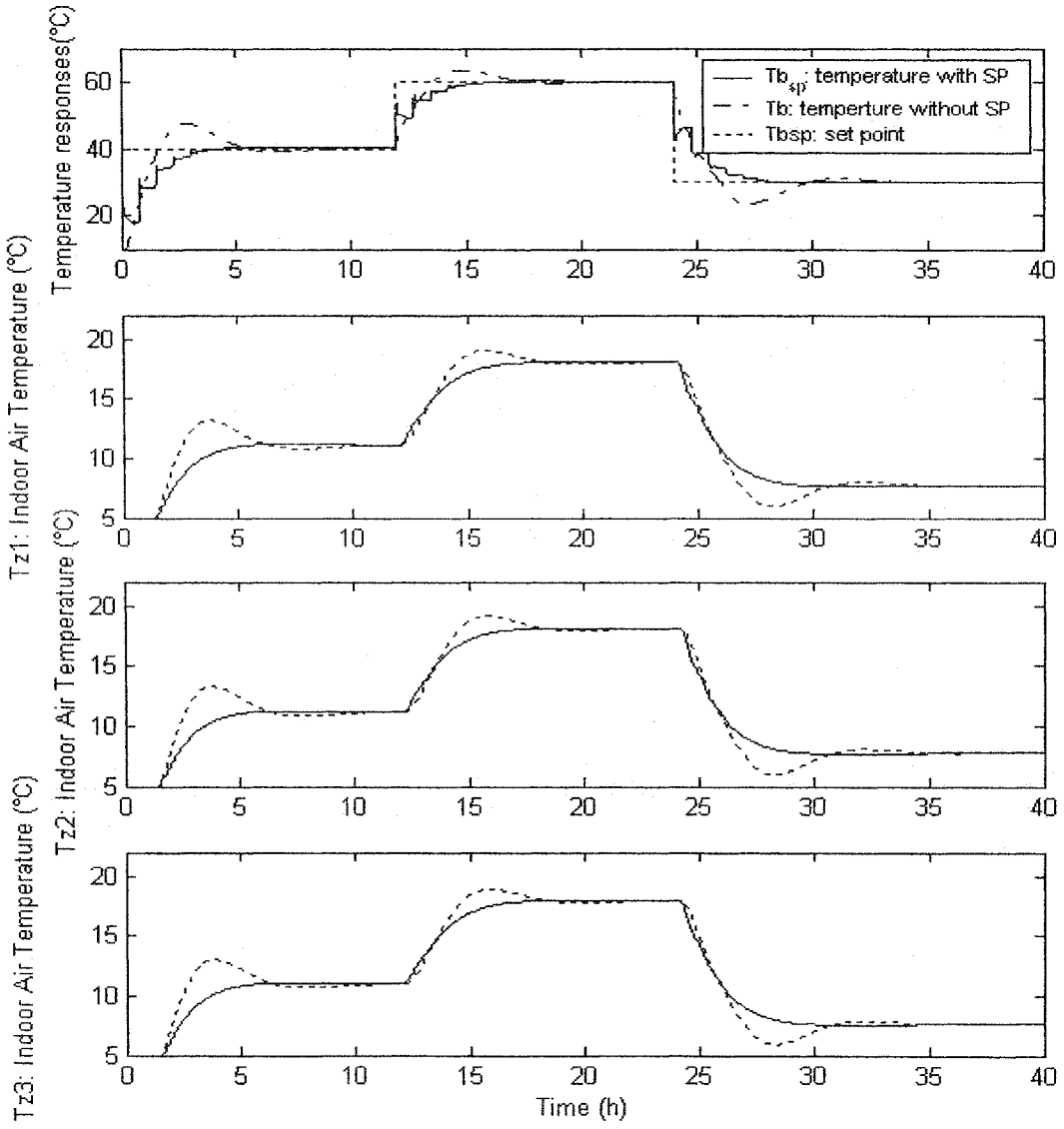

Figure 5.7 Responses of changes in set point T_{bsp} with and without SP

5.7.3 Typical daily operation

In order to simulate typical daily heating process, a typical five-day weather data with outside temperature ranging from 10.6°C to –8.5°C is chosen as shown in Figure 5.8. The temperature profile denotes warm day, cool weather, and cold day in winter. The optimal set points T_{bsp} corresponding to these outdoor temperature conditions is chosen from Figure 5.4. In addition, a disturbance of ±5°C in T_b was considered because such disturbance results from the fluctuations in the pressure and temperature of the transported fuel, as well as other uncertain factors. Lastly, the internal load is also considered in some simulations.

5.7.4 Temperature responses of the DDHS with disturbances in T_b

The responses of the control system with and without SP are compared in Figure 5.8 and 5.9 in the presence of disturbances in T_b acting on the system.

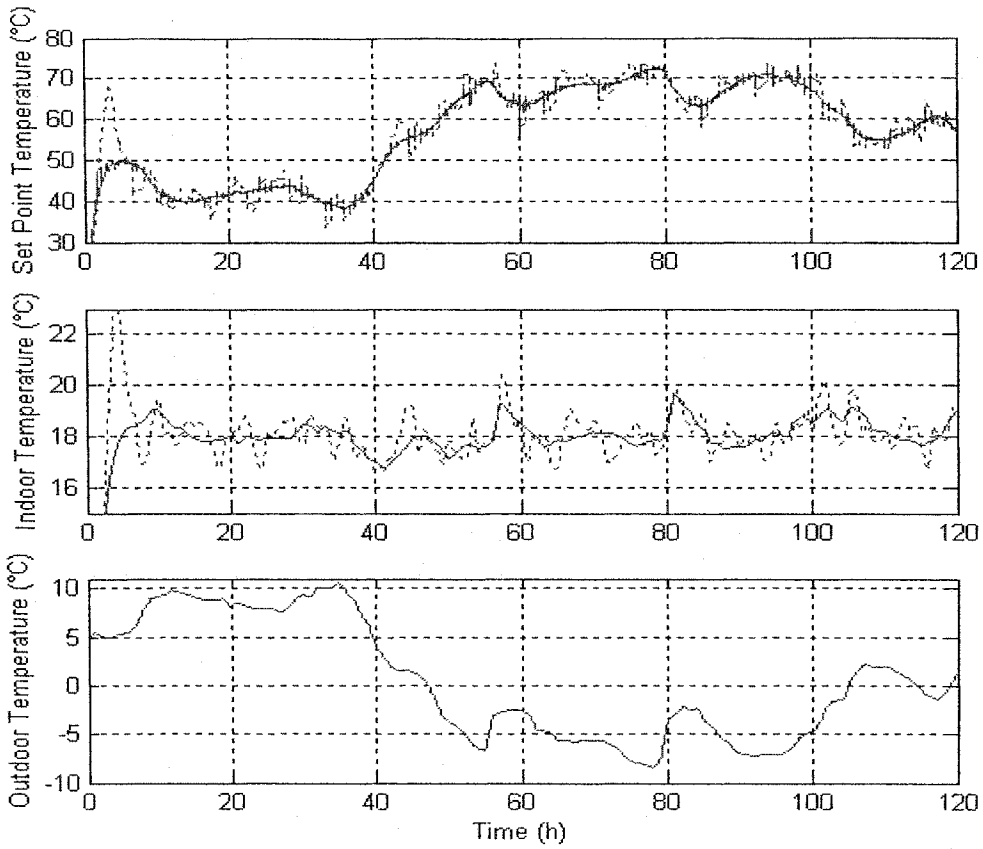

Figure 5.8 Real time responses with and without SP

The temperature responses of zone 1 in Figure 5.8 have obvious differences. Note that good disturbance rejection is achieved by using SP. From these responses, one can note that the biggest swing in T_b in the control system without SP is around 5°C, while the biggest swing in T_b in the control system with SP is about 1°C. As a result, indoor air temperatures in zone 1 also show clear differences. They fluctuate within a range of 18±0.5°C in most conditions in the control system with SP, while they vary from 18+1°C to 18-1.5°C in the control system without SP. Therefore, it is obvious that the control

system with SP is more effective in handling long transport delay and in disturbance rejection.

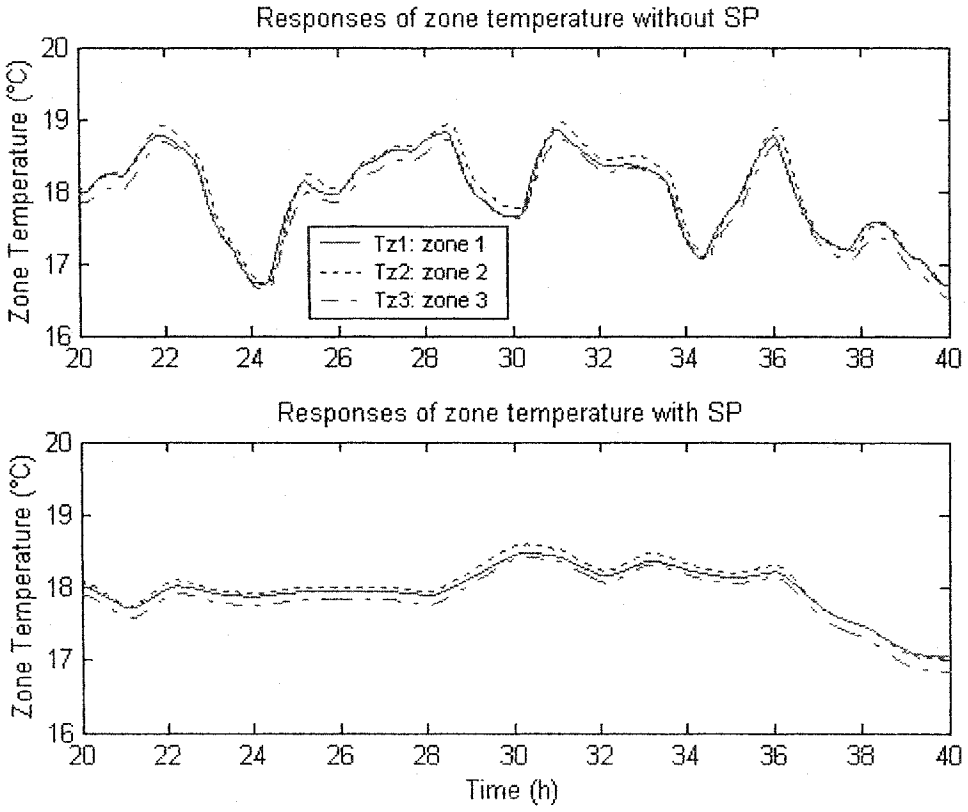

Figure 5.9 Real time responses of zone temperature with and without SP

The indoor air temperature responses in each zone are shown in Figure 5.9. For example, the indoor air temperature response in zone 1 is somewhat faster than that in zone 2 because of the transport time delay. In addition, the indoor air temperature responses in each zone are slightly different. The reason is that each zone has different load patterns and has their own T_b set points. However, this difference is around 0.1°C ~0.3°C, and is not significant.

5.7.5 The effect of changes in transport time delay

In practice, the time delay can change since the heating load and circulating water flow rate may be varied in the heating season. Hence, simulation runs are made to study the effect of a ±25% change in time delay. The results are shown in Figure 5.10. It can be seen that the heating system shows a slight difference in responses between the cases with increasing and decreasing time delay compared to no time delay. The reason is that the varying transport delay means the change in circulating water flow rate. However, it is known that the effect of changing circulating water flow rate on indoor air temperature is smaller than changing supply water temperature. Therefore, the cases with increasing and decreasing time delay at this range show no significant differences. Another reason for this is that the PI controller can also compensate for these changes as well.

It is also shown in Figure 5.10 that the tendency of changing transport time delay. When the time delay increases, the indoor air temperature response is faster than that in decreasing time delay.

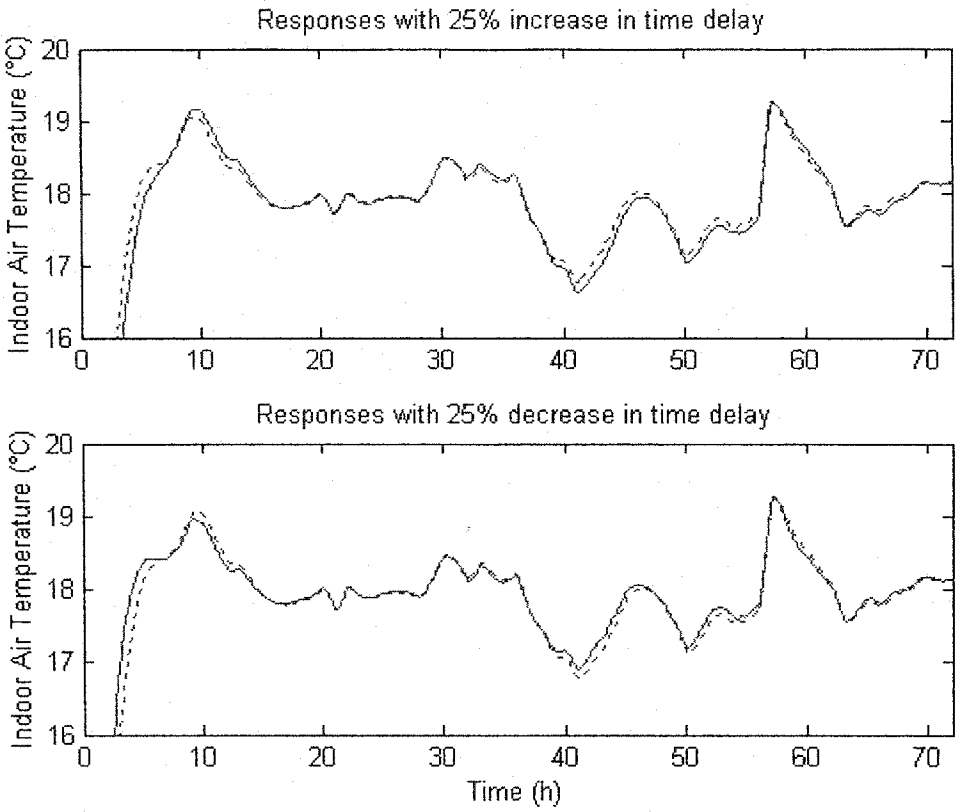

---- Responses with no time delay change —— Responses with time delay change

Figure 5.10 Response of changing time delay with SP

5.7.6 The effect of changes in model parameters

Because the physical properties of the building materials and heat transfer coefficients are variable, the parameters of the analytical model should be varied accordingly. In order to simulate this case, a simulation with a 40% increase in the capacities of all zones was considered, and the results are presented in Figure 5.11.

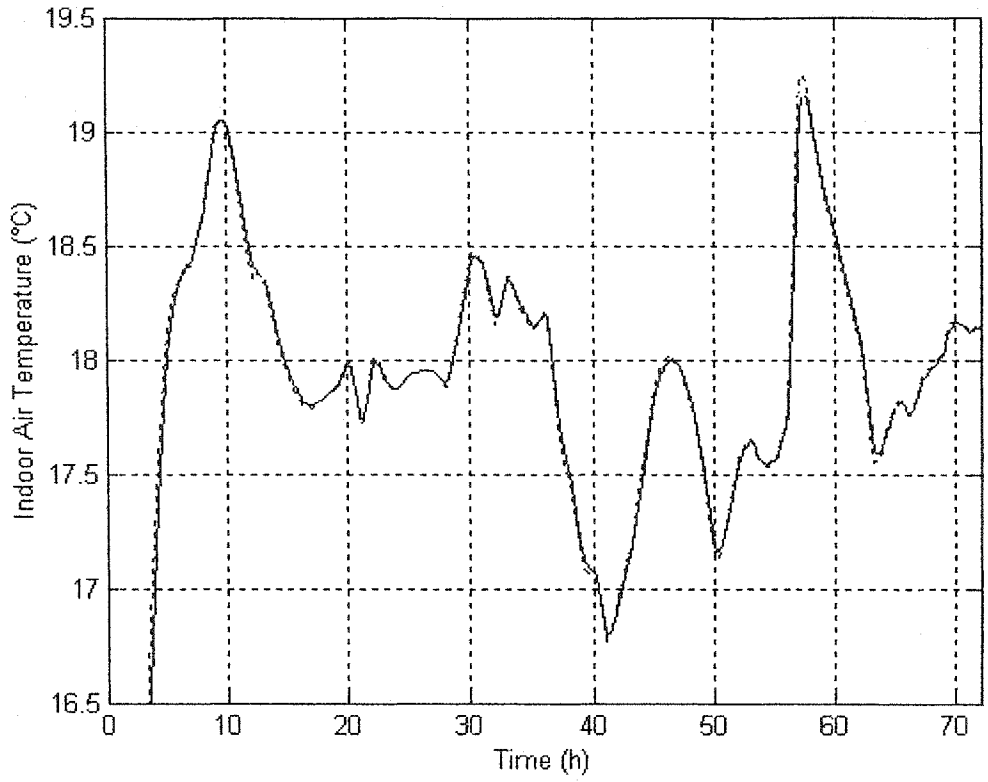

—— Responses with change in parameters ---- Responses with no change in parameters

Figure 5.11 Response of model parameter change

The responses depicted in Figure 5.11 show that the SP is able to reject the effect of changing capacities of the building.

5.7.7 The effect of internal loads

Internal loads always exist, and sometimes they have clear influence on indoor air temperatures. This case is presented in Figure 5.12. It can be seen from this figure that the indoor air temperatures fluctuate greatly by internal loads. The greatest swing in the indoor air temperature is about 5.8°C compared to the design indoor air temperature.

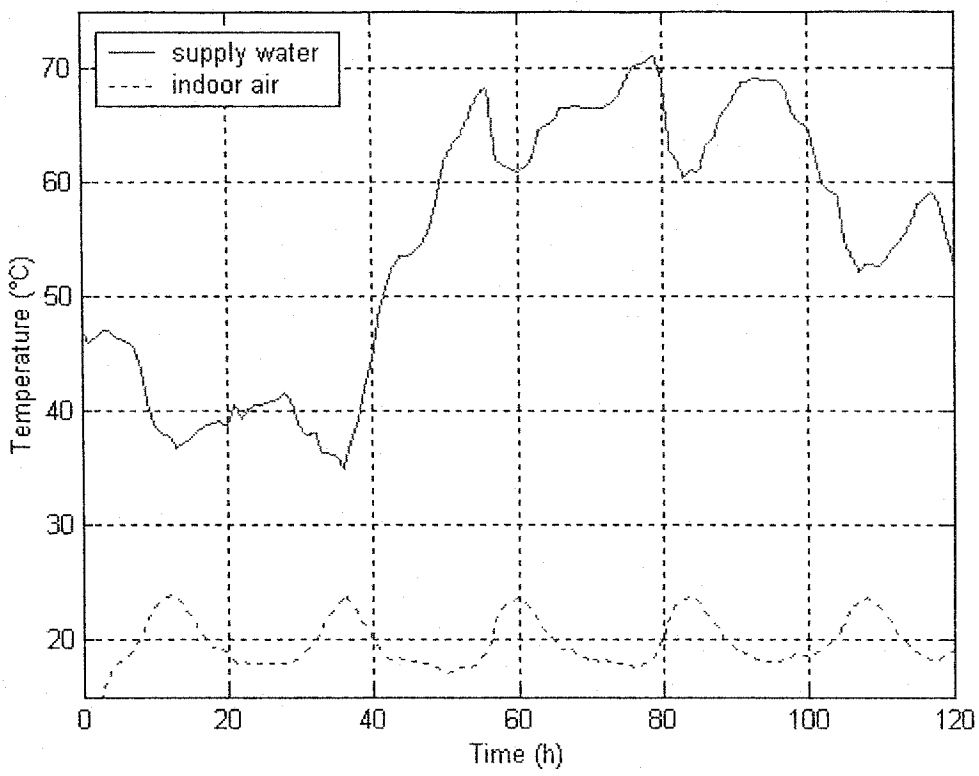

Figure 5.12 Responses of indoor air temperature with internal loads

5.7.8 Methods for reducing indoor air temperature fluctuation

The fluctuations in the indoor air temperature shown in Figure 5.12 are not desirable, and it should be reduced by appropriate means. This can be achieved by predicting internal loads and compensating for them in the selection of optimal boiler water temperature. Therefore, adjusting the optimal set points in T_b with internal loads is considered. Based on the actual outdoor air temperature and the internal loads, the equivalent outdoor air temperature can be determined.

Since each zone has its own internal load, the maximum internal loads in the three zones are chosen at any given time in order to calculate the equivalent outdoor air temperature. Using the maximum internal loads, the equivalent outdoor air temperature is

plotted in Figure 5.13. For example, the temperature affected by internal loads, actual outdoor air temperature, and equivalent outdoor air temperature at 36:00 hours are 3.6, 10.1, and 13.7°C respectively. Therefore, the supply water temperature will be decreased if the optimal supply water temperature is determined based on the increased outdoor air temperature.

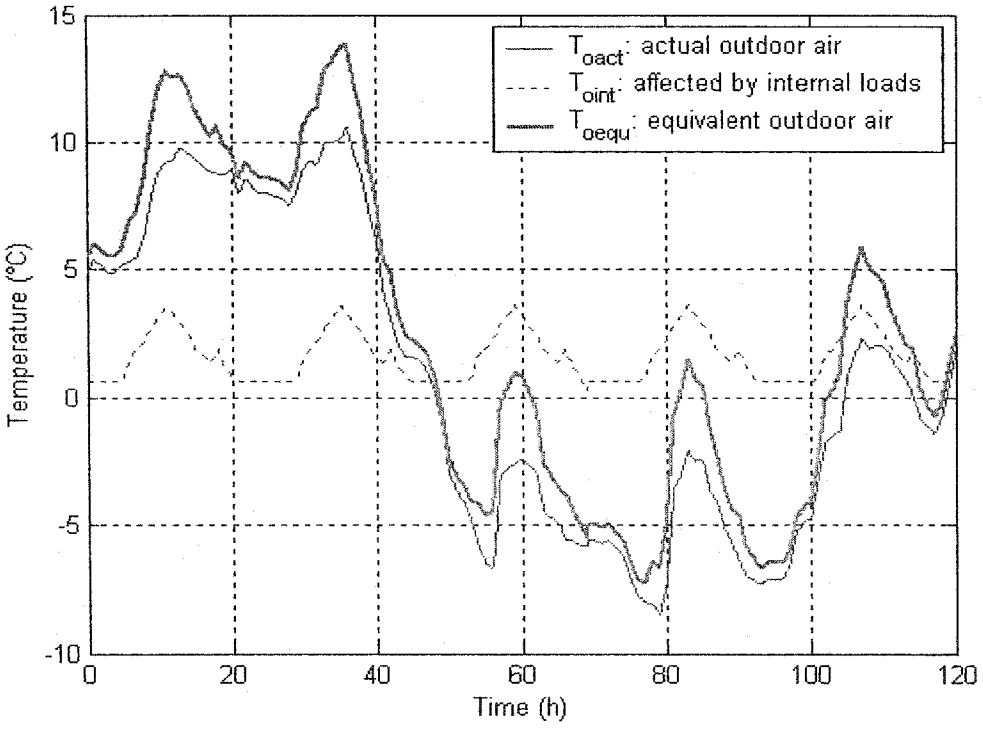

Figure 5.13 Equivalent outdoor air temperature by considering internal loads

The temperature responses of the DDHS with the equivalent outdoor air temperature based T_b set points are presented in Figure 5.14. The temperature responses with average and instantaneous internal load are shown in the figure. The set points of the supply water temperatures with instantaneous internal loads decrease compared to the average case, especially around the noon. As a result, indoor air temperatures are also reduced. The peak indoor air temperature is decreased by 1°C~1.5°C.

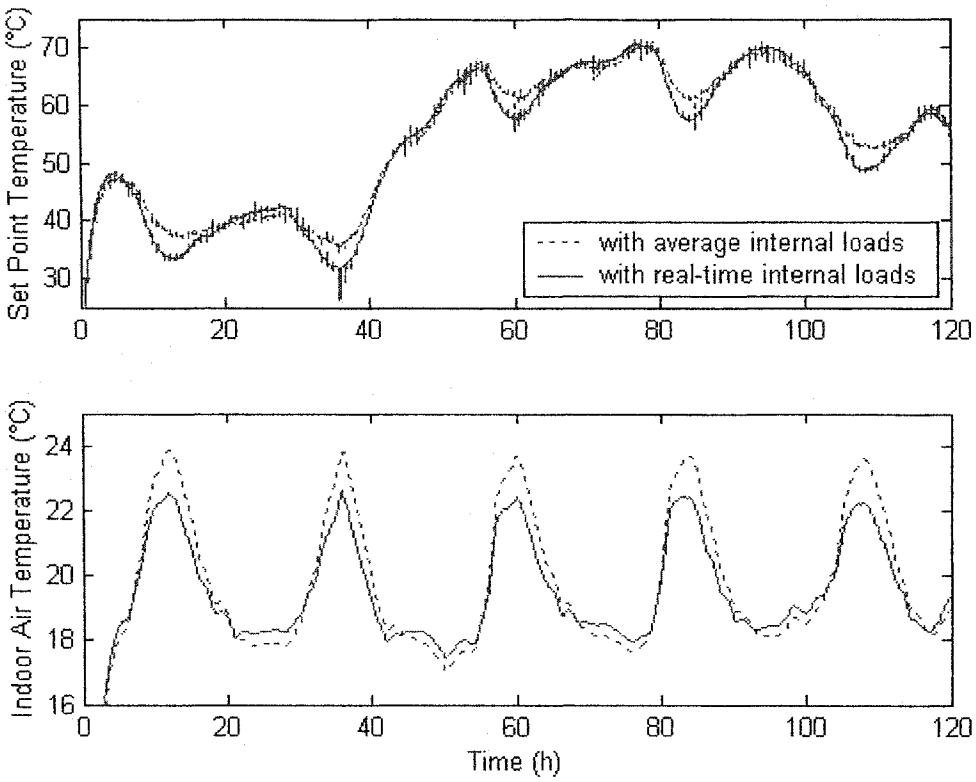

Figure 5.14 Responses with set points T_b based on Figure 5.13

However, the indoor air temperature still shows large swings. In order to lower the fluctuations in indoor air temperature, adjustment of the set points in T_b were obtained by fine tuning the boiler set point temperature. The results are presented in Figure 5.15. It is apparent that indoor air temperatures are within a reasonable range (18±1°C).

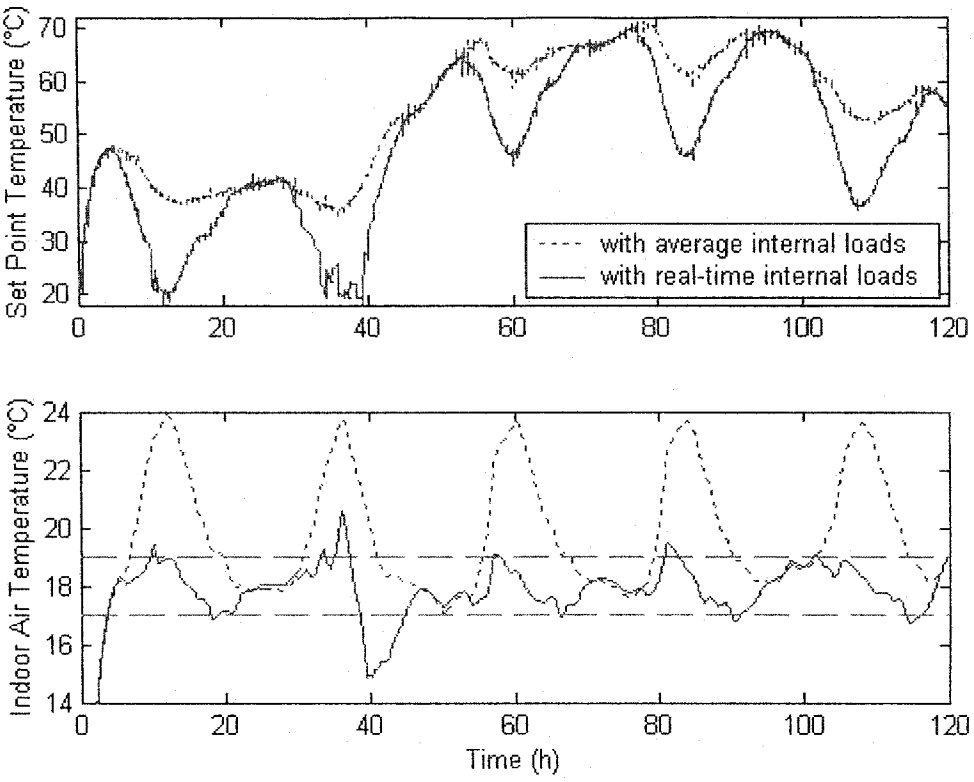

Figure 5.15 Responses with tuned supply water temperature set points

5.7.9 Comparison of energy consumption

In order to assess the energy saving potential of the developed optimal control strategy, four cases are simulated.

Case 1: arbitrary T_{bsp1} set points without internal load

T_o>5°C, T_{bsp1}=42°C;

T_o>0°C and T_o≤5°C, T_{bsp1}=53°C;

T_o>-5°C and T_o≤0°C, T_{bsp1}=65°C;

For all other outdoor air temperatures, T_{bsp1}=72°C,

Case 2: optimal T_{bsp2} set points without internal load,

Case 3: optimal T_{bsp3} set points with internal load, and

Case 4: adjusted optimal T_{bsp4} set points with internal load.

The simulation results are depicted in Figure 5.16. In this figure, the magnitude of the set point T_{bsp1} is the highest, while the set point T_{bsp4} is the lowest because of the internal loads considered in Case 4. For example, at 50:00 hours, the T_{bsp1}=65°C. Whereas, T_{bsp4}=60.2°C. In addition, Figure5.16 shows higher temperatures in zone 1 in Case 1 compared with Case 2. Also, the variations in indoor temperature in Case 3 are somewhat large because of the influence of internal loads. In order to tightly regulate the zone temperatures, adjusted equivalent outdoor air temperature is utilized, and the temperature responses are presented as in Case 4. It can be seen from Case 4, the indoor air temperatures are regulated in the range of 17°C~19°C. In addition, the lower indoor air temperatures that occur around 40:00 hours because of the change of outdoor air temperatures are too fast.

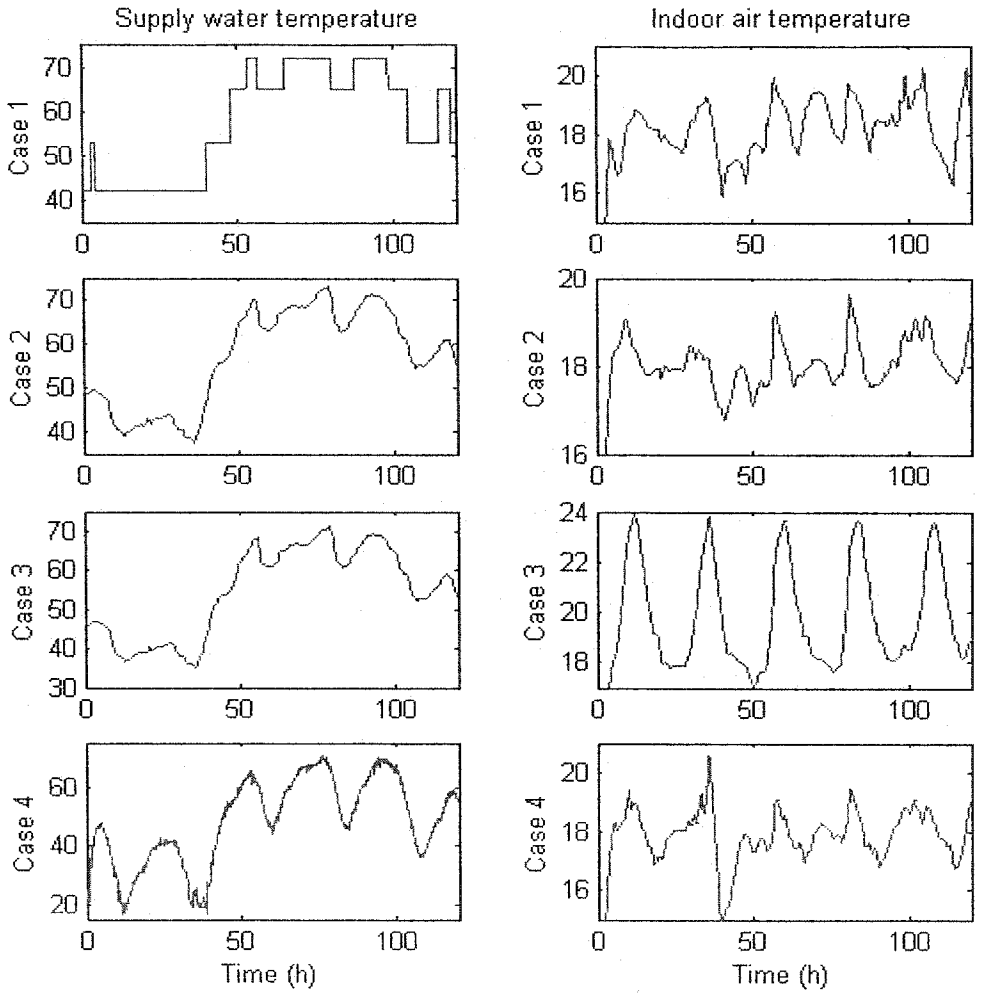

Figure 5.16 Responses of set point T_{bsp} change in four cases

The energy consumption of the four cases discussed above is compared in Table 5.1. Average outdoor air temperatures of warm, cool, and cold day are 6.4°C, -0.73°C, and –5.84°C respectively. From this table, the energy saving achieved by using the adjusted optimal supply water set points with internal loads (Case 4) is 19% compared to the Case 1 on a cold day. This is a significant saving in large systems such as the DDHS. Moreover, from the simulation, the fuel consumption for the five-day period in Case 1, 2, 3, and 4 were calculated. They are 47663, 47328, 42631, and 37617kg respectively. The

energy saving between Case 1 and 2 is about 1%, while the energy saving between Case 2 and 3 is about 10%. The biggest energy saving occurs in Case 4 is about 12% compared to Case 3.

Table 5.1 Energy consumptions in four cases (kg)

Item	Case 1	%	Case 2	%	Case 3	%	Case 4	%
Warm day	6260	100	6410	102.4	5457	87.17	4363	69.7
Cool day	10546	100	10341	98.06	9410	89.23	8294	78.65
Cold Day	12941	100	12430	96.05	11512	88.96	10513	81.24

In Figure 5.17, the energy consumption for a typical 15-day period is simulated. It can be seen that the largest energy saving are achieved in Case 4. For instance, the total energy consumption over the 15-day period for Case 1, Case 2, Case 3, and Case 4 are 167206, 166387, 151793, and 139174kg respectively. In other words, energy saving obtained in Case 2, Case 3, and Case 4 are 0.5%, 9.2%, and 16.8% compared with Case 1. Therefore, the largest energy savings occur in Case 4. Note that in the arbitrary set point case, sometimes the energy consumption is lower than Case 2 because its indoor air temperature is lower than that in Case 2.

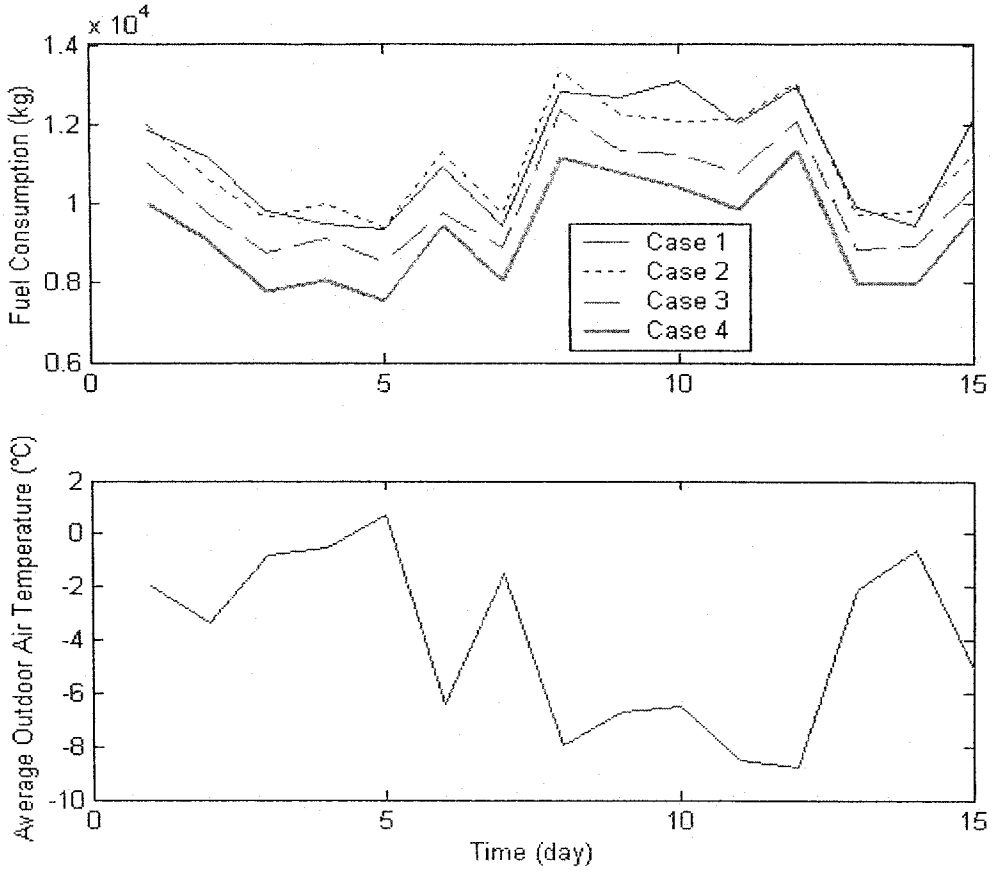

Figure 5.17 Energy consumption of four cases

Chapter 6 Contributions, Conclusions, and Recommendations for Future Research

6.1 Contributions and Conclusions

The contributions of this research are in the design, dynamic modeling, and optimal control of district heating systems. The specific contributions and conclusions in each of these areas are summarized below.

The contributions of the research work in terms of steady state design methodology are:

(1) Steady state methods were used to design and size two typical DDHS and IDHS.

(2) The influence of varying circulating water flow rate, heat transfer area of terminal heaters, and area of heat exchangers were investigated using aggregate models of DHS.

From steady state analyses the following conclusions were drawn.

(1) The most important parameters affecting the operation of DHS are circulating water flow rate and heat transfer area of terminal heaters in DDHS.

(2) The most important parameters affecting the operation of IDHS were circulating water flow rate in the primary side and heat transfer area of terminal heaters.

The contributions in the area of dynamic model development are summarized below.

(1) Dynamics responses of overall heat transfer process in the DDHS and the IDHS are influenced by heat losses due to water leakage and piping network as well as

building loads.

(2) A boiler model was developed based on the type of boiler and actual measured operating data.

(3) Large number of buildings and heat exchangers typically used in DHS were aggregated and the concept of equivalent building (or zone) and equivalent heat exchange station were used in the analyses.

(4) Nonlinear heat exchanger and terminal heater characteristics were taken into account in the dynamic models.

From the open loop tests conducted on the dynamic models the following conclusions were drawn.

(1) The time needed for the boiler temperature to reach steady state is influenced by outdoor temperature and initial conditions. Typically 12 hours to 15 hours were required for the boiler temperature to reach steady state.

(2) A typical daily breakdown of heat losses and heat utilization efficiency were found to be 12.6% and 87.4% respectively.

The contributions in optimization of operating parameters are summarized below.

(1) A multi-variable constraint optimization problem was formulated and solved to determine optimal operating parameters of DHS.

Results show that:

(2) Operating cost is significantly influenced by the makeup water used followed by pumping costs of water flow in the system.

(3) Optimal operating strategy of DHS can be implemented by modulating water flow rate, changing the airflow rate of the supply and exhaust fan of the boiler, and adjusting supply water temperature of the boiler using outdoor air temperature as a load discriminating signal, and predicting optimal set points given in Chapters 4.

The contributions in energy-optimal operation are summarized as follows:

(1) A control strategy augmented with Smith Predictor is designed to compensate the large transport time delays in the piping network.

From the closed loop simulation results the following conclusions were drawn.

(2) The developed optimal control strategy combined with a Smith Predictor controller gives superior performance in terms of temperature regulation and disturbance rejection.

(3) Simulation results show that significant savings in energy can be achieved by using optimal set points to operate the boiler as well as by considering the building's internal loads. For instance, energy savings from 19% to 25% can be realized compared with the conventional approach of using arbitrary set points.

(4) A small amount of fine tuning of optimal supply water temperature set points can reduce the fluctuation in indoor air temperatures effectively.

(5) The designed control strategy is found to be robust to changes in time delay and building parameters and give good temperature control under set point changes and variable outdoor air temperature.

6.2 Recommendations for future research

Research results conducted in the thesis present opportunities for further developments in control strategy study and optimal operation.

(1) Varying circulating water flow rate together with optimal control of supply water temperature could save greater energy.

(2) Comprehensive model-based computer programs of DHS will be very useful in analyzing and simulating the impact of design and operating conditions.

(3) It is important to develop a control strategy involving multiple control loops in IDHS.

(4) Dynamics of makeup water systems should be examined carefully by modeling the pressure responses of the system.

(5) Adding zone control loop may improve indoor air temperature responses in DDHS with fluctuating internal loads.

References

[1] *ASHRAE Handbook HVAC Systems and Equipment*, ASHRAE, American society for heating refrigerating and air conditioning engineers, Atlanta, GA, 2000;

[2] A.K. Athienitis, *Building Thermal Analysis*, Concordia University, 2000, pp 87-108, 129-189;

[3] B. BΦhm, *On the Optimal Temperature Level in New District Heating Networks*, Fernwärme International, 1986, 15(5) pp 301-306;

[4] B. BΦhm, *Energy-economy of Danish District Heating System: A technical and Economical Analysis*, Laboratory of Heating and Air Conditioning, Technical University of Denmark, Lyngby, Denmark, 1988;

[5] Chen Tingyao, *A methodology for Thermal Analysis and Predictive Control of Building Envelope Heating System*, Concordia University, 1997, pp 47-105;

[6] E.G. Hansen, *Hydronic System Design and Operation, A Guide to Heating and Cooling with Water*, McGraw-Hill Book Company, New York, 1985, pp 93-144, 259-312;

[7] G.E. Phetteplace, *Simulation of District Heating Systems for Piping Design*, International Symposium on District Heat Simulation, Reykjavik, Iceland, 1989;

[8] IDHA, *District Heating Handbook*, 4th ed, International District Energy Association, Washington, D.C., 1983;

[9] John M. House, Theodore F. Smith, *A System Approach to Optimal Control for HVAC and Building Systems*, ASHRAE Trans, 1995, Part 2, pp647-660;

[10] K. Larsson, Y.EL Mahgary, *Urban District Heating Using Nuclear Heat :An Energy Model for Overall Optimization of a Nuclear Based District Heating System*, International Atomic Energy Agency Vienna, 1977, pp 45-67;

[11] K.M. Letherman, *Automatic Controls for Heating and Air Conditioning Principles and Applications*, Pergamon Press, v15, 1981, pp 96-195;

[12] K. Watanable, M. Ito, *A Process-model Control for Linear Systems with Delay*, IEEE Trans, On Automatic Control, 26(6), 1981, pp 1261-1266;

[13] Liu Jianjiang, Ni Weidou, Yang Yanping, *New Method for Designing Robust Smith Predictor*, Journal of Tsinghua University Science and Technology, 1999,v39;

[14] Liu Xianying, Chen Yanlin, Shun Cunwu, Huang Zhong, *The Calculating Method of Design and Selection on Plate Heat Exchanger, Air Conditioning Design*, China Hunan Science and Technology Publishing House, 1997, v1, pp 82-107;

[15] Lu Yaoqing, *Practical Heating and Air-conditioning Design Handbook*, China Construct Industry Press, 1993;

[16] Li Yingcai, He Ping, *Heating Engineering*, China Construct Industry Press, 1980, pp 112-127, 201-212;

[17] M. Zaheer-Uddin, R.V. Patel, *The Design and Simulation of a Sub-Optimal Controller for Space Heating*, ASHEAE Trans, vol. 99, part 1, 1993, pp 554-564;

[18] O. J. Smith, *A Controller to Overcome Dead Time*, ISA J.6 (2), 1949, pp 28-33;

[19] P.E. John Siegenthaler, *Modern Hydraulic Heating for Residential and Light Commercial Buildings*, Mohawk Valley Community College Utica, New York, 1995, pp 163-166;

[20] P.L. Martin, D.R. Oughton, *Faber and kell's Heating and Air-conditioning of buildings*, 8th edition, Butterworth-Heinemann Ltd, Linacre House, Jordan Hill, Oxford 0X2 8DP, 1995, pp 620-622;

[21] Prabir Basu, Cen Kefa, Louis Jestin, *Boilers and Burners Design and Theory*, 2000, pp 21-50;

[22] P.B. Deshpande, Raymond H.Ash, *Elements of Computer Process Control with Advanced Control Applications*, Instrument Society of America, 1980, pp 227-250;

[23] Reijo Kohoner, *Intermittent Heating of Buildings, Performance of HVAC Systems and Controls in Building*, Proceeding of a CIB International Symposium (W79) at the Building Research Establishment, Garston, 1984, pp 233-246;

[24] S.H. Saboksayr, *Neural Network based Decentralized Control of an MZSH System*, Concordia University, 1995;

[25] S. Ljubiša, Milić. Draganović, R. Stojić, Milan S. Matijević, *A New Smith Predictor for Controlling a Process with an Integrator and Long Dead-Time: Design and Tuning*, Electronic and Energetics, 2001, Vol (14), No.1, pp1-18;

[26] Spyros G. Tzafestas, J.K. Pal, *Real Time Microcomputer Control of Industrial Processes*, Kluwer Academic Publishers, London, 1991, pp90-91;

[27] Steve Glickman, Roland Kulessky, Gregory Nudelman, *PID-Control Design for Power Station Processes Based on Time-Delay Compensation – Smith Predictor*, http://www.geocities.com/ugf4aggnn/CSTPMenu;

[28] W.E. Stewart, C.L. Dona, *Water Flow Rate Limitations*, ASHRAE Trans 1993 part 2, pp 811-825;

[29] W. Bobenhausen, *Simplified Design of HVAC Systems*, John Wiley & Sons, INC., 1994, pp 49-62, 249-272;

[30] Zheng Guorong *Dynamic Modeling and Global Optimal Operation of Multi-zone Variable Air Volume HVAC Systems*, Concordia University, 1997, pp 35-184;

[31] Zhang Zhilong, *Temperature Control Strategies for Radiant Floor Heating System*, Concordia University, 2001, pp 16-84;

[32] Z. Zhang, R.M. Nelson, *Parametrical Analysis of a Building Space Conditioned by a VAV System*, ASHRAE Trans, 1992, Part 2, pp43-48.

Appendix Design Calculation Tables of the DHS

The following design parameters are used in the design of DHS.

Table A.1 Design parameters of the DHS

Number	Item	Unit	Data
1	Supply water temperature in the primary system	℃	130
2	Return water temperature in the primary system	℃	80
3	Supply water temperature in the secondary system	℃	95
4	Return water temperature in the secondary system	℃	70
5	Total heated floor area	m^2	851031
6	Indoor air temperature	℃	18
7	Outdoor air temperature	℃	-11
8	Fouling factor of exchangers	℃	0.85
9	Terminal heaters		Radiator
10	Resistance of valves and piping network in each building	Pa	50000
11	Heat value of fuel (Fuel oil: No.6)	MJ/kg	43.3485
12	Type of heat exchanger		Plate heat exchanger
13	Resistance of each HES at primary side	10^4 Pa	15

Table A.2 Heated floor area and design heating load in the DDHS

Number	Floor Area	Design Heating Load	Building Type	Design Circulating Water Flow Rate	Elevation of Lowest Floor (Sea Level)	Elevation of Highest Floor (Sea Level)
	m^2	w		t/h	m	m
1	2325	144409	Residential	4.971	32.25	47.25
2	3598	218618	Residential	7.525	33.02	54.02
3	256	31109	Commercial	1.070	32.55	35.55
4	3244	199299	Residential	6.860	35.23	56.23
5	3244	199299	Residential	6.860	35.23	56.23
6	4256	244233	Residential	8.407	33.45	54.45
7	2589	164302	Residential	5.655	32.65	50.65
8	1254	98206	Commercial	3.380	33.84	45.84
9	1254	98206	Commercial	3.380	33.84	45.84
10	5369	304478	Residential	10.481	35.02	56.02
11	7523	424599	Residential	14.616	34.65	55.65
12	5632	319392	Residential	10.994	33.84	54.84
13	5621	318768	Residential	10.973	33.84	54.84
14	3587	256696	Commercial	8.836	33.75	44.75
15	756	79621	Commercial	2.740	32.26	37.55
16	1258	84931	Residential	2.923	32.48	47.48
17	1258	84931	Residential	2.923	32.48	47.48
18	2367	151812	Residential	5.225	34.11	52.11
19	2367	151812	Residential	5.225	34.11	52.11
20	5684	360715	Commercial	12.417	32.55	46.55
21	2985	185402	Residential	6.382	32.98	53.98
22	2985	185402	Residential	6.382	32.98	53.98
23	5658	359065	Commercial	12.360	32.64	49.35
24	3567	252857	Commercial	8.704	32.58	49.55
25	4562	267951	Residential	9.223	33.56	54.56

26	2587	162428	Residential	5.591	33.21	54.21
27	6541	370942	Residential	12.769	32.68	53.68
28	5310	336980	Commercial	11.602	32.77	46.75
29	1250	84390	Residential	2.904	32.65	47.65
30	1250	84390	Residential	2.904	32.65	47.65
Total	100137	6225243		214.294		

Table A.3 Heated floor area and design heating load in the IDHS

Number	Floor Area	Design Heating Load	Design Circulating Water Flow Rate	Elevation of the HES (Sea Level)	Design Exchanger Area
	m^2	w	t/h	m	m^2
HES_1	100137	6225243	107	31.86	160
HES_2	250495	14757193	254	32.66	360
HES_3	35485	2155713	37	33.21	40
HES_4	110361	6704440	115	32.85	130
HES_5	53682	3275675	56	30.28	62
HES_6	95232	5913909	102	31.58	110
HES_7	73528	4446970	77	32.79	90
HES_8	25641	1574958	27	32.84	30
HES_9	55417	3366584	58	34.02	80
HES_10	51053	3046336	52	31.84	72
Total	851031	51467024	885		1134

Table A.4 Piping network selection and water circulating resistance calculation for the DDHS

Pipe Segment	Design Water Flow Rate	Calculating Water Flow Rate	Nominal Diameter	Length	Equivalent Length Factor	Velocity	Friction Rate	Resistance
	t/h	t/h	mm	m		m/s	Pa/m	Pa
A-B	214.3	235.73	250	75	0.55	1.28	69	8021
B-C	128.88	141.768	200	112	0.5	1.23	84.2	14145
C-D	55.66	61.226	150	278	0.45	1.01	86.3	34787
B-B1	85.42	93.962	150	220	0.45	1.52	104	33176
B1-B2	52.35	57.585	150	84	0.45	0.95	77.9	9488
B2-B3	30.77	33.847	125	87	0.41	0.8	70.1	8599
B3-B4	11.97	13.167	80	96	0.32	0.72	97.1	12304
B4-B5	6.38	7.018	50	75	0.28	1.03	387.6	37209
B4-B6	5.59	6.149	50	85	0.28	0.92	291.5	31715
C-C1	73.22	80.542	200	58	0.5	0.7	27.8	2418
C1-C2	48.12	52.932	150	122	0.45	0.87	64.6	11427
C2-C3	39.08	42.988	125	114	0.41	1.02	112.3	18051
C3-C4	35.7	39.27	125	32	0.41	0.92	92.4	4169
C4-C5	29.66	32.626	100	85	0.37	1.2	109.2	12716
C5-C6	15.27	16.797	80	180	0.32	0.91	157.3	37374
D-D1	39.38	43.318	125	57	0.41	1.02	112.3	9025
D1-D2	33.54	36.894	125	120	0.41	0.87	83.2	14077
D2-D3	21.96	24.156	100	63	0.37	0.89	114.1	9847
D2-D4	11.58	12.738	65	80	0.3	1.01	240.3	24991
Note: The biggest resistance loop is A-B-B4-B5, and the value is 2x108799Pa.								

Table A.5 Piping network selection and resistance calculation for the IDHS

Pipe Segment	Design Water Flow Rate	Calculating Water Flow Rate	Nominal Diameter	Length	Equivalent Length Factor	Velocity	Friction Rate	Resistance
	t/h	t/h	mm	m		m/s	Pa/m	Pa
A-B	885	973.5	500	672	0.85	1.36	33.7	41895
B-C	598	657.8	450	908	0.75	1.13	26.1	41472
C-D	446	490.6	350	466	0.65	1.37	52.9	40674
D-E	192	211.2	300	840	0.6	0.8	22	29568
E-F	165	181.5	250	521	0.55	0.99	41.4	33432
F-G	107	117.7	200	467	0.5	1.02	60.2	42170
B-H	287	315.7	300	492	0.6	1.2	48.8	38415
H-I	129	141.9	250	1104	0.55	0.77	25	42780
Note: The biggest resistance loop is A-B-G, and the value is 2x187318Pa.								

Table A.6 Equipment selection in the DDHS (Boiler house approach)

Item	Unit	Data
Design heating load	Mw	6.225
Calculated heating load	Mw	6.853
Circulating resistance of external pipe	10^4 Pa	21.76
Resistance in the end of the biggest resistance loop	10^4 Pa	5
Filter resistance in the boiler house	10^4 Pa	3
Circulating water resistance of the boiler	10^4 Pa	10.69
Circulating water resistance of pipe in the boiler house	10^4 Pa	3
Rotational speed of the circulating pump	rpm	1426
Pressure head of the circulating pump	10^4 Pa	43.45
Calculated water flow rate of the pump	t/h	236
Set pressure of the makeup water system	10^4 Pa	24
Size and nominal parameters of equipment		
Circulating pump:		IS150-125-400
Nominal water flow rate	t/h	200
Nominal pressure head	10^4 Pa	50
Nominal efficiency	%	75
Nominal shaft work	KW	36.3
Nominal rotation speed	rpm	1450
Boiler:		
Nominal boiler capacity	Mw	7
Density of No.6 fuel oil	kg/m^3	988.5
Nominal boiler efficiency	%	91.2
Design oil consumption	kg/h	688
Design circulating water flow rate	t/h	250
Design circulating water resistance	10^4 Pa	12
Design permeable pressure	10^4 Pa	160

Table A.7 Equipment selection in the HES_1

Item	Unit	Data
Design heating load	Mw	6.23
Calculated heating load	Mw	6.853
Circulating resistance of external pipe	10^4 Pa	21.76
Resistance in the end of the biggest resistance loop	10^4 Pa	5
Filter resistance	10^4 Pa	3
Exchanger water resistance in secondary side	10^4 Pa	8.35
Water resistance of internal pipe	10^4 Pa	3
Rotational speed of the circulating pump	rpm	1426
Pressure head of the pump	10^4 Pa	43.45
Circulating water flow rate of the pump	t/h	236
Set pressure of the makeup water system	10^4 Pa	24
Size and nominal parameters of equipment		
Circulating pump:		
Type		IS150-125-400
Nominal water flow rate	t/h	200
Nominal pressure head	10^4 Pa	50
Nominal efficiency	%	75
Nominal shift work	Kw	36.3
Nominal rotation speed	rpm	1450
Exchanger:		
Calculated heating load	Mw	6.853
Design supply water temperature in the primary system	℃	130
Design return water temperature in the primary system	℃	80
Design supply water temperature in the secondary system	℃	95
Design return water temperature in the secondary system	℃	70
Logarithmic mean temperature difference	℃	19.96

Conductance of the plate heat exchanger	$w/m^2℃$	3000
Fouling factor		0.85
Total transfer area of exchangers	m^2	134.7
Type		BB0.8
Quantity		2
Transfer area of each exchanger	m^2	80
Circulating water flow rate in primary side	t/h	50
Circulating water flow rate in secondary side	t/h	100
Circulating water resistance in primary side	10^4 Pa	6
Circulating water resistance in secondary side	10^4 Pa	6
Design permeable pressure	10^4 Pa	160

Table A.8 Equipment selection of the heat source in the IDHS

Item	Unit	Data
Design heating load	Mw	51.47
Calculated heating load	Mw	56.617
Circulating water resistance of external pipe	10^4 Pa	37.46
Circulating resistance in the EHS of the biggest resistance loop	10^4 Pa	15
Filter resistance in the heat source	10^4 Pa	3
Boiler circulating water resistance	10^4 Pa	15.7
Circulating water resistance of pipe in the boiler house	10^4 Pa	5
Rotational speed of the circulating pump	rpm	1283
Pressure head of the pump	10^4 Pa	76.2
Circulating water flow rate of the pump	t/h	885
Set pressure of the makeup water system in primary side	10^4 Pa	32
Circulating pump:		14sh-9
Nominal water flow rate	t/h	1260
Nominal pressure head	10^4 Pa	75
Nominal efficiency	%	82
Nominal shift work	Kw	314
Nominal rotation speed	rpm	1450
Boiler:		
Nominal boiler capacity	Mw	58
Density of No.6 fuel oil	kg/m^3	988.5
Nominal boiler efficiency	%	91.3
Design oil consumption	kg/h	5276
Design circulating water flow rate	t/h	1000
Design circulating water resistance	10^4 Pa	25
Design permeable pressure	10^4 Pa	250